Development of traceable Rituximab modified polymeric micelles for active targeting of B-cell Lymphoma

by

Asma Ali Saqr

A thesis submitted in partial fulfillment of the requirements for the degree of

Master of Science

in
Pharmaceutical Sciences

Faculty of Pharmacy and Pharmaceutical Sciences
University of Alberta

Abstract

B-cell Non-Hodgkin Lymphoma (NHL) accounts for more than 90% of all adult cases of lymphomas and in most cases it is CD20 positive. B-cell NHL is usually treated by combination of conventional chemotherapeutics and the monoclonal antibody against CD20, rituximab. This combination regimen leads to severe side effects reducing the quality of life in lymphoma patients and/or forcing clinicians to use suboptimal doses of the medication. With current treatment, the survival of lymphoma patients is only around 50%. There is a need for the development of more effective and less toxic therapies for NHL.

Towards this goal, we pursued development and optimization of traceable CD20 targeted nano-carriers that can stay stable upon dilution in blood and potentially deliver a high payload of conventional chemotherapeutics preferentially to NHL cells, as compared to normal cells that do not express CD20. Such nano-carriers may be used for targeted therapy of CD20 positive malignant cells as well as following the progression of the disease. In this context, preparation of immune-mixed micelles was pursued through incubation of rituximab conjugated poly(ethylene glycol)-1,2-distearoyl-sn-glycero-3-phosphoethanolamine (PEG-DSPE) and methoxy poly(ethylene glycol)-poly(ε-caprolactone) (PEG-PCL) with degree of polymerization (DP) of 15 or 22 in the PCL block, or methoxy poly(ethylene glycol)-poly(ε-benzyl carboxylate-ε-caprolactone) (PEO-PBCL) with DP of 22 in the PBCL block. The effect of the hydrophobic block (PCL_{15}, PCL_{22}, and $PBCL_{22}$) on the thermodynamic and kinetic stability of mixed micelles was then studied by dynamic light scattering. The mixed micelles were made traceable, by introducing Cy5.5 to rituximab, and/or conjugating Cy3 to propagyl capped PEO-PCL or PEO-PBCL. The uptake of plain versus rituximab modified mixed micelles by KG-15 ($CD20^+$) and SUP-M2 cells ($CD20^-$) was then evaluated by flowcytometry at emission wavelengths of 570 and 707 nm, for Cy3 and Cy5, respectively.

Paclitaxel was loaded in mixed micelles; and it's *in vitro* release was evaluated. The *in-vitro* cytotoxicity of paclitaxel loaded micelles against KG-15 and SUP-M2 cells was measured by MTT assay. Our data showed mixed micelles composed of PCL_{22} or $PBCL_{22}$ to be thermodynamically and kinetically more stable than those with PCL_{15}. Accordingly, rituximab modified mixed micelles containing PCL_{22} or $PBCL_{22}$ showed the highest percentage of Cy3/Cy5 double positive association with KG-15 cells. The interaction of the rituximab modified mixed micelles was significantly higher by KG-15 than SUP-M2 cells. Pre-incubation of KG-15 cells with free antibody eliminated this difference, confirming the involvement of CD20 mediated micellar uptake. Paclitaxel release from mixed micelles with PCL_{22} and $PBCL_{22}$ core was slower than that of PCL_{15}. The *in-vitro* cytotoxicity study showed no significant difference in the cytotoxic effect of paclitaxel loaded rituximab mixed micelles compared to paclitaxel loaded in plain mixed micelles in KG-15 and SUP-M2 cells at 24 and 72 h, however, perhaps reflecting the non-internalizing function of CD20 receptor. In summary, the results of this study showed successful development of traceable immune-mixed micelles for active targeting of B-cell NHL based on rituximab-PEG-DSPE and PEO-PCL_{22} or PEO-$PBCL_{22}$. Mixed micelles of PEO-PCL_{15} were found to be not stable enough for this purpose.

Preface

This thesis is an original work by Asma Saqr. The research project, of which this thesis is a part, will be submitted to a Pharmaceutical Journal.

Dedication

I dedicate this thesis to my mother and father, whose prayers and encouragement gave me strength and courage; to my dear husband Ali who has been in my side all the way with his love, support, and patience; and to my beautiful daughters Zain and Ruba.

Acknowledgement

I would like to express my deepest gratitude to.

- My supervisor Dr. Afsaneh Lavasanifar for giving me the opportunity to pursue my studies in her lab. Her encouragement, guidance and academic support throughout the program enabled me to develop an understanding of the field. I cannot thank her enough for her endless help and motivation throughout my studies.

- My supervisory committee members, Dr. Hoon Sunwoo and Dr. Raimer lobenberg for their generous guidance and valuable comments and suggestions.

- Dr. Michael Doschak for accepting to be on my examining committee.

- M y previous lab mates Shyam Garg, Qi Zhang and Hoda Soleymani for helping me in the beginning of my studies.

- My current lab mates Dr. Mohammad Vakili, Dr. Forughalsadat Sanaee, Abdulsalam Alharbi, Hanan Al Lawati , Nasim Ghasemi, sams Sadat, Zahra Shire and Igor Paiva for their support and help.

- Dr. Vishwa Somayaji for his help with the ^{1}HNMR spectrometry.

- Dr. Aja Rieger and Sabina Baghirova, University of Alberta Faculty of Medicine and Dentistry Flow Cytometry facility, for their help with the flow cytometry analysis.
- Faculty staff, in particular, Joyce Johnson, Diseray Schamehorn, Matthew Barnett Cory Thorp and Drew Price for their help and support throughout the whole program.
- My dear husband, Ali and my lovely kids, Zain and Ruba who accompanied me throughout the whole journey and helped me in every way with their love and support. My mother, father and my dear brothers and sisters for their love, encouragement and support throughout my whole life. ™

- Finally, I would like to thank the following institutions: -
  - ❖ Alberta Innovates Health Solutions CRIO grant for funding of the research project.
  - ❖ The Libyan Ministry of Education and Scientific Research for providing me with the scholarship that supported me and my family throughout my Master study.
  - ❖ Canadian Bureau for International Education for facilitating and managing my tuition fees and my expenses.
  - ❖ Graduate Student Association, University of Alberta for the professional development and travel grant.
  - ❖ Faculty of Graduate Studies and Research, University of Alberta for the Travel Award.

Table of Contents

List of Figures

List of Tables

List of Schemes

List of Abbreviations

ADCC	Antibody dependent cellular cytotoxicity
ADR	Adriamycin
ADR	Adriamycin
ANP	Aminopeptidase N
asODNs	Antisense Oligonucleotides
BCL	α-benzyl carboxylate ε-caprolactone
BSA	Bovine serum Albumin
CD20	Cluster differentiation 20
CDC	Complement dependent cytotoxicity
$CDCl_3$	Deuterated chloroform
CDR	Complementary determining region
CHOP	Cyclophosphamide, doxorubicin, vincristine, and prednisone
CMC	Critical micellar concentration
CRR	Complete remission rate
CXB	Cetuximab
DLS	Dynamic light scattering
DMF	Dimethyl formamide
DOX	Doxorubicin
DP	Degree of polymerization
DSMN	DOX loaded mesoporous silica nanoparticles
DSPE	1,2-Distearoyl-sn-glycero-3-phosphoethanolamine
DTX	Docetaxel
EGFR	Epidermal growth factor receptor

EPR	Enhanced permeability and retention effect
ER	Endoplasmic reticulum
Fab	Fragment antigen binding
FBS	Fetal bovine serum
Fc	Fragment crystallizable
FN	Fibronectin
GR	Glucocorticoids
H_2O_2	Hydrogen peroxide
HA	Hemolytic adhesion
HUVECs	Human umbilical vein endothelial cells
I.V	Intravenous
mAbs	Monoclonal antibodies
MAC	Membrane attack complex
MM	Mixed micelles
MTT	3-(4,5- dimethylthiazol-2-yl)-2,5-diphenyltetrazolium bromide
NADPH	Nicotinamide adenine dinucleotide phosphate
NHL	Non- Hodgkin lymphoma
NHS-PEG-DSPE	1, 2-Distearoyl-sn-glycero-3-phosphoethanolamine-N-[succinimidyl (polyethylene glycol)]
NK	Natural killer cells
NUT	Nutlin -3
PBS	Phosphate buffer saline
PCD	Programmed cell death
PCL	α-propagyl-carboxylate-ε-caprolactone

PE	Phosphatidylethanolamine
PEG-PG	Poly (ethylene glycol)-poly(L-glutamic acid)
PEO	Methoxy poly ethylene oxide
PEO-PBCL	Polyethylene oxide- poly α-benzyl carboxylate ε-caprolactone
PEO-PBCL-PPCL	Polyethylene oxide- poly α-benzyl carboxylate ε-caprolactone- Poly α-propagyl-carboxylate-ε-caprolactone
PEO-PCL	Poly (ethylene oxide)- poly caprolactone
PEO-PCL-PPCL	Polyethylene oxide- poly caprolactone- Poly α-propagyl-carboxylate-ε-caprolactone
PEO-PLA	Poly (ethylene oxide)- block- poly (lactide)
PLGA	Poly (lactide-co- glycolide) nanoparticles
PMs	Polymeric micelles
PT	Cisplatin
PTK	Protein tyrosine kinases
PTX	Paclitaxel
RA	Rheumatoid Arthritis
RDMSN	Rituximab Mesoporous silica nanoparticles loaded with DOX
RES	Reticular endothelial system
ROS	Reactive oxygen species
RTX	Rituximab
SB	Human lymphoblastiod cell lines
SDS	Sodium dodecyl sulfate
SPIO	Super magnetic oxide anion
SPION	PEGylated Iron oxide NPS
TBTA	(Tris[(1-benzyl-1H-1,2,3-triazol-4-yl)methyl]amine)

Chapter one

Introduction

1 Introduction

Lymphoma can be defined as neoplasm of lymphoid origin. It is mainly characterized by abnormal proliferation of B- cells or T-cells. There are more than 25 different histological subtype of Lymphoma. However, B-cell Non-Hodgkin Lymphoma (NHL) accounts for more than 90% of all adult cases most of which are CD20 positive.[1, 2] According to Canadian cancer society statistics 2017, NHL accounts for 4.5% of new male cases and 3.8 of new female cases of cancer. NHL is the 6th leading cause of cancer death.[3]

Lymphoma is usually treated by combined chemotherapy consisting of cyclophosphamide, doxorubicin, vincristine, prednisone (CHOP) or surgery.[4] It can also be treated by Radiotherapy that uses high energy X-rays to kill the tumor cells or stop them from growing. However, the survival of patient with aggressive lymphoma has been reported to be less than 50%, which urges the need of new therapies. [5]

The development in the molecular characterization and the improved knowledge of the pathophysiology and the microenvironment of cancer in general and NHL in particular had led to the identifying of key proteins that are either exclusively expressed or overexpressed by the tumor cells. B-cell antigens especially the cluster differentiation 20 (CD20) antigen has been extensively studied since the early 80s. However, it wasn't until 1988 were it was fully identified. [6, 7] This has led to the development of antibodies against CD20, e.g., rituximab (RTX), that are now part of regular treatment in CD20 positive NHL patients.

In addition to its application as a therapeutic agent in NHL patients, application of rituximab as a ligand for targeted delivery of radiopharmaceuticals as well as chemotherapeutic drugs

has been studied in the literature. Our objective in the current thesis was to develop traceable CD20 targeted nanoparticles for the delivery of conventional therapeutics to NHL cells. In this chapter, an overview on the background knowledge on the role of CD20 and its antibody in NHL treatment will be provided first. Development of antibody targeted nano-delivery systems; in general and rituximab modified nanocarriers as well as actively targeted polymeric micelles will be briefly discussed, as well.

1.1 Cluster of differentiation 20 (CD20)

Cluster of differentiation 20 (CD20) (Molecular weight 35kDa) is a multi-transmembrane non-glycosylated hydrophobic phosphoprotein that crosses the membrane four times and has two extracellular loops. The extracellular loop, provides a large surface for the exposure of epitopes to monoclonal antibodies (mAb)s (Figure 1-1).[6, 8] Cluster differentiation 20 is expressed extensively by normal and malignant pre-B and mature lymphocytes (around 250,000 molecule per cell), but not by pro-B-cells, normal plasma cells, stem cells or other normal tissue.[6, 9]

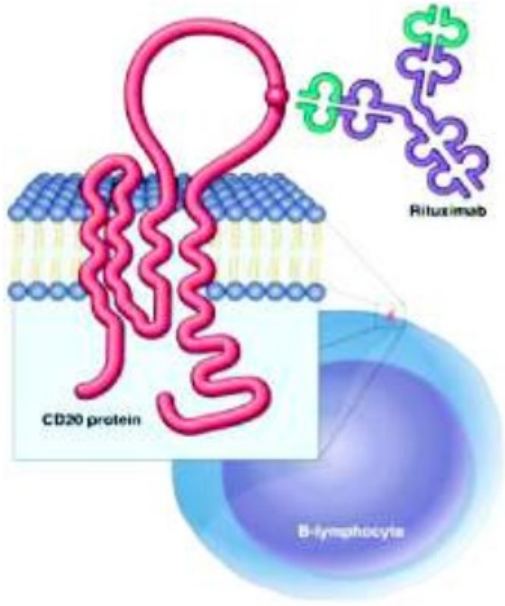

Figure 1-1 CD 20 antigen expressed on the surface of B-cells. CD20 is a nonglycosyted tetramer phosphoprotein. Rituximab is a chimeric anti CD20 monoclonal antibody. This figure was reproduced from reference [10] with permission.

The role of CD20 antigen on the B-cells is not fully understood. However, it is believed to serve as a Ca^{+2} channel that plays an important role in cell differentiation and proliferation.[11]

The binding of CD20 to its antibody does not lead to the shedding of this antigen from the B-cell surface or its internalization into the cells. These properties are believed to be important for initiation of an immune response leading to cell death following antibody-CD20 interaction. Moreover, the resistance of RTX against cell internalization allows for a sustained immune attack as long as the effector cell is available. Antibody antigen binding in case of CD20 can trigger three different responses in the biological system, depending on the density of the antigen on the cells and its proximity to the cell membrane, the type and the density of mAb used and more importantly the ability of the mAb to cluster in the membrane microdomains. There are three different pathways in response to CD20 binding on NHL cells to its antibody: complement dependent cytotoxicity (CDC), antibody dependent cellular cytotoxicity (ADCC) and programmed cell death (PCD). [12]

Complement dependent cytotoxicity (CDC) usually takes place when the CD20 antigen is expressed heavily on the surface of the B-cells and there is high density of the mAb available. Once the mAb binds to the antigen, it reorganize itself into dense clusters at the membrane microdomain then this interaction initiates the classical complement pathways that starts with C1q which crosslinks the fc domain of the adjacent mAbs. Cascade events will then follow leading to the formation of C3 and C5 convertase enzyme complex. These enzymes will then activate C3 and C5 which will eventually lead to the release of chemoattractants (C3a and C5a), opsonization of surface with C3b and osmotic cell lysis because of the assembly of the membrane attack complex (MAC) together with C6, C7, C8 and several C9 molecules (Figure 1-2, step 1).[8, 13, 14]

For the antibody dependent cellular cytotoxicity (ADCC) only moderate numbers of CD20 mAbs is required. This reaction starts with the recognition of the fc domain by the fc receptor on the effector cells (Natural killer cells NK, eosinophils, neutrophils or macrophages). This interaction, initiates a series of signaling pathways leading to the release of a variety of immune modulators including cytokines, chemokines, proteases and reactive oxygen species, which are either inflammatory or cytotoxic or both. The effector cells will then release cytotoxic compounds that will lead to Phagocytosis or programmed cell death in CD20 over expressing cells (Figure 1-2, step 2). [12, 14]

Finally, programmed cell death is a direct process that can cause cell death without involvement of any effector cells or serum proteins. Direct programmed cell death by CD-20 antibody, is not depend on the antigen density or the antibody density. Its activation relies mainly on the target molecule and its associated signal transduction cascade.[12, 15] Programmed cell death can be caspase independent cell death, where the binding of the mAb to the CD20 antigen triggers redistribution of actin cytoskeleton filaments and the hemolytic adhesion (HA). Actin redistribution results in structural changes within the lysosomes that will swell and then disperse their contents, which includes cathepsin B, into the cytoplasm. This will lead to the loss of the plasma membrane integrity and eventually cell death.[16] Programmed cell death can also be reactive oxygen species (ROS) dependent cell death. In this case, ROS can cause irreversible oxidative damage to lipids, proteins, and DNA, which lead to cell death. The excessive production of ROS was explained to be the result from the binding of the mAb to the antigen leading to HA, redistribution of the actin filaments and the release of the lysosomes proteases. Nicotinamide adenine dinucleotide phosphate (NADPH) oxidase will then. Transfer one electron to the molecular oxygen converting it to superoxide, two molecules of superoxide will then bind to form hydrogen peroxide (H_2O_2) this process will continue leading to accumulation of ROS that will eventually lead to cell death.

Furthermore PCD can be triggered by the ligation of the mAb with antigen leading to phosphorylation of the protein tyrosine kinases (PTK) that can erupt the endoplasmic reticulum (ER) and increase the level of intracellular Ca^{++}. These events will then initiate a caspase- apoptosis [17-19] (Figure 1-2, step 3). According to the type of response triggered, mAbs are classified to: class I (like rituximab) where the mechanism of action is mainly CDC mediated; and class II (like obinutuzumab) where the response is through direct induction of PCD. Both classes can still be inducing ADCC response.[14, 20]

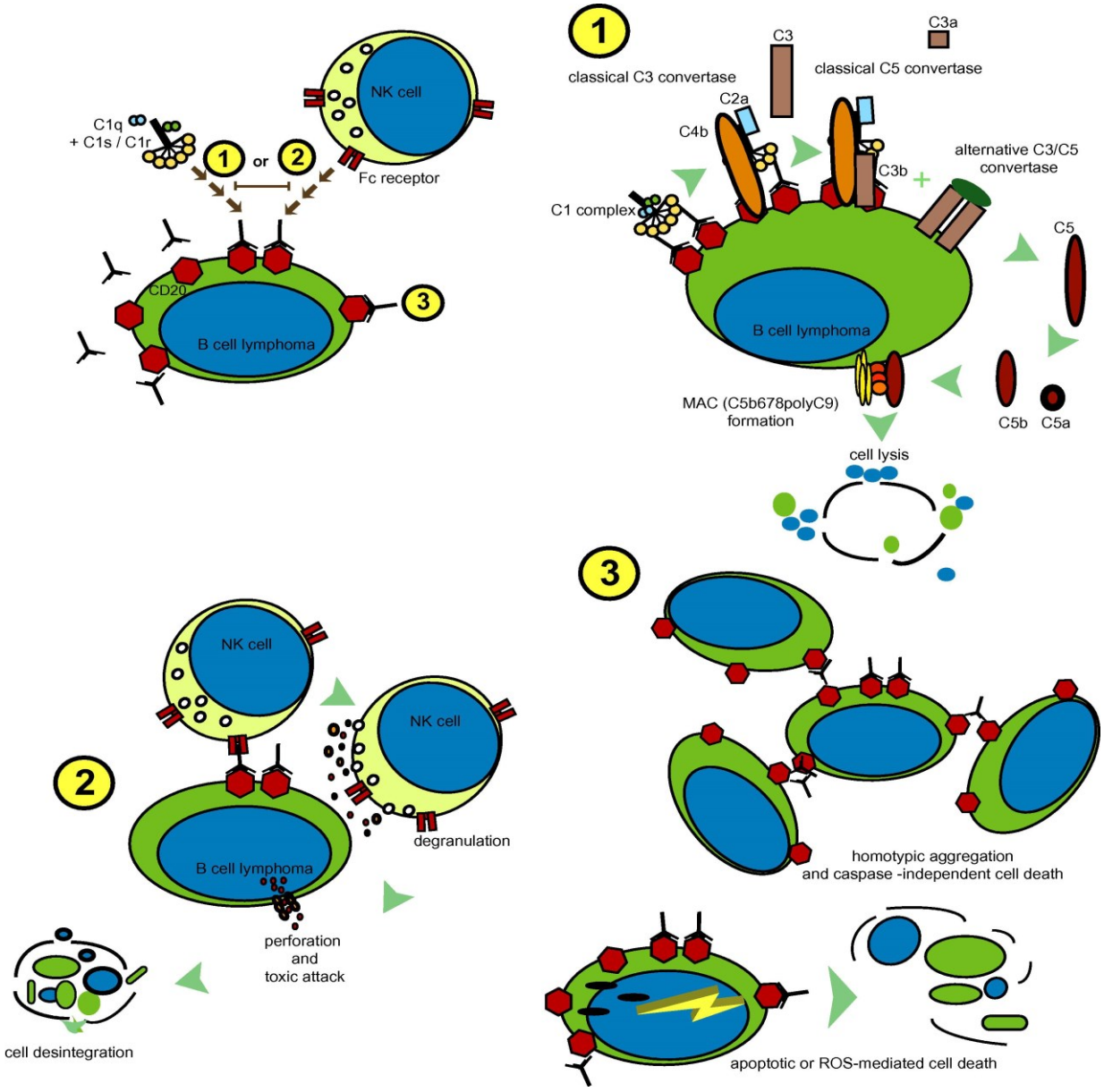

Figure 1-2 Possible outcomes that result from the binding between anti-CD20 mAb and CD20 on the surface of B-cells (1)-CDC, (2)-ADCC and (3)- Apoptosis. This figure was reproduced from this reference [12] with permission.

1.2 Rituximab overview

Kohler and Milstein discovered the hybridoma technology in 1975.[21] It is considered a significant milestone in immunology and biomedicine. Hybridoma technology is composed of several technical steps, that includes antigen preparation, animal immunization, cell fusion (between the splenocytes and the myeloma cells), hybridoma screening, generation and sub-cloning, as well as characterization and production of specific antibodies known as mAbs. This technology allowed the unlimited production of pure and highly specific antibodies against wide variety of antigens.[22-24] Since the identification of CD20 antigen, scientist tried to design a mAb against it. Early studies suggested the use of murine mAb. Despite its effectiveness severe immunotoxicity was observed by its use, however.[22, 25] A murine human (chimeric) mAb was then developed by INGENE and ONCOGEN at 1987 using recombinant DNA technology.[26] At 1994 IDEC developed another chimeric anti CD20 antibody which was named rituximab® and approved by FDA in 1997.[22, 27]

Early studies done by IDEC showed the effectiveness of the chimeric anti-CD20 antibody both *in-vitro* and *in-vivo*. The *in-vitro* results showed 50% lysis of the human lymphoblastiod cell lines (SB) cells (CD20+) when treated with the chimeric anti-CD20 antibody compared to the no significant difference seen with the cells treated with the murine anti- CD20 or with the CD20 (-) T-cell leukemia HSB cells. The *in-vivo* studies were done on monkeys where they were treated with 16.8 mg/kg of the chimeric anti- CD20 antibody weekly for four weeks. The results showed a 40 to 70% depletion of the B-cell from the lymph node for the

monkey receiving the antibody compared to the monkey receiving normal saline, with no observed toxicity.[27]

Phase I clinical trials was conducted on 15 low-grade relapsed B-cell Lymphoma patients, receiving a single intravenous (I.V.) infusion dose of the antibody (0, 50, 100, 250, or 500 mg/m^2). The results showed specific depletion of CD20 B-cells from the circulation within 72 hours and they remain depleted for up to three months. The most common side effect that was observed was low-grade fever. Other side effects occurred such as nausea, orthostatic hypotension, bronchospasm, and thrombocytopenia.[28]

Phase II clinical study was conducted to evaluate the safety, pharmacokinetic and the clinical effect of the chimeric anti-CD20 antibody, RTX. The study was designed as an open label multi- center trial, 37 patients with low grade relapsed B-cell lymphoma were enrolled in this trial each receiving $375mg/m^2$ weekly for 4 weeks. The results showed clinical remission in 17 of the patients (3 complete remissions and 14 partial remissions). The median time to progression was 10.2 months. The toxicity profile was similar to the one seen in the phase I trial.[29]

A multi-center pivotal phase III study was conducted recruiting 166 patients with recurrent low-grade lymphoma, in which they received 37 $5mg/m^2$ weekly doses for 4 weeks. The results showed 48 % remission including 6% with complete remission with 13.2 months median time to progression. The pharmacokinetic data showed the half-life of RTX was significantly increased from the first infusion (76.3 hours) to the forth infusion (205.8 hours).[30] This study led to the FDA approval of RTX as a single agent to treat B-cell NHL that are resistant to chemotherapy.[22]

Rituximab is chimeric anti CD20 monoclonal antibody approved in Canada to treat B-cell NHL, Chronic Lymphocytic Leukemia (CLL) and other non-cancer condition such as Rheumatoid Arthritis (RA) and Granulomatosis.[31] It consists of murine fragment antigen binding (Fab) region and the human kappa and IgG1 constant heavy chain.[27] RTX (Molecular weight 145 kD) is composed of 2 heavy chains of 451 amino acids and 2 light chains of 213 amino acids. [10] RTX binds to the CD20 antigen with comparable affinity and specificity of the murine anti- CD20 antibody (approximately 8 nM).[27]

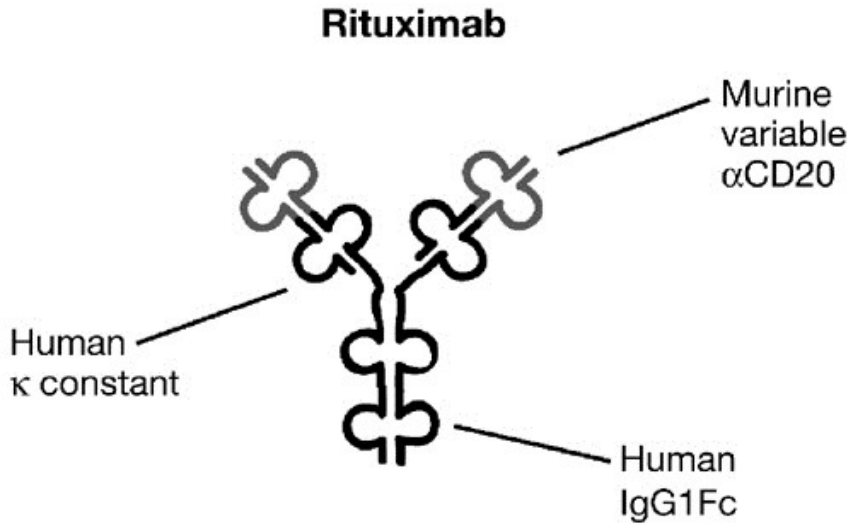

Figure 1-3 Rituximab chimeric anti-CD20 antibody. Fab regions are from the murine anti-human CD20, are fused to human IgG1 heavy-chain (fc) and human kappa light-chain constant regions. This figure is reproduced from this reference [32] with permission.

1.3 Combination of rituximab with other cytotoxic agents

The extensive research done on RTX and its use to treat B-cell lymphoma as single agent has shown it was rarely curative and the effect was not durable.[33] Clinical studies over the years

showed the huge impact of adding RTX to other drugs that are known to be cytotoxic to B-Lymphocytes disease.[34] Glucocorticoids (GR) are known to be cytotoxic to cells through binding to the GR receptor and either suppressing the transcription of genes responsible for cell survival or up-regulating the genes that cause inhibition of cell growth or cause cell death.[35] Rose *et al*. studied the synergistic effect of RTX and dexamethasone on 9 different CD20 positive B-cell NHL cell lines. The results pointed out that 6 of the NHL cell lines treated with rituximab and dexamethasone show synergetic effect on the inhibition of cell growth.[34] Furthermore, an *in-vitro* and an *ex-vivo* study on CD20 positive B-cell lymphoma cells conducted by Chow *et al*. used the combination of RTX with different cytotoxic drugs used to treat lymphoma such as Doxorubicin (DOX), Mitoxantrone, Cladribine and Bendamustine. The results showed significant drop in the dose of chemotherapy that can cause apoptosis. However, the use of RTX alone showed only minor induction of cell death. It was concluded that RTX can increase the sensitization of the lymphoma cells to the cytotoxic agents.[36] In addition to that several studies in the literature tried to combine RTX for instance with Lenalidomib (an immunomodulator). This combination enhanced the ADCC due to the expansion of NK cells and monocytes caused by Lenalidomib.[37]Others combined RTX with Alemtuuzumab an anti – CD52 mAb and showed an increase in the cytotoxic effect mainly by inducing apoptosis.[38]

In 2006, the FDA approved the use of RTX in combination of cyclophosphamide, doxorubicin, vincristine, prednisone (CHOP) to treat low grade B-cell NHL based on a randomized study (399 patients) conducted by 86 centers in France, Belgium and Switzerland. The trial showed a significantly higher rate of complete remission (CRR) in the patient receiving rituximab along with CHOP (76% vs. 63% receiving CHOP only; P=0.005). The median follow up survival rate for 2 years was also significantly improved (57% vs. 38%; P=0.001).[39] Another study conducted over the period of seven years emphasized the

huge advantage of addition of rituximab to the course of chemotherapy. It showed a significant improvement of the event free survival (42% for rituximab with CHOP vs. 25% for CHOP alone; P<0.0001).[40]

1.4 Rituximab as part of antibody drug conjugates and radio immunoconjugates

Despite the significant advantage seen with the addition of RTX to the conventional chemotherapy regiments, there is still a long road to achieve absolute remission from NHL. In addition to that severe side effects are still observed as a result of this combination. In search for targeted drugs for NHL, those that are more effective yet less toxic to patients, antibody drug conjugates (ADCs) and radio-immunoconjugate have also been studied extensively.[41, 42] Application of CD20 targeted radio-immunoconjugates, have achieved significant improvement in the therapeutic activity. For Instance, a clinical study of ibritumomab tiuxetan, a yttrium-90-conjugated monoclonal antibody to CD20, showed an overall response rate of 80% with (90)Y-ibritumomab tiuxetan vs. 56% for rituximab (p = 0.002).[43] Despite this, harsh and long required conjugation conditions associated with the use of radio-immunoconjugates has limited the application of these targeted drugs.[42]

ADCs are extensively studied to treat NHL. However, only internalized antigens such as CD19 and CD22 were targeted for this purpose.[44]Jiang *et al.* designed a genetically engineered antibody anti-CD19 (Fab)-Lidamycin(LDM) that exhibited enhanced cytotoxicity compared to LDM alone.[45] The use of ADCs has other down sides that include the low drug/antibody molar ratio, the need for the presence of a linker for the formation of ADCs, as well as low conjugation efficiency.[44, 46]

An alternative approach is the use of nano-delivery systems modified on their surface with rituximab that can carry several moles of drug or radiochemical inside. [47] This approach has several advantages over the use of ADCs and radio-immunoconjugates; it can overcome the limitation of low antibody to drug ratio, take advantage of the physical barrier provided by the Nano-carrier against drug distribution and toxicity in normal organs, and also be used for the delivery of drug combinations to cancerous cells in NHL. Furthermore, for the development of anti-body modified nanocarriers, the drug does not need to bear functional groups in its structure. Besides, there is no need for drug cleavage from the mAb inside the cells, thus, eliminating the need for the use of internalizing mAbs, as non-internalizing mAbs can still provide the advantage of targeted delivery of the encapsulated drug in the vicinity of the diseased cells.

1.5 The use of rituximab as a targeting moiety on the surface of nano-carriers

Rituximab conjugated immunoliposomes or immunomicelles can prolong drug circulation in blood, sustain drug release to cancerous cells and actively target lymphoma cells in circulation and/or those residing in lymphoid organs, at the same time. Moreover, immunoliposomes or immunomicelles can reduce the interaction of chemo or radionuclide with other immune cells such as T-cell, and ensure minimal effect on the immune system by therapy.[48]

This approach has been exploited in several previous studies through conjugation of rituximab to the surface of liposomes and nanoparticles (Table1-1). A study conducted by *Cong Wu et al.* on NHL xeno-transplant model showed that the anti-CD20 fab fragment modified liposomes containing Adriamycin (ADR) were significantly more effective in

reducing the tumor burden than plain liposomes loaded with ADR and the free ADR.[49]In addition to immunoliposomes, immunonanoparticles were also extensively studied. *Shoubing Zhou et al.* designed mesoporous silica nanoparticles decorated with rituximab and loaded with DOX (RDMSN). Both *in-vitro* and *in-vivo* studies were conducted. The *in-vitro* study was carried on Raji, Daudi cell lines (CD20 +) and Jurkat cell lines (CD20-). They treated the cells with free DOX, DOX loaded mesoporous silica nanoparticles (DSMN) and RDMSN. Their results pointed to a significant higher cytotoxic effect by RDMSN compared to plain DMSN and free DOX on Raji and Daudi cell lines while no significant difference was noticed on Jurkat cell lines. The *in-vivo* study was conducted on Raji cells grafted mice the result showed that the mice treated with RDMSN to show significantly reduced rate of growth in tumor volume compered to mice treated with DMSN and free DOX. [50]

Table 1-1 Examples of rituximab targeted nano-carrier systems

Nano carrier	Active molecule	*In-vitro* results	*In-vivo* results	Ref.
Mesoporous NPs	Doxorubicin	The RTX modified NPs showed higher anti-tumor activity compared to the plain NPs and free DOX.	The RDMSN significantly reduced the tumor volume compared to DMSN and free DOX.	[50]
Liposomes	Doxorubicin	Increase in the cellular uptake 4 times compared with the Bovine serum Albumin (BSA) decorated liposomes. Decrease in the IC50 to one fourth compared to the free Adriamycin. On Daudi and Raji cell lines (CD20+ Lymphoma cell lines)	Remarkable decrease in tumor burden compared to the BSA liposomes loaded with ADR and frees ADR. Significantly prolonged the survival of tumor-bearing mice compared to BSA liposomes loaded with ADR and free ADR. With a complete remission percentage of 4/10 while the plain liposomes were 1/10	[49]
Liposomes	-	The in-vitro study was done on Z138C (mantle cell lymphoma cell line) showed 5-fold	-	[51]

		increase in the association of the RTX liposomes compared to free liposomes. The in-vitro cytotoxicity showed that the IC50 of the RTX liposomes (150μg/mL) was significantly reduced compared to free RTX (up to 1mg-mL did not affect the viability)		
Liposomes	Antisense Oligonucleotide (Oligonucleotide complementary to mRNA) (asODNs)	Selectively and effectively reduce the expression of BCL2 (Anti-apoptotic gene) in Daudi cells (CD20+) versus its effect on Jurkat T (CD20-) cells. The selectivity was shown when the RTX targeted liposomes selectively interacted with the CD20+ cells (Daudi) when they were mixed with CD20- (Jukart T) cells.	The study was done on Burkitt's lymphoma CD20+ tumor-bearing NOD/SCID mice. The results showed high efficiency of the RTX targeted liposome carrying the anti-BCL2 asODN against tumor development (0 mm^3tumor volume up to 70 days) compared to the control (RTX targeted liposomes carrying the scrambled asODN) where the tumor volume reached 400-1200 mm^3 at 61 -70 days	[52]
Poly(lactide-co-glycolide) nanoparticles PLGA NP	Nutlin -3 (Nut)	No significant difference between the RTX targeted NP loaded with Nut and the NP loaded with Nut in cytotoxicity against JVM-2 was detected.	Targeted NP loaded with Nut significantly reduced the tumor volume by 1.5 fold (after 9 days of treatment) compared to the plain NP. Also the targeted NP enhanced the overall survival (35 days) compared to the plain NP (27.5 days) in JVM-2 xenograft SCID mice model	[53]
Lipid NPs	-	CDC and ADCC both enhanced compered to free RTX in two different lymphoma cell lines (Z138 and JVM2)	No significant difference was noticed in term of cytotoxicity.	[54]
PEGylated Iron oxide NPS (SPION)	Rhenium 188 ^{188}Re	The relative numbers of B cells were significantly decreased by the ^{188}Re-RTX-SPION compared to bare-SPIONs (91.6 ± 2.7%)and RTX-SPIONs (70.8±3.2%) on the CD20 overexpressing B-cells	-	[55]

To the best of our knowledge, surface modification of polymeric micelles (PMs) with rituximab has not been reported, to date. However, modification of PMs with other targeting moiety such peptides, mAbs or its fragments, hormones, mono and polysaccharides, lipoproteins or other low molecular weight ligands have been tried and reported (Table 1-2). [56]

Table 1-2 Example of ligand modified polymeric micelles in literature for cancer targeting.

Cellular target for the ligand	Ligand	Micellar system	Active molecule	Indication	Ref.
GLUTs1-14	Glucose	Polyvinyl caprolactam–polyvinylacetate–polyethylene glycol copolymer and D-α-tocopheryl polyethylene glycol 1000 succinate (TPGS)	Paclitaxel	Breast cancer	[57]
Neu1 sialidase	oseltamivir	Poly (polyethylene glycol methyl ether methacrylate)-block-poly (methyl methacrylate)	Coumarin	Pancreatic carcinoma	[58]
memHsp 70	TKD	Poly (d,l-lactide-*co*-glycolide)-*b*-poly(ethylene glycol) (PEG-b-PLGA)	Doxorubicin	Breast cancer	[59]
CD22	CD22 streptavidin-conjugated monoclonal	Propylacrylic acid (PAA), butyl methacrylate (BMA), and poly 2, (Dimethylamino) ethyl methacrylate (DMAEMA) **1.6**	SiRNA	NHL	[60]
2C5 antigen	2C5 monoclonal	Poly(ethylene glycol) – phosphatidylethanolamine	Taxol	Lewis Lung carcinoma	[61]

	antibody	(PEO-PE)			
Tissue factor (TF)	Anti-TF Fab fragment	Poly(ethylene glycol)-*b*-poly(glutamic acid) (PEG-*b*-P (Glu))	1,2-diaminocyclohexane platinum (II) (DACHPt)	Pancreatic cancer	[62]
Epidermal growth factor receptor (EGFR)	Anti EGFR antibody	Poly(ethylene oxide)–block-poly(ε-caprolactone) (PEO-b-PCL)	DOX	Colorectal cancer	[63]
Keratin-1	P18 Peptide	PEO-b-PCL	-	Breast cancer	[64]
$\alpha_V\beta_3$ Integrin	GRGDS peptide (Gly-Arg-Gly-Asp-Ser)	Poly (ethylene oxide)-block-poly (α-benzyl-carboxylate-ε- caprolactone) (PEO-b-PBCL)	DOX	Breast cancer	[65]
HER2	Trastuzumab Fab	PEO-PCL	Electron emitter indium-111 (^{111}In)	Breast cancer	[66]

1.7 Polymeric micelles overview

Polymeric micelles (PMs) represent one class of Nano-delivery systems that have been extensively explored for application in cancer therapy because of their unique and favorable properties.[67] PMs were first introduced as drug delivery systems by Ringsdorf in the 1980s. PMs consist of amphiphilic block copolymer that can self-assemble in aqueous environment and form core/shell structure, where the core is hydrophobic and can solubilize lipophilic drugs; and the shell is hydrophilic and biocompatible providing stealth properties protecting the carrier from aggregation and early uptake by the reticular endothelial system (RES). Polyethylene glycol is mostly used for the latter purpose.[68, 69] PMs have the ability to solubilize hydrophobic drugs and also control their release. [70]

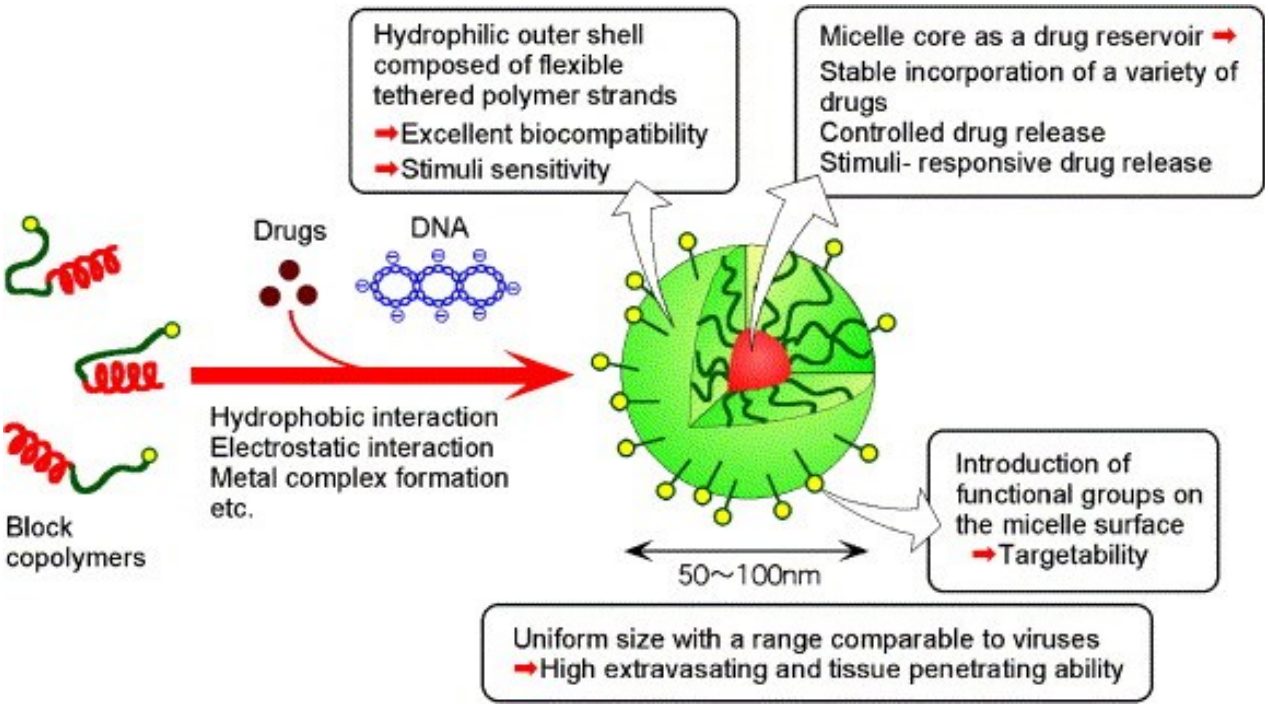

Figure 1-4 Polymeric micelles structure. Reproduced from reference [69] with permission

Polymeric micelles are characterized by their critical micellar concentration (CMC), which is defined as lowest concentration of the polymer required to self-assemble and form micelles. The major driving force for micelle formation is the hydrophobic effect, where the hydrophilic chains form a shield over the hydrophobic chains preventing its interaction with water and reducing the interfacial energy between the water and the polymer.[71] [72] Block copolymers have relatively low CMC compared to surfactants, which allow them to remain intact in a micellar form upon dilution in the bloodstream. In addition to that, PMs are known to dissociate slowly in the surrounding media upon dilution below CMC levels.[69]

Because of their nanometer size range (10-100 nm), PMs have the ability to accumulate in the solid tumors passively via the enhanced permeability and retention effect (EPR). The EPR phenomenon usually occurs in solid tumors because of the increased expression of angiogenesis driving proteins. In addition, owing to rapid tumor growth and production of waste, the lymphatic vessels are collapsed and faulty in effective drainage, leading to enhanced retention of nanocarriers accumulated in tumor. [73] For the PMs to accumulate into the tumor site effectively, they have to be designed to be long circulating in blood. In order to achieve that, the PMs must be smaller than 200nm and have a hydrophilic biocompatible shell (stealth) to avoid early elimination by RES. On the other hand, PMs must be larger than 42-50 kDa to avoid the glomerular filtration by the kidney.[69, 74, 75] Furthermore, the surface of the PMs can be easily modified with specific ligands that have high affinity to a surface receptor expressed on the cancer cells without affecting the stability of the micellar system. These surface modified micellar systems will then have the ability to actively target the tumor cells.[67]Other advantages of the PMs include: simple formulation, good loading efficiency of hydrophobic drugs and also their ability to control drug release; thereby alter its pharmacokinetics and bio distribution, *in vivo*.[76, 77]

1.8 Example polymeric micelles used in cancer therapy

1. Poly (ethylene oxide*)-block*-poly (lactide) (PEO-*b*-PLA)

Poly(lactide) (PLA) is an FDA approved synthetic hydrophobic biodegradable polymer. PEO-PLA can self-assemble and form micelles with a size that ranges between 10-100nm depending on the molecular weights of the polymer forming units.[78] Genaxol PM® is a recent clinically approved micellar formulation of Paclitaxel in PEO-PLA.[67] PEO-PLA is also in the preclinical formula of Paclitaxel along with Vitamin E TPGS.[79]

PEO-PLA has been conjugated to different ligands for the purpose of active targeting. In one study CLT-1 peptide was conjugated to PEO-PLA loaded Paclitaxel. CLT-1 peptide has high affinity to fibronectin FN (overexpressed in the tumor microenvironment). The results of this study showed the targeted PMs penetrated glioma cells more efficiently compared to plain PMs, and also prolonged the median survival time of glioma bearing mice.[80] In another study Folic acid was conjugated to DOX loaded PEO-PLA. The *in-vitro* results on multi-drug resistant breast cancer showed increase in the cellular uptake and cytotoxicity compared to the plain micelles and free DOX for targeted PM formulations of DOX. While the *in-vivo* study done on Nude mice bearing MCF-7Adr tumor showed large reduction in the mortality rate, 60% of the mice receiving free DOX died versus 0% death in mice receiving the same concentration of DOX loaded in PEO-PLA. Moreover, the mice receiving the targeted PEO-PLA did not significantly loose body weight compared to the control (receiving 5%glucoce). While mice treated with free DOX lost 15 % of their body weight.[81]

2. Poly(ethylene oxide)-–*block*-poly (Lactic acid-*co*-glycolic acid) PEO-*b*-PLGA

PLGA is a hydrophobic biocompatible biodegradable polymer that is approved by the FDA as a drug delivery system. PEO-PLGA was also modified with different ligands to achieve active drug targeting. A study conducted by Wang *et.al.* Conjugated APRPG (Ala-Pro-Arg-Pro-Gly) that specifically targets αvβ3 integrin (over-expressed during angiogenesis) to Maleimide–PEO–PLGA co-polymer. The peptide-decorated micelles were then loaded with an angiogenesis inhibitor TNP-470. The *in-vitro* study done on HUVECs cell line (Human umbilical vein endothelial cells) showed significant increase in the cytotoxic effect of TNP-470 loaded peptide decorated micelles compared to the TNP-470 loaded plain micelles and free TNP-40. An *in-vivo* study was done on a SKOV3 human ovarian cancer bearing mice,

showed much higher reduction of the tumor growth on mice treated with TNP-470 loaded targeted micelles compered to free TNP-470 or TNP-470 loaded plain micelles.[82]

3. Poly(ethylene oxide)-*block*-poly(caprolactone) (PEO-*b*-PCL)

PCL is a polyester, biodegradable synthetic polymer with low toxicity. It is commonly used for drug delivery because it can be simply synthesized and modified.[83] PEO-PCL has been successfully tested for solubilization of several cytotoxic drugs such as Paclitaxel, DOX and Cisplatin.[84-86] Active targeting of PEO-PCL has also been studied. Nguyen-Van Cuong *et.al.* synthesized a star-shape Folate–PEO–PCL encapsulated with DOX for targeted delivery in breast cancer. Folate receptors are over-expressed in tumors of breast and ovarian cancer. The result showed that the uptake of DOX-loaded folate PEO–PCL micelle was higher than that of free DOX in MCF-7/adr cells (adriamycin-resistant breast cancer cell line). [85]

Another research group designed Cetuximab (CXB) anti EGFR (Epidermal growth factor receptor) mAb conjugated to PEO-PCL that was loaded with DOX and super magnetic oxide anion (SPIO). The in-vitro uptake of CXB conjugated micelles by A431 (EGFR+) was significantly enhanced by 1.45 times compared to the plain micelles. In contrast there was no significant different in the uptake between the decorated and the plain micelles on MDA-MB-435 (EGFR-). This was translated into enhancement in the cytotoxic effect of the decorated micelles compared to the plain micelles. In addition to that the MRI signaling intensity was decreased to 40% on A4311cells treated with the decorated micelles compared to the plains due to the enhance of uptake. In the other hand this reduction was not seen on the MDA-MB-435.[87]

4. Polyethylene glycol- -phospholipids

PEG-lipid copolymer differ from the other PEG block copolymer, is that the hydrophobic part is made from lipid. The most used lipid for the purpose of drug delivery is phosphatidylethanolamine (PE) and 1,2-Distearoyl-sn-glycero-3-phosphoethanolamine (DSPE).[88]

The PEG-phospholipids are also commonly used for the purpose of active targeting. For instance Torchilin group commonly uses the PEG-PE for this purpose. In one study they formulated an anti- nucleosome 2C5 antibody conjugated to DOX loaded PEG-PE. This delivery system was then tested on NCI-ADR-RES ovarian cancer spheroid cell line. The results showed significant enhancement of the cytotoxicity for the 2C5 harboring DOX PEG-PE compared to the free DOX, plain DOX micelles and the control isotope-matched DOX-micelles.[89]

Furthermore, Paclitaxel loaded PEG-DSPE in one study was decorated with NGR peptide (Asn, Gly, Arg) (NGR-M-PTX). NGR is a ligand known to bind with high affinity to Aminopeptidase N (ANP); a membrane- bound metalloproteinase expressed in the pericytes associated with blood brain barrier this enzyme plays an important role in cancer invasion and angiogenesis. An *in-vitro* study was carried on C6 glioma cell line (Rat neural cells) showing significant decrease in the IC_{50} of NGR-M-PTX (189.4±14.1ng\mL) compared to free PTX (359.6±33.7ng/mL) and M-PTX (241.3±13.9ng/mL). In addition to that the *in-vivo* study done on C6 glioma bearing rats showed significant reduction in the tumor weight compared to the control (receiving saline) by NGR-M-PTX (70.90±10.37 %) versus Taxol® (10.97±30.74%) and M-PTX 49.07±22.3). [90]

5. Poly(ethylene glycol)-*block*-poly(amino acid)s

In this category the hydrophobic compartment is composed of polymerized amino acids. The most commonly used amino acids are lysine, aspartic acid, glutamic acid and histadine. Poly (amino acid)s have some favorable criteria that include its biocompatibility and biodegradability into naturally occurring amino acids. In addition to that the poly (amino acid) can be easily modified due to presence of a wide variety of functional groups such as the amino, hydroxyl, thiol and carboxyl group.[67, 91]

Poly(amino acid)s have also been studied to harbor active ligands. A research group designed an anti C225 antibody (against epidermal growth factor receptor EGFR) conjugated to DOX loaded poly(ethylene glycol)-poly(L-glutamic acid) (C225-PEG-PG-DOX). There results showed that the C225-PEG-PG-DOX (5mins to internalize) selectively binds to the human vulvar squamous carcinoma cell lines A431; that over express EGFR, while the plain PEG-PG-DOX (24hrs to internalize) did not. In addition to that the C225-PEG-PG-DOX was more potent in inhibiting the tumor growth comparing to the plain DOX micelles.[92]

A group designed an $\alpha_V\beta_3$ Integrin targeting c(RGDfK) peptide decorated on α-tocopherol and polyethylene glycol grafted to poly(L-glutamic acid) PLG-g-Ve/PEG loaded with docetaxol(DTX) and Cisplatin (PT). The targeted DTX-PT-loaded micelles showed synergistic cytotoxicity and enhanced internalization rate in mouse melanoma (B16F1) cells compared to plain micelles with DTX and PT (M-DTX-PT), plain micelles with DTX (M-DTX) and plain micelles with PT (M-PT). *In vivo* studies in B16.F1 melanoma established on C57BL/6 mice demonstrated remarkable long circulation, anti-tumor and anti-metastasis efficacy of c(RGDfK) decorated M-DTX-PT compared to M-DTX-PT, M-DTX and M-PT.[93]

1.9 Paclitaxel overview

Paclitaxel (PTX) is hydrophobic drug with a relatively large molecular weight (853.9 g/mol). It is widely used to treat breast, lung and ovarian cancer [94] . In addition to that it has been studied to treat recurrent Non-Hodgkin Lymphoma.[95]Paclitaxel cause cytotoxicity by binding to and enhancing the assembly of tubules to form microtubules, which will lead to chromosomal missegregation. These effect will inhibit the mitosis and proliferation and eventually lead to cell death.[96]

Paclitaxel has very low water solubility (0.006mg/mL) and in order to be injected intravenously it should be solubilized in a vehicle. Taxol is the clinically approved formulation of PTX in Cremophor® EL (Polyoxyethylated castor oil) and dehydrated alcohol.[97]

Another approach to solubilize PTX was to encapsulate it in nanocarriers and more specifically polymeric micelles because of its hydrophobic core that can accommodate such hydrophobic drugs. Genexol PM is a clinically approved formulation of PTX loaded in PEG-PLA polymeric micelles.[98, 99] Beside that there are some PTX loaded PMs that entered the clinical trials. NK105 is PTX formulation of PEG-*b*-poly(α,β-aspartic acid) that entered a multi-center phase III clinical trials in Japan.[100, 101] In addition to PMs, PTX was also loaded to albumin nanoparticles, the formulation known now as Abraxane® is clinically approved to treat lung, breast and pancreatic cancer.[102]

1.10 Rationale:

Non-Hodgkin Lymphoma is the sixth cause of death in Canada. The treatment of CD20 positive NHL is majorly relied on the use of rituximab in combination with a chemotherapy cocktail known as CHOP. This combination has shown to improve the event free survival

from 25% to 42% in NHL cases. Although this is a very significant improvement, still more than 50% of the cases remain uncured. This in addition to the emergence of severe side effects in patient going through the combination therapy has urged the need of new treatment strategies with better anti-cancer effects and less toxicity. Targeted drug delivery to NHL tumors may potentially lead to better therapeutic index for anti-NHL drugs or drug combinations.

Direct conjugation of radiopharmaceuticals and small anti-cancer drugs to mAbs against CD20 for use in NHL therapy has been tried with some success. An alternative approach uses conjugation of mAbs or other targeting ligands to nano-delivery systems for the purpose of drug targeting. The advantage of this approach over direct drug conjugation to targeting antibody is the enhanced drug to targeting ligand ratio, no requirement for the presence of functional groups on the drug of choice, and potential for combination drug delivery.

Different ligands interacting with receptors overexpressed on cancer cells have been extensively studied for the purpose of targeted drug delivery to tumor cells. This includes peptides, mAbs or mAb fragments, hormones, mono and polysaccharides, folic acid, transferrin, etc. Among these, mAbs stand out because of their high specificity and affinity for their target receptors. However, the use of mAb is controversial especially in targeting solid tumors because of their large size particularly in cases where they are used as ligands for nano-carriers. The increase in size caused by using mAb as the active targeting ligand can impede the movement of the nanocarrier within the tumor mass. In contrast, the use of mAb as an active ligand is still beneficial in hematological cancers such lymphoma and leukemia. Another potential shortcoming of mAbs as active targeting ligands on the surface of nanocarries is the possibility of their neutralization in the circulation or opsonization and

uptake by the RES before reaching the tumor target. In cases where target antigen does not shed from the cell surface, such as CD20, mAb neutralization that will not be an impeding issue. Opsonization and uptake by the RES can be managed by application of stealth nanocarriers and by adjusting the density of mAb on the surface of the carrier, so that its stealth properties are not compromised.

Among the different nanocarriers used for tumor targeting, polymeric micelles stand out because of their advantageous properties which include small size appropriate for tumor extravasation and penetration, as well as capacity for the solubilization and detainment of hydrophobic drugs in systemic circulation, that is required for their drug targeting by nanocarriers.[103] Despite these advantages, development of mAb modified polymeric micelles for the purpose of active drug targeting, has been limited to PEO-phospholipid micelles that are not very stable under sink condition, thus not suitable for active drug targeting. Reports on the development of mAb modified micelles for other type of block copolymers are scarce in the literature.

The objective of this study was to develop more stable mAb modified micellar structure for the purpose of active drug targeting in NHL. We also aimed to make these micelles traceable, so that their fate following cell treatment or systemic i*n vivo* administration can be easily followed. The information generated from the following traceable nanocarriers in cells or animals can be used to map the relationships between nanocarrier structure and their biological behavior. Moreover, a traceable nano-drug delivery system that can light up the tumor upon accumulation, can guide the optimum timing and/or localization of the simultaneous chemo or radiation treatment.

1.9. Objective

To develop traceable polymeric micelles for active drug targeting to CD20 positive NHL cells.

1.10. Hypothesis

Stabilized mixed micelles based on rituximab-PEG-DSPE and PEO-PCL-prepared through application of PEO-PCLs of enhanced hydrophobicity, can be used to increase the specific interaction and PTX delivery of polymeric micelles for CD20+ NHL cells

1.11 1. 11. Specific Aims

1. To prepare traceable rituximab modified mixed micelles through incubation of Cy5 labeled rituximab-PEO-DSPE with Cy 3 labeled PEO-poly(ester)s (i.e., PEO-PCL or PEO-PBCL) of different molecular weights.
2. To assess the effect of poly(ester) block on the thermodynamic and kinetic stability of mixed micelles.
3. To investigate the effect of poly(ester) block on the specific interaction of mixed micelles with CD20 + KG-15 cells over CD20 - SUP M2 cells.
4. To investigate the effect of poly(ester) block on the *in vitro* release and specific cytotoxicity of encapsulated PTX in mixed micelles against CD20 + KG-15 cells over CD20 - SUP M2 cells.

Chapter two

Methods

2 Materials and Methods

2.1 Materials:

Methoxy poly (ethylene oxide) (PEO) (MWt 5000 Da), sodium dodecyl sulfate and L-Ascorbic acid (99%) were purchased from Sigma (St Louis, MO). ε-Caprolactone was purchased from Lancaster synthesis (UK). α-Benzylcarboxylate-ε-caprolactone (BCL) and α-propagyl-carboxylate-ε-caprolactone were synthesized by Alberta Research Chemicals Inc. (ARCI, Edmonton, AB, Canada) based on methods published previously by our group.[104] 1, 2-Distearoyl-sn-glycero-3-phosphoethanolamine-N-[succinimidyl (polyethylene glycol)] (DSPE-PEG3400-NHS) and methoxy poly(ethylene oxide) (Mwt 2000 Da), covalently linked to distearoyphosphadidyl ethanolamine (mPEO2000-DSPE) were purchased from Nanocs Inc. (USA). Paclitaxel (PTX) (purity> 99.5) was purchased from LC Laboratories (Woburn, MA, USA). Rituximab (anti CD20 antibody) and Taxol were a generous gift from Cross Cancer Institute. Stannous octoate was purchased from MP Biomedicals Inc. (Germany). Spectra/por dialysis tubing (MWCO, 3.5kDa) was purchased from Spectrum Laboratories (Rancho Dominguez, CA). Cy3 azide, Cy5.5 NHS dye and Cu (II) (Tris[(1-benzyl-1H-1,2,3-triazol-4-yl)methyl]amine)(TBTA) complex were purchased from Lumiprobe (Hallandale Beach, Florida). All other chemicals and reagents used were of analytical grade.

2.2 Cell culture:

Cell culture media RPMI 1640, fetal bovine serum (FBS) and penicillin –streptomycin-L-glutamine were purchased from GIBCO, Life Technologies INC. (Burlington, ON, Canada). KG-15 cell line (CD20 +) and SUP-M2 cell line (CD20 -) were received from the laboratory of Dr. Raymond Lai, Department of Pathology and Medicine, University of Alberta.

2.3 Synthesis of PEO-PCL and PEO-PBCL di-block copolymers

Methoxy poly (ethylene oxide)-*block*-poly (ε-caprolactone) (PEO-PCL) with different degrees of polymerization in the PCL block were synthesized by ring opening polymerization of ε-caprolactone using PEO (5000 Da) as the initiator and stannous octoate as catalyst (Scheme 2-1).[105] Briefly, melted PEO (0.5 g), and dried ε-caprolactone (0.285 mg or 0.170 mg) were mixed in a vial with stannous octoate (2 drops). The vials were then sealed under vacuum. The reaction was preceded by placing the vial in the oven at 140 °C for 6 hours and vortexing every 30 minutes for the first 2 hours. Cooling the vials at room temperature terminated the reaction. For the PEO-PBCL block copolymer methoxy PEO (5000 Da) 0.5 g, α-benzyl carboxylate ε-caprolactone (BCL) 0.545 g and stannous octoate were used as initiator, monomer and catalyst, respectively, under the identical reaction condition as described above (Scheme 2-2). The product of this reaction was purified by dissolving it in dichloromethane and then precipitating it in n-hexane. The product was then washed with n-hexane twice and dried in vacuum oven overnight at room temperature. The samples were dissolved in deuterated chloroform ($CDCl_3$) and then subjected to ^1H NMR spectroscopy 600 MHz (Bruker 300 AM; Billerica MA) for characterization. The degree of polymerization in the PCL and PBCL blocks was determined from the ^1H NMR based on the peak intensity ratio of the protons from the ethylene moiety of the PEO (δ=3.65 ppm) to peak intensity of the proton from the methylene of the caprolactone (δ=4.06ppm) considering a molecular weight of 5000 Da for the PEO block. The degree of polymerization (DP) for each block is represented as a subscript in the abbreviated name of polymers from here on.

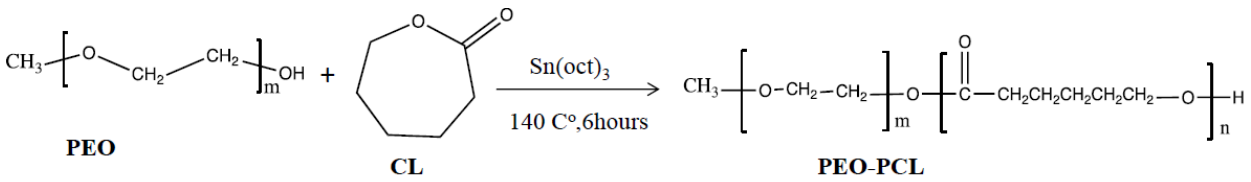

Scheme 2-1Synthesis route for PEO-PCL di-block copolymer.

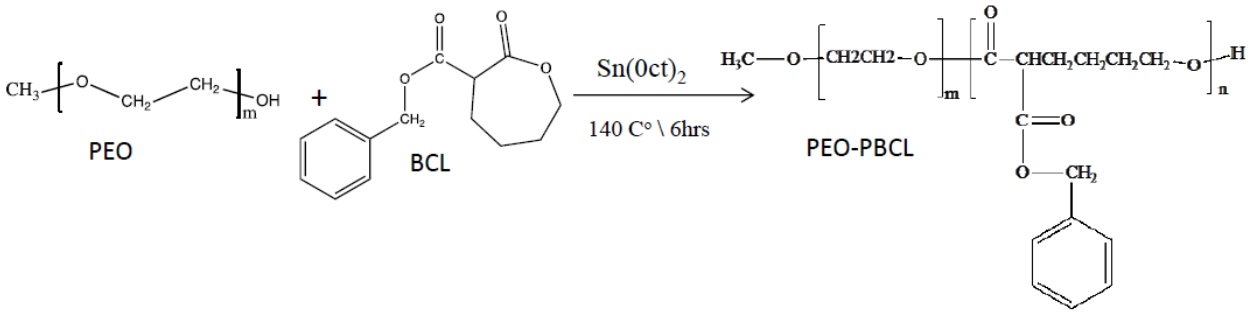

Scheme 2-2 Synthesis route for PEO-PBCL di-block copolymer.

2.4 Preparation of α-propagyl-ε-caprolactone end capped PEO-PCL and PEO-PBCL block copolymers

The α-propagyl-carboxylate-ε-caprolactone(PCL) was polymerized at the end of PEO_{114}-PCL_{22}, PEO_{114}-PCL_{15} or PEO_{114}-$PBCL_{22}$ through reflux in dry toluene (10 mL) for 24 hours using stannous octoate as catalyst (10 drops) (scheme 2-3 and 2-4).[106] The prepared PEO_{114}-PCL_{22}-$PPCL_4$, PEO_{114}-PCL_{15}-$PPCL_4$ and PEO_{114}-$PBCL_{22}$-$PPCL_4$ were purified by precipitating the solution in n-hexane. The precipitate was collected and dried in vacuum oven overnight. The samples were dissolved in $CDCl_3$ and then subjected to ^1H NMR spectroscopy 600 MHz (Bruker 300 AM; Billerica MA) for characterization. The degree of

polymerization of PPCL was calculated based on the peak intensity ratio of the protons from the ethylene moiety of the PEO (δ=3.65 ppm) to peak intensity of the proton from the methylene of the propargyl (δ=2.50 ppm), considering a molecular weight of 5000 Da for the PEO block.

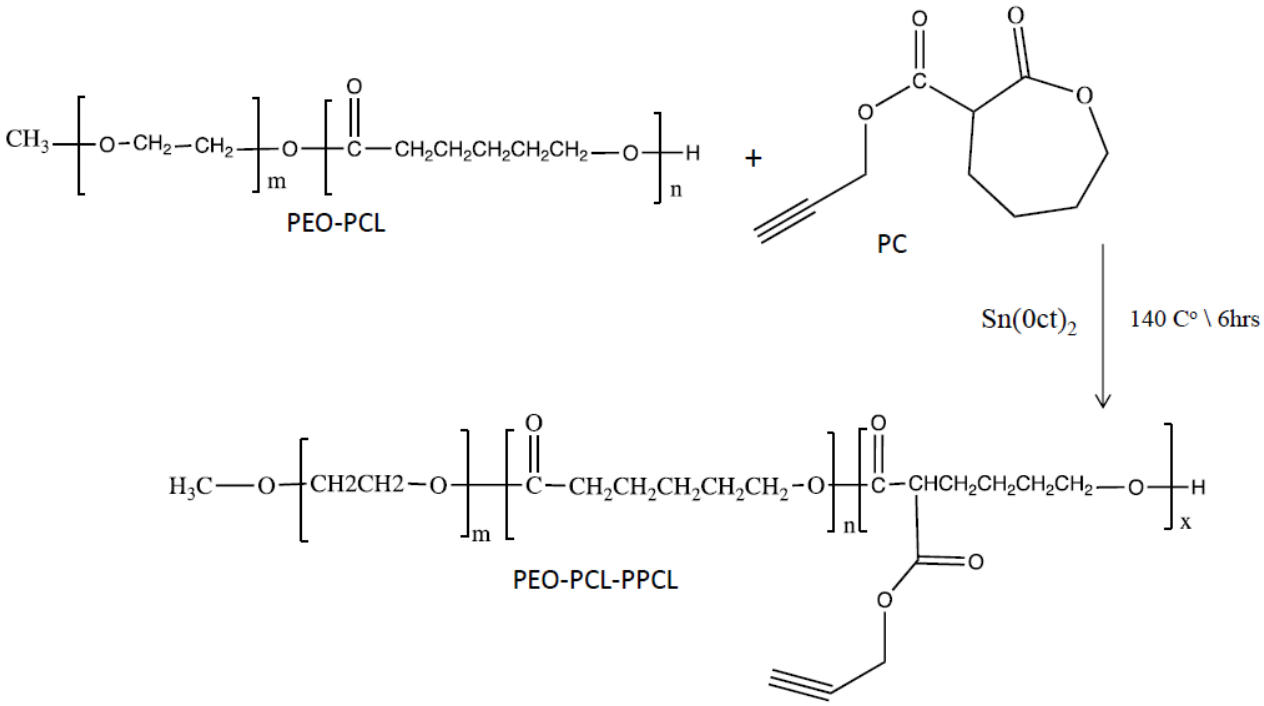

Scheme 2-3 Conjugation of the propargyl caprlactone to PEO-PCL block co-polymer end.

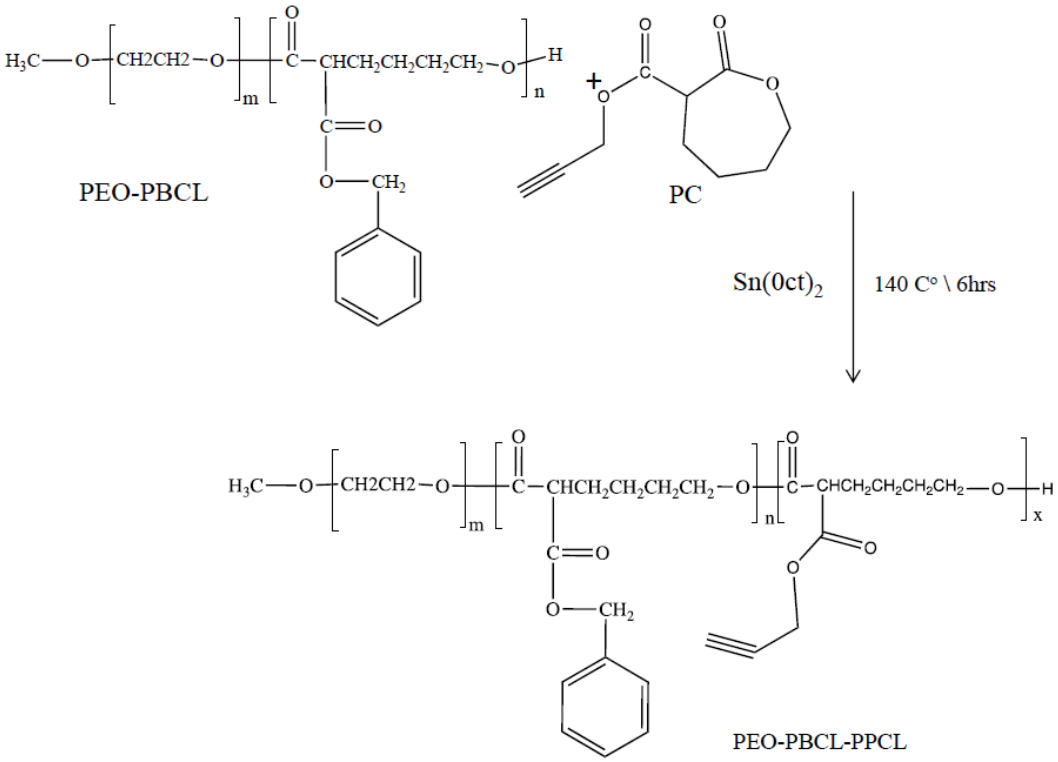

Scheme 2-4 Conjugation of the propargyl caprlactone to PEO-PBCL block co-polymer end.

2.5 Conjugation of Cy3 azide dye to PEO-PCL-PPCL and PEO-PBCL-PPCL block copolymers

Cy3 azide dye was conjugated to the propargyl end of the PEO-PCL-PPCL and PEO-PBCL-PPCL block copolymers by click chemistry. The reaction is copper catalyzed azide- alkyne cycloaddition that allowed the synthesis of 1, 4 substituted trizole. PEO_{114}-PCL_{22}-$PPCL_4$, PEO_{114}-PCL_{15}-$PPCL_4$ or PEO_{114}-$PBCL_{22}$-$PPCL_4$ polymer (0.01 mM); Cy3 azide (0.001mM); Cu (II) TBTA (0.0001mM) and ascorbic acid (0.0001Mm) were added to degassed DMSO. Cu (I) is the active form of the catalyst; however, Cu (II) was used because Cu (I) is unstable and cannot be stored; so it is generated in situ by reducing the Cu (II) to Cu (I) with the ascorbic acid. The TBTA complex was used to stabilize the Cu (I) towards

disproportionation. The reaction was kept stirring in dark for 24 hours.[107] The solution was purified by dialysis against double distilled water for 24 hours with changing the water every hour for the first 4 hours. The solution was then centrifuged for 5 minutes to remove any remaining free dye. The Cy3 conjugated polymers were then freeze-dried and stored (Scheme 2-5).

2.6 Conjugation of Cy5.5 NHS ester to Rituximab

Rituximab (Mwt.145 KD) was labeled with Cy5.5 NHS ester at an applied 1:200 molar ratios. The NHS ester dye was reacted with the primary amine from the antibody in PBS at slightly alkaline media pH=8.3 for 4 hours at room temperature in the dark to yield a stable amide bond.[108] The conjugate was than purified by size exclusion chromatography on Sepharose CL-6B column using PBS (pH 7.4) as the mobile phase (Scheme 2-6 step1).

2.7 Conjugation of Rituximab or Cy5.5 labeled Rituximab to the NHS-PEG-DSPE micelles

Micelles were prepared from the NHS-PEG-DSPE phospholipid by co-solvent evaporation method. Briefly, NHS-PEG-DSPE (0.001mM) was dissolved in acetone followed by drop-wise addition of this solution to 2 mL phosphate buffer saline (PBS) while stirring. The solution was left overnight to allow evaporation of the acetone. The Rituximab or Cy5.5 labeled Rituximab was added to NHS-PEG-DSPE micelles at 1:100 molar ratios. The NHS group from the micelles reacts with the primary amine from the antibody at pH 8 for 4 hours in the dark to form an amide linkage. The conjugate was than purified by Sepharose CL-6B column using PBS (pH=7.4) as the mobile phase (Scheme 2-6 step2 and 3).

2.8 Formation of mixed Micelles

Mixed micelles are formed by incubating PEO_{114}-PCL_{15}-$PPCL_4$, PEO_{114}-PCL_{22}-$PPCL_4$ or PEO_{114}-$PBCL_{22}$-$PPCL_4$ micelles (labeled with Cy3 dye at the poly(ester) block end) with the Rituximab-PEG-DSPE (plain or labeled with Cy5.5 NHS dye) at 1:1 Molar ratio in PBS for 24 hours. (Scheme 2-7)

A.

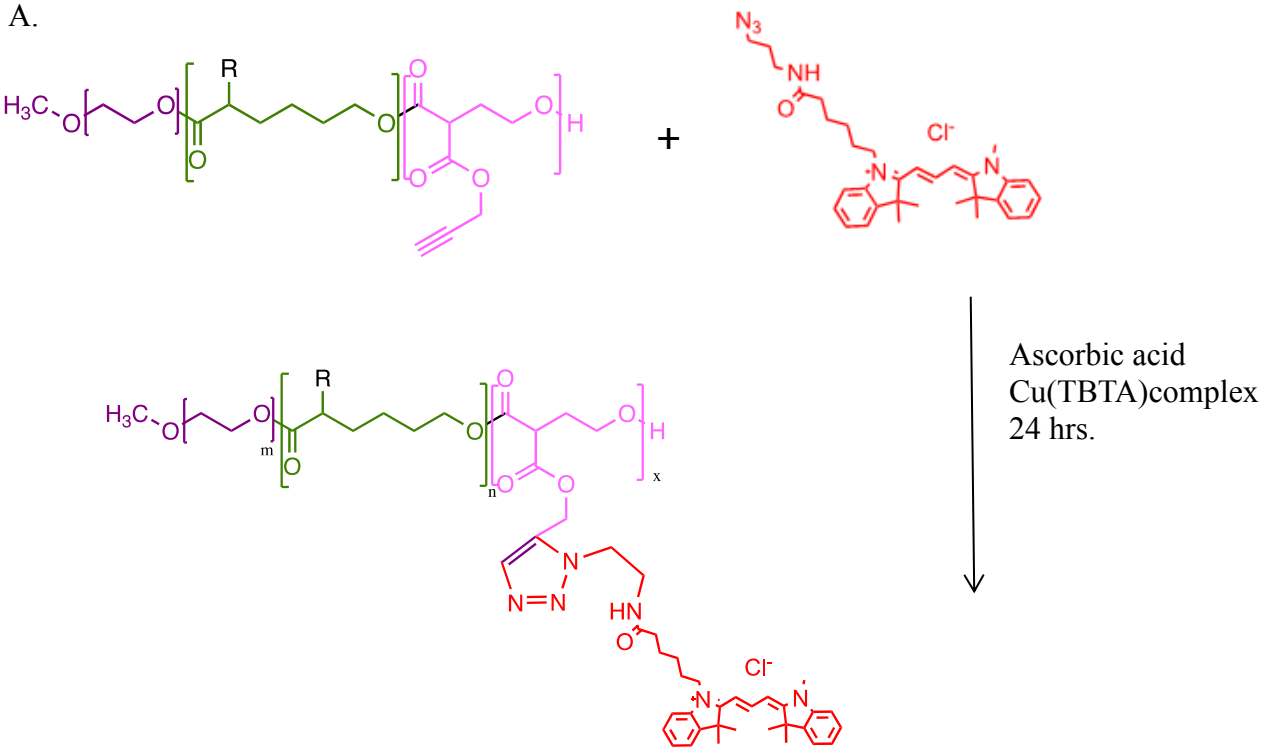

B.

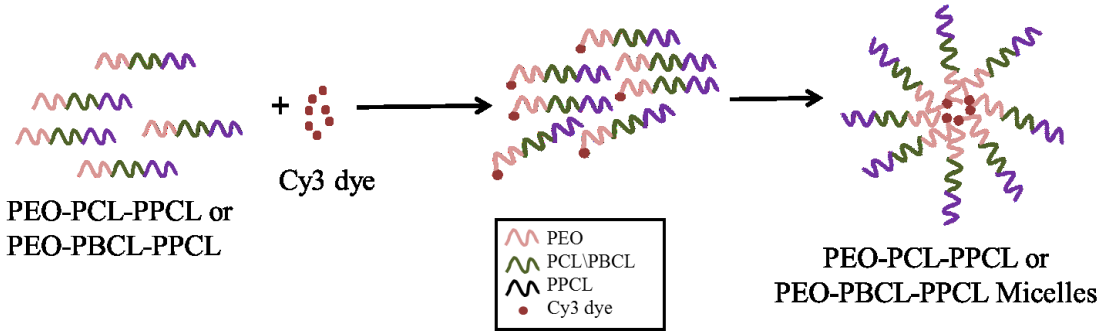

Scheme 2-5 A. Chemical synthesis of Cy3 -labeled polymers. B. Self-assembling of the Cy3 labeled polymers into micelles.

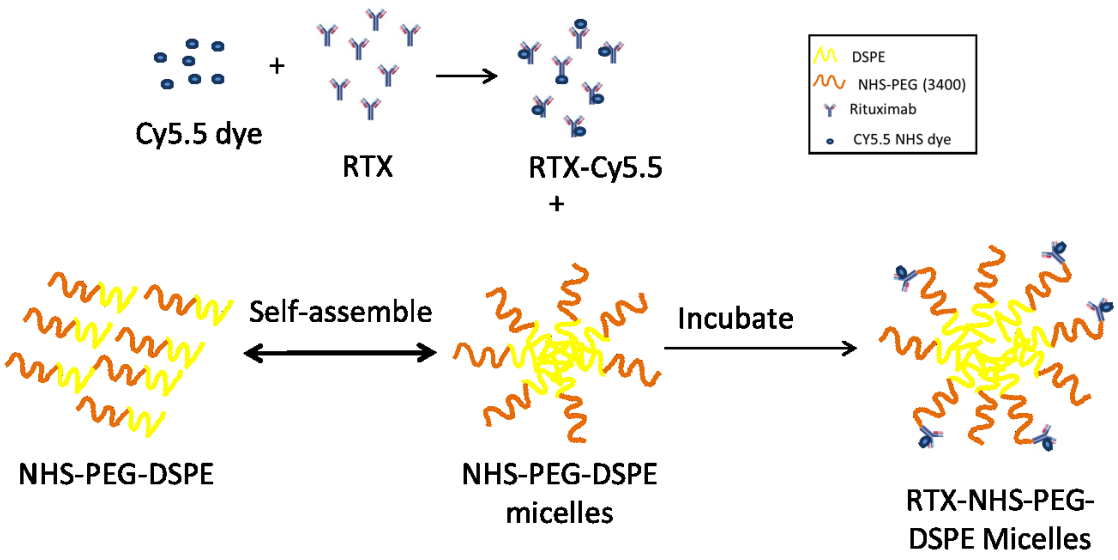

Scheme 2-6. 1- Chemical tagging of the Cy5.5 NHS ester dye to the RTX mAb. 2-Self-assembly of the NHS-PEG-DSPE to micelles. 3- Chemical conjugation of the RTX tagged Cy5.5 to the NHS-PEG-DSPE micelle.

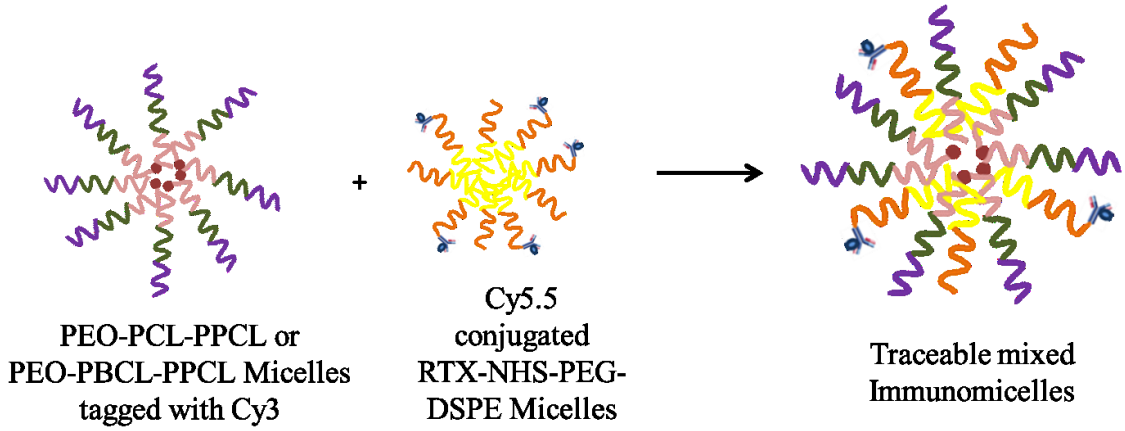

Scheme 2-7 Formation of mixed micelles from incubation of Cy5.5-Rituximab-PEG-PL micelles with either PEO_{114}-PCL_{15}-$PPCL_4$-Cy3, PEO_{114}-PCL_{22}-$PPCL_4$-Cy3 or PEO_{114}-

$PBCL_{22}$-$PPCL_4$-Cy3 micelles. The polymers compromising different mixed micelles (MM) under study are defined in Table 1.

2.9 Quantification of the conjugated mAb on the micelles

Mixed micelles composed of Rituximab-PEG-DSPE/PEO_{114}-PCL_{15}-$PPCL_4$ (RTX-MM-PCL_{15}), Rituximab-PEG-DSPE/PEO_{114}-PCL_{22}-$PPCL_4$ (RTX-MMPCL_{22}) or Rituximab-PEG-DSPE/PEO_{114}-$PBCL_{22}$-$PPCL_4$ (RTX-MM $PBCL_{22}$) with no dye were prepared using method described under section 2.8. The mixed micelles were then purified from free unconjugated mAb by passing through Sepharose column using PBS as the mobile phase. The eluent was collected in 32 fractions of 1 mL each, from the column. Each fraction was subjected to dynamic light scattering measurement of size to distinguish and separate the fractions containing free rituximab, rituximab modified micelles and that containing plain micelles. Micro BSA protein assay was used to quantify the concentration of antibody in each fraction according to the manufacturer instructions. Absorbance was measured at 560 nm (by Synergy Hybrid plate reader, Winooski, USA). This method was used to quantify the concentration of mAb in fractions containing rituximab conjugated micelles and that containing free rituximab.

2.10 Micelle size

The hydrodynamic diameter and polydispersity of PEO_{114}-PCL_{22}-$PPCL_4$, PEO_{114}-PCL_{15}-$PPCL_4$, PEO_{114}-$PBCL_{22}$-$PPCL_4$, NHS-PEG-DSPE micelles and that of Mixed Micelles (1 mg/mL) were measured using dynamic light scattering (DLS) ZETA-Sizer Nano (Malvern Instruments Ltd., Malvern, UK). The analysis was performed at a scattering angle of 173^o at 25 C^o.

2.11 Micelle stability

Critical micelle concentration (CMC) of PEO_{114}-PCL_{22}-$PPCL_4$, PEO_{114}-PCL_{15}-$PPCL_4$ PEO_{114}-$PBCL_{22}$-$PPCL_4$, NHS-PEG-DSPE and its mixed micelle counterparts with NHS-PEG-DSPE (without dye or antibody) was determined by dynamic light scattering (DLS) equipped with a laser operating at a wavelength of 633 nm.[109] Single attenuator index was used throughout all the measurements. The scattered light was detected at an angle of 173°. Measurements were carried out in polystyrene cells at 25 °C. Using the scattered light intensity as a function of polymer concentration, a series of micelle solutions (0.060–1000 μg/mL) in deionized water were prepared for different micellar formulations. The count rate (Kcps) as the function of the intensity of the scattered light was plotted against log concentration. The intersection of the two linear graphs in the sigmoidal curve was determined as the CMC.

Kinetic stability was measured with DLS by mixing the micelles formed from individual polymers and those of mixed micelles (without dye or antibody) solutions (1 mg/mL) with sodium dodecyl sulfate (SDS) (20 mg/mL) in 2:1 v/v ratio. The scattered light intensity and the PDI were measured at different incubation time intervals.[110]

2.12 Measuring the cellular association by flow cytometry

To evaluate the cellular association of micelles, *in vitro*, two different lymphoma cell lines; Kg-15 (CD20 +) and SUP M2 (CD20 -) were used. KG-15 and SUP M2 cells (1×10^6) were suspended in the media in a 24 well plate and incubated at 37^{oC} until the confluence was around 70 %. The cells were treated with the Cy5.5 labeled RTX-MM PCL_{15}-Cy3, PCL_{22}-Cy3 or $PBCL_{22}$-Cy3 as well as their plain (no rituximab) counterparts for 4 hours.

Competition study was also done by pretreating the cells with free rituximab at a concentration equivalent to 10 times the concentration of the conjugated antibody 2 hours prior to the micellar treatment. After the incubation, cells were centrifuged and washed twice with cold PBS before analysis using a BD FACS Caliber flow cytometer. The cells were gated using forward-versus side-scatter to exclude debris and dead cells before analysis of 10,000 cell counts. The data were analyzed with FlowJo cell analysis software version 10 (FlowJo, LLC, Ashland, Ore.) and plotted as Quadrant plot

2.13 Encapsulation of PTX in polymeric micelles and their characterization

Paclitaxel (PTX) loaded polymeric micelles were prepared by the dialysis method. [111] The block copolymers (PEO_{114}-PCL_{15}-$PPCL_4$ or PEO_{114}-PCL_{22}-$PPCL_4$ or PEO_{114}-$PBCL_{22}$-$PPCL_4$) and PTX were dissolved in dimethyl formamide (DMF) (0.5 mL). This solution was added to double distilled water (4 mL) in a drop-wise manner under moderate stirring for one day, followed by organic solvent removal by dialysis against double distilled water for another day (Spectrapor, MW cut-off 3500 Da). The micellar solution was then centrifuged at 11,600 × g for 5 min to remove any free unimers and un-encapsulated PTX. The PTX loaded PMs were than incubated with NHS-PEG-DSPE for another day to allow the formation of mixed micelles. The solution was analyzed for PTX content using LC-10AD SHIMADZU HPLC system at a flow rate of 1.0 mL/min at room temperature. The detection was performed at 227 nm using a SPD-10Avp SHIMADZU UV-VIS HPLC detector Reversed phase chromatography was carried out with a Microsorb-MV 5µ C18-100 Å column (4.6 mm × 250 mm) with 40 µL of sample injected in a gradient elution using 0.1% trifluroacetic acid aqueous solution and acetonitrile. The percent of acetonitrile was 40% at time zero and increased to 100% in 15 min. [112] The amount of loaded PTX was measured

and used to calculated PTX encapsulation efficiency and loading as described in the following equations.

$$\text{PTX loading (w/w\%)} = \frac{\text{amount of physically loaded PTX in mg}}{\text{amount of copolymer in mg}} \times 100$$

$$\text{Encapsulation efficiency (\%)} = \frac{\text{amount of physically loaded PTX in mg}}{\text{amount of PTX added in mg}} \times 100$$

2.14 Release of PTX from polymeric micelles

Release of PTX from MM-PCL_{15}, MM-PCL_{22} or MM-$PBCL_{22}$ and micelles prepared from individual PEO-PCLs or PEO-PBCL or PEG-PL polymer was determined in 0.01 M phosphate buffer (pH 7.4) containing 10% fetal bovine serum (FBS). The micellar solution (3 mL) was transferred into a dialysis bag (Spectrapor, MW cutoff 3500 Da) and placed into 500 mL of 0.01 M phosphate buffer (pH 7.4) with 10% FBS. The release study was performed at 37 ^{o}C in a Julabo SW 22 shaking water bath (Germany). At selected time intervals, the whole release media has been replaced with fresh one and aliquots of 200 µL were withdrawn from the inside of the dialysis bag for HPLC analysis and replaced with double distilled water. The amount of PTX released was calculated by subtracting the amount of PTX remained in the dialysis bag from the initial amount of PTX. The release profiles were compared using similarity factor, f2, and the profiles were considered significantly different if f2 < 50.

$$f_2 = 50 \times log\left(\left[1 + \left(\frac{1}{n}\right)\sum_{j=1}^{n}\left|R_j - T_j\right|^2\right]^{-0.5} \times 100\right)$$

Where n is the sampling number, Rj and Tj are the percent released of the reference and test formulations at each time point j.

2.15 *In-vitro* cytotoxicity study

The cytotoxicity of free PTX and PTX encapsulated in RTX-MMPCL$_{15}$, RTX-MM PCL$_{22}$ or RTX-MM PBCL$_{22}$ and their non-targeted counterparts against 2 different cell lines (KG-15 and SUP-M2) was tested using 3-(4,5- dimethylthiazol-2-yl)-2,5-diphenyltetrazolium bromide (MTT) assay. The cells were grown in RPMI media supplemented with 10% FBS and 1% P/S (Penicillin and Streptomycin) antibiotics, and maintained at 37 °C with 5% CO2 in a tissue culture incubator. Growth medium containing 5000 cells was placed in each well of a 96 well plate and incubated until the confluence was around 50%. PTX loaded micellar solutions; free PTX and empty micelles at different concentrations were incubated with the cells for 24, 72 hours. MTT solution (5 mg/mL) was added to each well and the plates were then incubated for another 4 hours. The plates were centrifuged at 1000 × G for 10 mins and the media was aspirated and replaced by DMSO to dissolve the formazan crystals. The cell viability was detected by measuring the optical absorbance at 570 nm using Synergy Hybrid plate reader (Winooski, USA). The mean absorbance of each treatment was determined and converted to the percentage of viable cells relative to the control.

2.16 Statistical analysis

Statistical analysis was performed using either unpaired Student's t test or one-way ANOVA with Tukey post-test analysis, as indicated in the text. The significance level (α) was set at 0.05. For non-linear regression analysis, Graphpad prism was used (version 7.00, Graphpad Software Inc., La Jolla, CA, USA). All experiments were conducted in triplicate unless mentioned otherwise in the text. In tables or graphs data points are represented as mean ± standard deviation (SD).

Chapter Three

Results

3 Results

3.1 Characterization of synthesized block copolymers

The ^{1}H NMR spectra of synthesized PEO-PCL, PEO-PBCL, PEO-PCL-PPCL and PEO-PBCL-PPCL and peak assignments are shown in Fig. 3-1, 3-2, 3-3 and 3-4, respectively. ^{1}H NMR spectra of the individual polymers were used to calculate the number average molecular weight of block copolymers as described in the experimental section. The characteristics of prepared block copolymers are summarized in Table 3-1.

a.

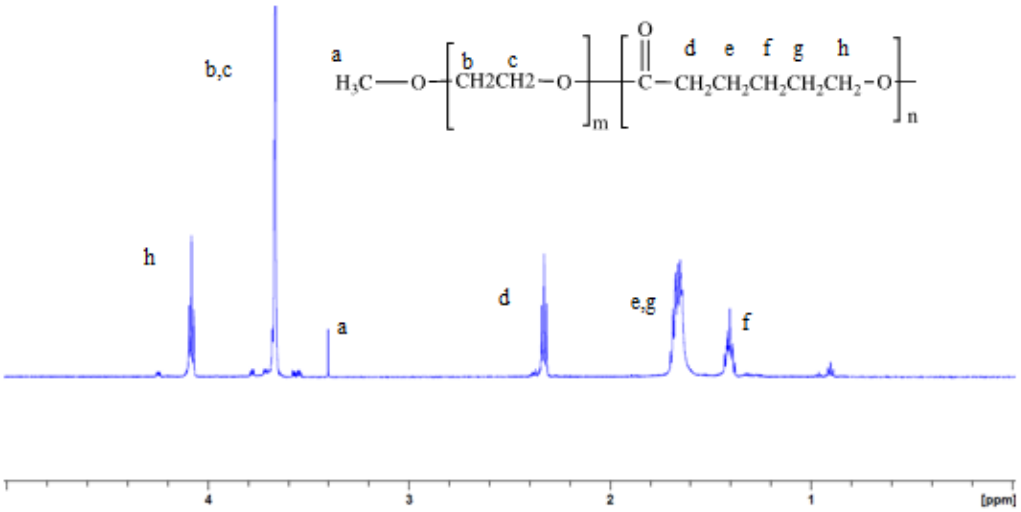

b.

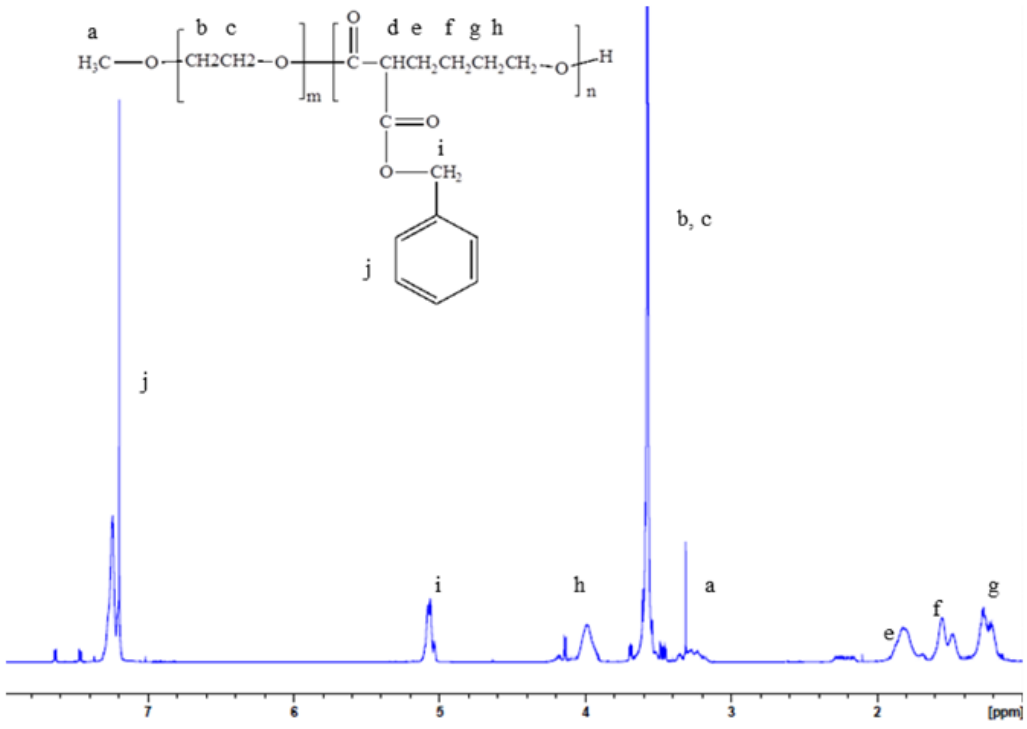

Figure 3-1^{1}H NMR Spectra of a. PEO-PCL and b. PEO-PBCL in $CDCl_3$

a.

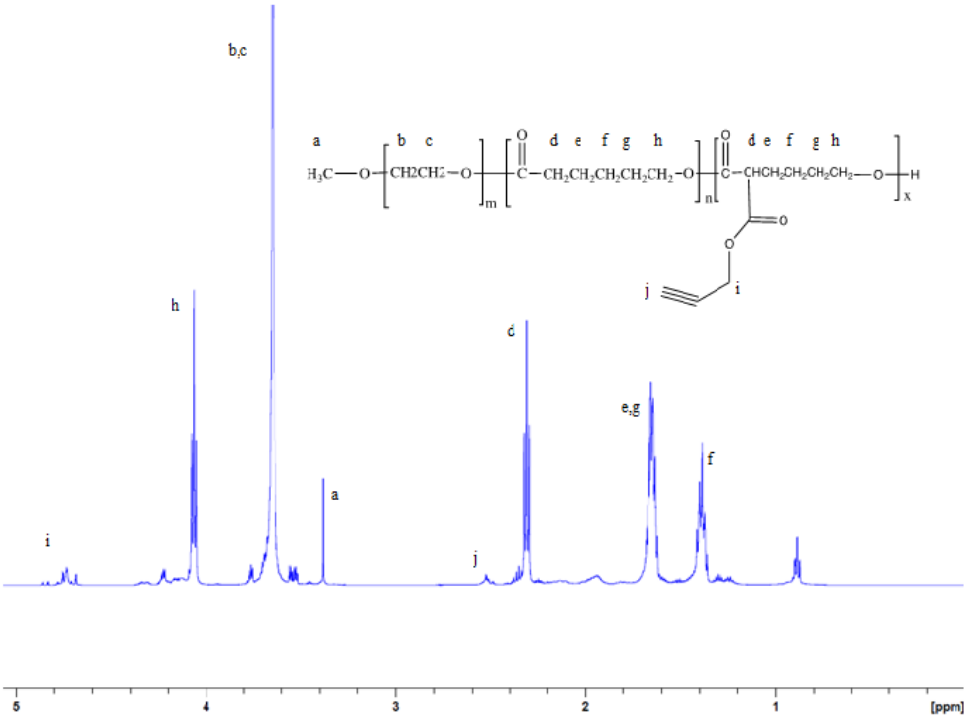

b.

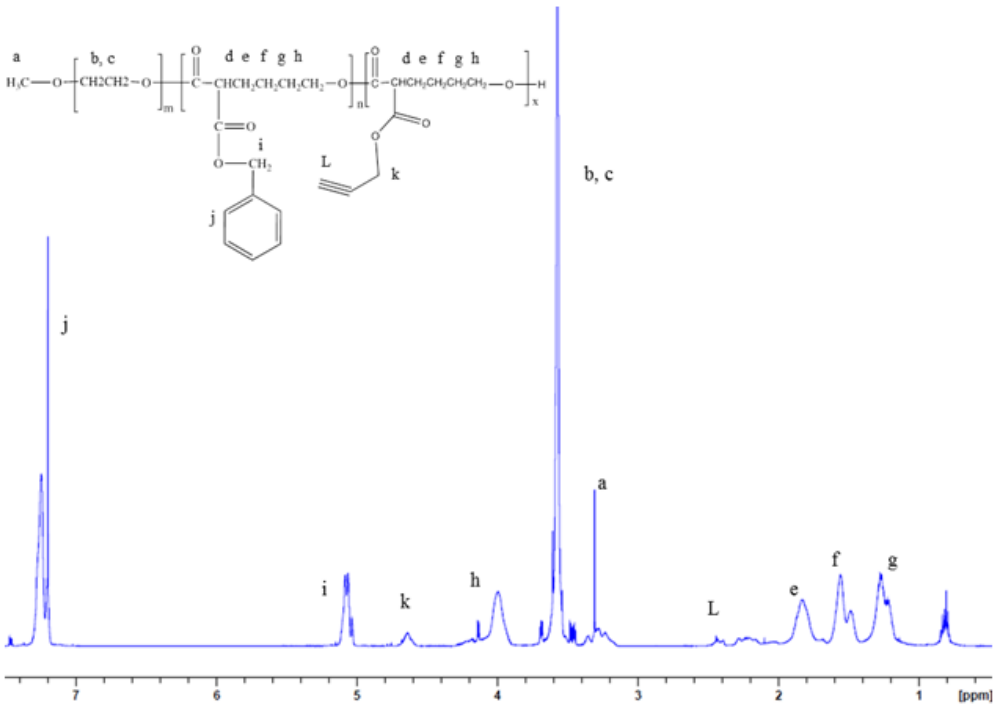

Figure 3-2 1HNMR Spectra of a. PEO-PCL-PPCL and b. PEO-PBCL-PPCL in CDCl3

3.2 Characterization of the micelle structures

The characteristics of the micelles prepared by solvent evaporation method are reported in Table 3-1. All micelles showed a CMC in μg/mL range (Table 3-1 and Figure 3-3). Among the prepared mixed micelles, the MM-$PBCL_{22}$ micelles had the lowest CMC (12.3 μg/mL), which indicates that this formula is the most thermodynamically stable one. On the other hand, the MM-PCL_{15} micelles showed a high CMC around (74.9 μg/mL). The CMC of the MM-PCL_{22} and MM-$PBCL_{22}$ were higher than the CMC of the single micelles prepared from individual PEO_{114}-PCL_{22}-$PPCL_4$ or PEO_{114}-$PBCL_{22}$-$PPCL_4$ block copolymers. However, it was significantly lower than the CMC of micelles prepared from NHS-PEG-DSPE.

The Z average diameter of the self-assembled structures was below 100 nm and they showed a relatively narrow polydispersity index. To confirm the successful formation of the mixed micelle system, the size of micelle formed from individual block copolymers, i.e., PEO_{114}-PCL_{15}-$PPCL_4$, PEO_{114}-PCL_{22}-$PPCL_4$, PEO_{114}-$PBCL_{22}$-$PPCL_4$, or NHS-PEG-DSPE, was measured separately before the incubation of block copolymers. After incubating either of PEO_{114}-PCL_{15}-$PPCL_4$/NHS-PEG-DSPE or PEO_{114}-PCL_{22}-$PPCL_4$/NHS-PEG-DSPE or PEO_{114}-$PBCL_{22}$-$PPCL_4$/NHS-PEG-DSPE pairs, the size of the mixture was also measured at different incubation time intervals. At few minutes after incubation, two peaks reflecting the size of each individual micelle appeared. As the incubation continued to 24 h, until only one peak was formed, possibly reflecting the size of the mixed micelles. The average diameter of mixed micelles was shown to be significantly different from the average diameter of micelles from individual polymers as shown in Table 3-1.

Table 3-1Characteristics of synthesized block copolymers and micelles self-assembled from mixed versus single polymers.

Block copolymers forming micelles[a]	Micelle name used	M_n ($gmol^{-1}$)[b]	Average micellar size[c]± SD (nm)	PDI[d]±SD	CMC[e]±SD (µg/mL)
PEO_{114}-PCL_{15}-$PPCL_4$	PCL_{15}	6500	57±0.6	0.215±0.003	5.1±0.6
PEO_{114}-PCL_{22}-$PPCL_4$	PCL_{22}	7800	50±3.4	0.263±0.002	2.2±0.1
PEO_{114}-$PBCL_{22}$-$PPCL_4$	PBCL $_{22}$	9960	71±0.4[$]	0.127±0.019	2.2±0.4
NHS-PEG-DSPE	DSPE	3400	23±2.1	0.368±0.1	45.1±4.8
NHS-PEG-DSPE/ PEO_{114}-PCL_{15}-$PPCL_4$	MM-PCL_{15}	-	78±0.6^	0.268±0.003	74.9±3.7*
NHS-PEG-DSPE/ PEO_{114}-PCL_{22}-$PPCL_4$	MM-PCL_{22}	-	84±2.9^	0.399±0.0170	18.2±2.5*
NHS-PEG-DSPE/PEO_{114}-$PBCL_{22}$-$PPCL_4$	MM-$PBCL_{22}$	-	93±3.6^	0.242±0.02	12.3±3.1*
Rituximab-NHS-PEG-DSPE/ PEO_{114}-PCL_{15}-$PPCL_4$	RTX-MM-PCL_{15}	-	93±7.5	0.234±0.07	-
Rituximab-NHS-PEG-DSPE/ PEO_{114}-PCL_{22}-$PPCL_4$	RTX-MM-PCL_{22}	-	95±20.6	0.284±0.068	-
Rituximab-NHS-PEG-DSPE/ PEO_{114}-$PBCL_{22}$-$PPCL_4$	RTX-MM-$PBCL_{22}$	-	110±11.6	0.216±0.01	-

[a]The number shown as subscript indicates the degree of polymerization of each block deteremined by ^{1}H NMR.

[b] The average nubmer molecular weight determined by ^{1}H NMR.

[c] Hydrodynamic diameter estimated from DLS.

[d] Poly dispersity index measured by DLS.

[e] Critical micellar concertration measured by DLS.

[^] Significantly different from its counterpart micelles from single block copolymer (unpaired student t test $P<0.05$)

[$] Significantly different from PCL_{15} micelles (unpaired student t test $P<0.05$)

[*] Statistically different from its counterpart micelles from single block copolymer (unpaired student t test $P<0.05$)

A.

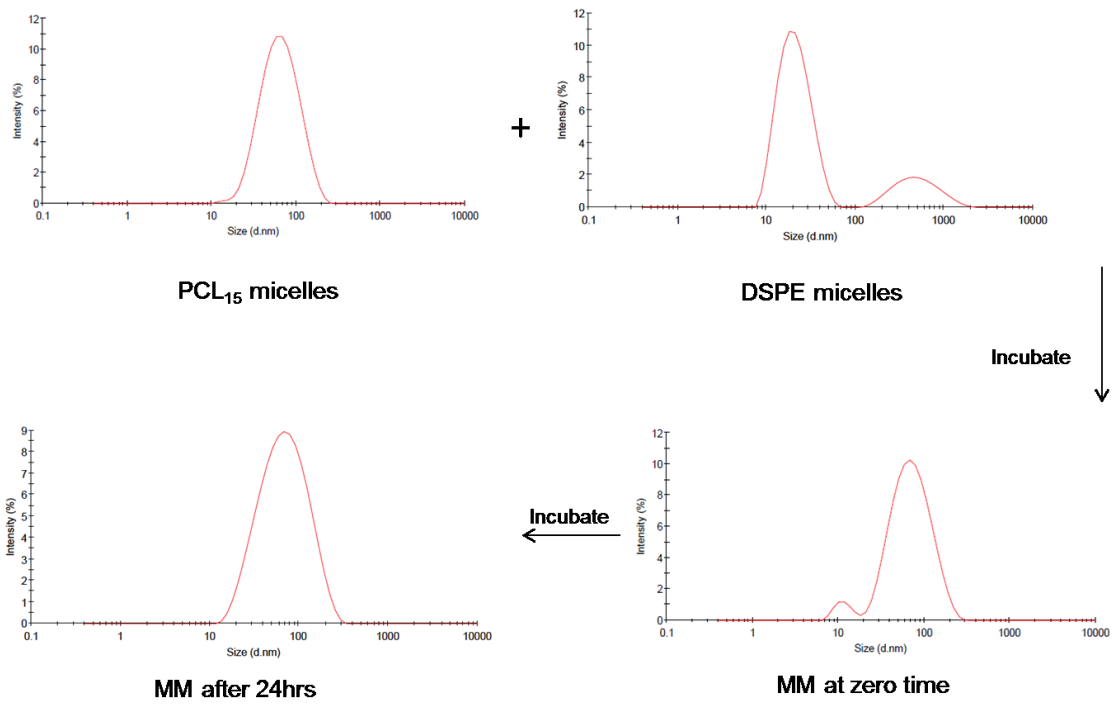
Intensity (%)
Size (d.nm)
PCL15 micelles
+
DSPE micelles
Incubate
MM at zero time
Incubate
MM after 24hrs

B.

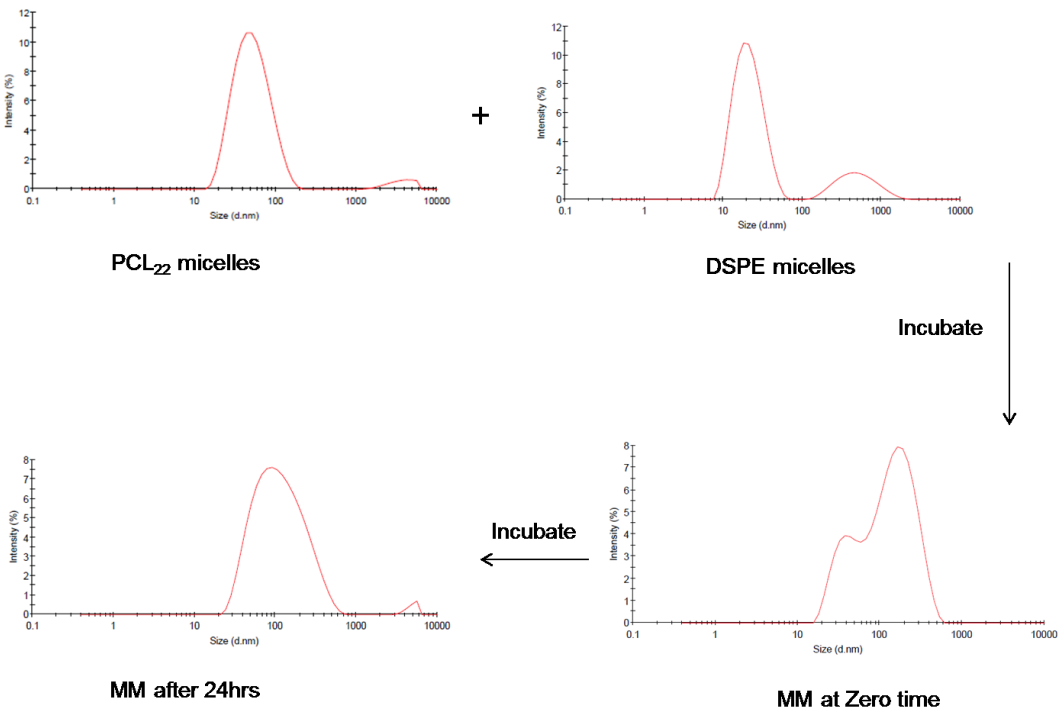
Intensity (%)
Size (d.nm)
PCL22 micelles
+
DSPE micelles
Incubate
MM at Zero time
Incubate
MM after 24hrs

C.

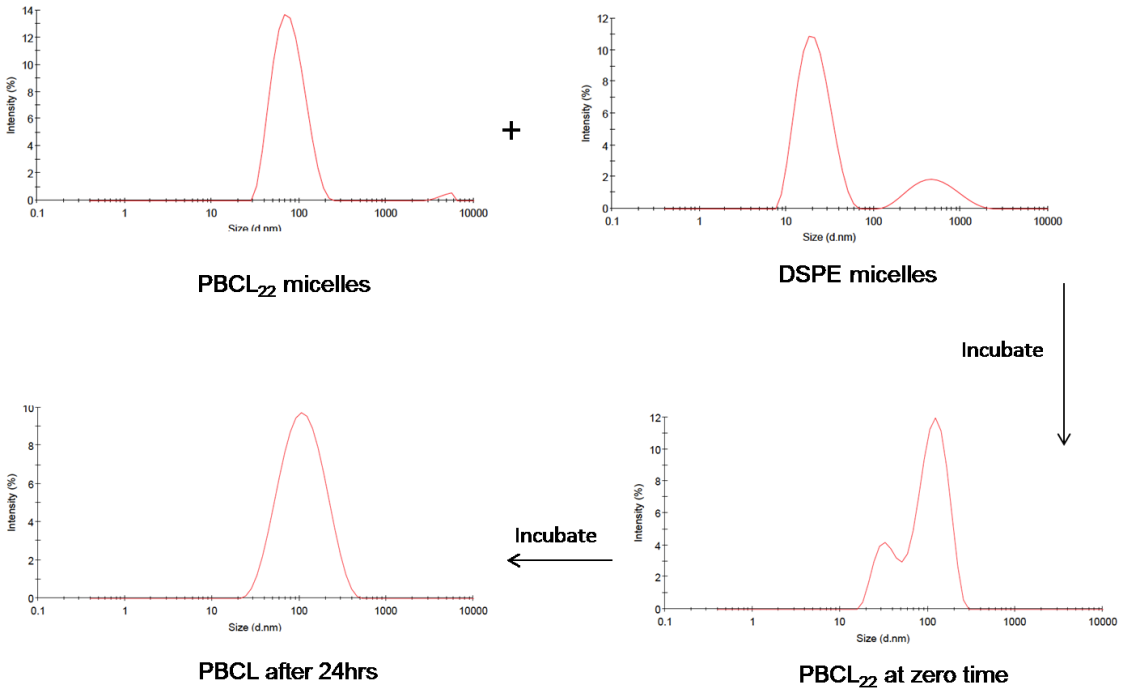

Figure 3-3 Tracking the formation of the mixed micelles by DLS. In this experiment, block copolymers of. PEO and A. PCL_{15}, B. PCL_{22} or C. $PBCL_{22}$ (description of block copolymers is provided in Table 3.1) were each incubated with NHS-PEG-DSPE and the formation of mixed micelles was monitred at time zero after incubation and after 24h by DLS.

3.3 Quantification of the conjugated dye and rituximab on the micelles

The amount of rituximab conjugated to the mixed micelles was quantified colorimetrically by micro BSA protein assay. This was done after separating different populations formed following mixing of PCL_{15}, PCL_{22} or $PBCL_{22}$ based block copolymers with PEG-DSPE ones, chromatographically using the Sepharose column. All of the 32 portions collected were subjected to identification primarily according to their size by DLS. After that the micro BSA

assay was conducted to identify the portions containing the mAb. The BSA reading was also used to quantify mAb concentration and conjugation efficiency in these sections. Combining the data from experiments mentioned above, we found that the first 7 portions collected from the column had neither micelles nor antibody (only PBS) (Table 3-2). This was evidenced by no absorbance in the BSA assay or reading in the DLS. Portions 6 to 11 was estimated to have Rituximab conjugated mixed micelle because DLS measurement showed existence of colloidal particles at 90-110 nm size range for these samples. Additionally, we had a high absorbance in the BSA assay. Fractions 12 to 14 had only the plain micelles. This was implicated by the absence of BSA response and a reading in the DLS similar to the size we identified for plain micelles (from 45 to 65 depending on the micelles). Fractions 15-16, on the other hand, were responsive to BSA assay and showed a size similar to that identified for the RTX conjugated NHS-PEG-DSPE micelles (30 nm) with the DLS study. Fractions 17-22 included the free antibody because again there size with DLS is around 16nm (similar to the size identified for RTX) and fractions 23 to 28 are estimated to have a mixture of free RTX and plain NHS-PEG-DSPE micelle because the DLS reading had a mixture of two size one similar to that identified for the free RTX (12nm) and the other similar to the size of plain NHS-PEG-DSPE micelles (25nm). In addition to that there was an absorbance with the BSA assay. While the rest until fraction 32 were just PBS. This was recognized by no size reading detected by DLS and no absorbance measured by the BSA assay.

Table 3-2 Characterization of the different fractions separated during the purification of different mixed micelles (RTX-MM-PCL15, RTX-MM-PCL22 and RTX-MM-PBCL22) by Sepharose column. The fractions were identified using the combination of data from size measurement by DLS and RTX concentration by BSA assay (n=1).

Identified Composition of fraction	Fraction	diameter (nm)±SD	PDI±SD	RTX conc. µg/mL	RTX conjugation efficiency [a] (%)
RTX –MM-PCL_{15}	6 to 11	93.3±7.5	0.234±0.07	0.255	17.5%
RTX-MM-PCL_{22}		95.3±20.6	0.284±0.06	0.257	18%
RTX-MM-$PBCL_{22}$		110±11.6	0.216±0.01	0.276	19%
PCL_{15} Micelles	12 to 14	52.6±5.2	0.198±0.02	0.025	1.7%
PCL_{22} Micelles		48.86±7.3	0.378±0.026	0.043	2.9%
$PBCL_{22}$ Micelles		65.4±5.6	0.106±0.007	0.01	0.6%
RTX conjugated NHS-PEG-DSPE micelle	15-16	30.2±5.7	0.432±0.01	0.136	9.3%
Free RTX	17 to22	16.05±4.4	0.568±0.075	0.853	59%
Free Ab and traces of NHS-PEG-DSPE micelles	23 to 28	-	-	0.214	14%

[a]RTX conjugation efficiency is calculated as (conjugated RTX/added RTX) × 100

3.4 Kinetic stability of polymeric micelles

The kinetic stability of the micelles was studied by DLS after the addition of SDS, which acts as a destabilizing agent. Figure 3-4.a shows the % intensity of the micellar peak for PCL_{15}, PCL_{22}, $PBCL_{22}$, NHS-PEG-DSPE as well as the MM-PCL_{15}, MM-PCL_{22}, and MM-$PBCL_{22}$ (desription given in Table 3.1.) over time in the presence of SDS. NHS-PEG-DSPE showed dramatic drop in the signal intensity of the micellar peak immediately after the incubation with SDS. After 2 hours of incubation the intensity of the micellar peak was less than 5%. In the case of $PBCL_{22}$ micelles and MM-$PBCL_{22}$ there were neither a change in the intensity of the micellar peak or the PDI even after 24 hours incubation, which means that the micelles remained intact throughout the whole period of incubation. For PCL_{22} micelles and MM-PCL_{22} the signal intensity of the micella peak dropped around 60% after only 6 hour. Their PDI also started to increase above 0.5, around the same time. However, the behaviour of MM-PCL_{15}, was signifiacntly different from micelles prepared from single PCL_{15} block copolymer. The PDI of the MM-PCL_{15} reached 1, only after 2 hours implying micellar dissociation. For micelles of PCL_{15} from single block copolymer, the PDI remined intact for upto 4 hours and then increased. Overall, among block copolymers under study, the PEO-PBCL based micelles (from single block copolymer or mixed) seem to be the most stable ones, kinetically.

a. b.

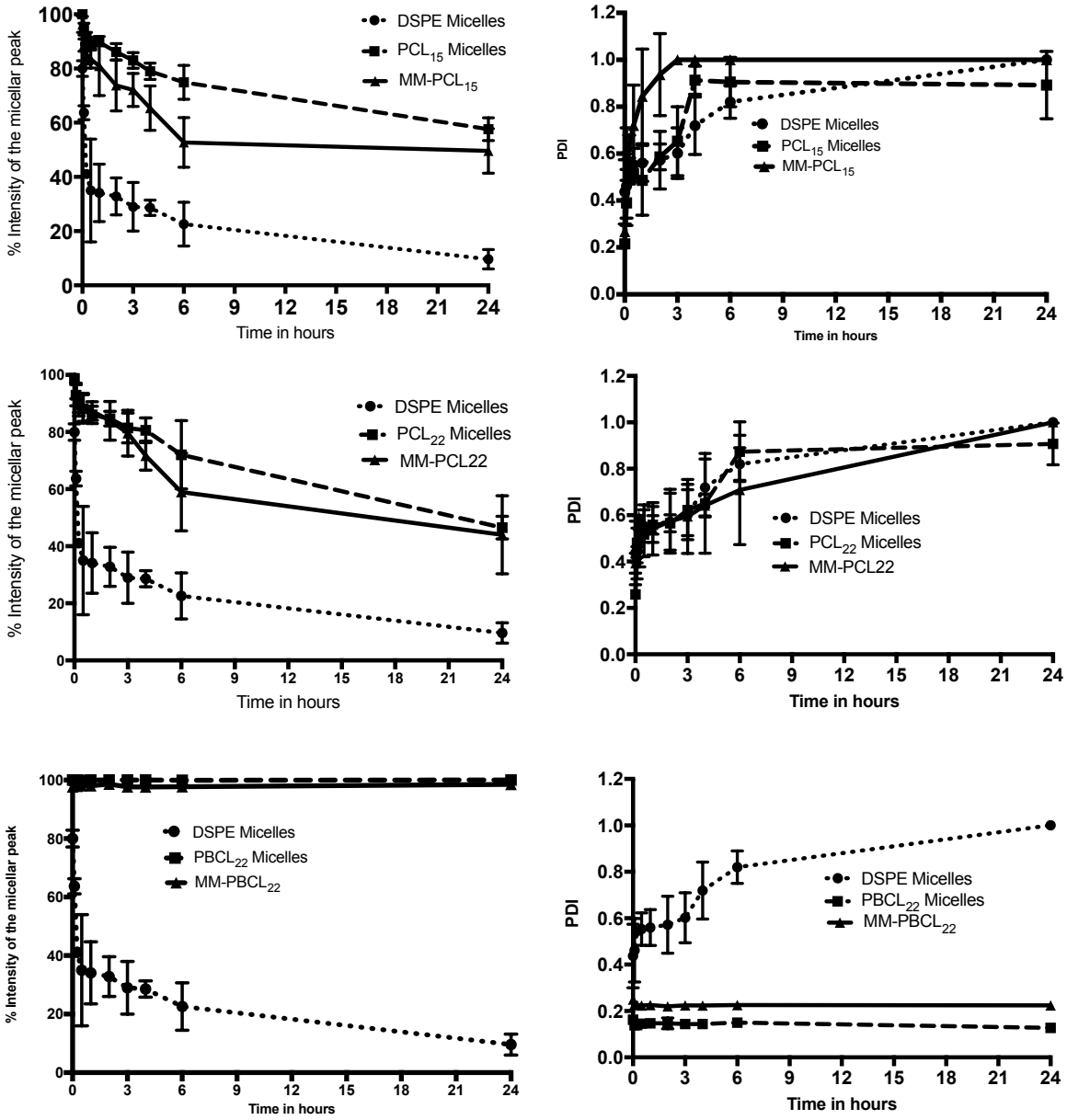

Figure 3-4 Kinetic stability measurements of micelles formed from individual polymers, i.e., PEO_{114}-PCL_{15}-$PPCL_4$, PEO_{114}-PCL_{22}-$PPCL_4$, PEO_{114}-$PBCL_{22}$-$PPCL_4$, NHS-PEG-DEPE versus associated mixed micelles. Polymers (at 1 mg/mL) were incubated with SDS (6.7mg/mL) a. The time dependent change in the peak intensity. (b) Time dependent change in the polydispersity index. Data represent average ± SD (n=3). The data related to NHS-PEG-DSPE micelles is related in all graphs for comparison with associated mixed micelles.

3.5 *In-vitro* cellular association

The association of the RTX-MM PCL_{15}, RTX-MM PCL_{22} and RTX-MM $PBCL_{22}$ with KG-15 cells (CD20+) or SUP-M2 cells (CD20-) was assessed by flow cytometry. The rituximab modified mixed micelles were labeled with 2 fluorescent dyes; Cy5.5, which was conjugated to RTX and Cy3, which was conjugated to the end of poly (ester) block in the core of micelles. The association of RTX conjugated to MM-PCL_{22} and MM-$PBCL_{22}$ were mostly positive for both Cy3 and Cy5.5, which suggests that these micellar systems remained intact in the media when incubated with the cells. For RTX modified MM-PCL_{15}, the vast majority of the cells were only positive for Cy5.5 dye, which suggest that our mixed micelles dissociated in the media and the Cy5.5 labeled RTX-PEG-DSPE micelle is associating with the CD 20 + cells alone. Despite the breaking down of the mixed micelles, still the RTX conjugated DSPE micelles had significantly higher uptake than the plain micelles by KG-15 cells (unpaired student test, $P<0.05$). Moreover, the association of the RTX conjugated DSPE micelles was significantly higher in KG-15 cells (CD20+) compared to its association with the SUP-M2 cells (CD20-) (unpaired student t test, $P<0.05$).

Furthermore, the flow cytometry dotplot (Figure 3-5) showed significant increase in the association of RTX conjugated MM-PCL_{22} and MM-$PBCL_{22}$ with KG-15 cells when compared to non-targeted MM-PCL_{22} and MM-$PBCL_{22}$ (unpaired student test, $P<0.05$). In addition, the association of the RTX modified MM-PCL_{22} and MM-$PBCL_{22}$ with KG-15 (CD20+) was 3.7 and 4.2 folds respectively enhanced compared to its association with SUP-M2 (CD20-) (unpaired student test, $P<0.05$).

To assess the effect of the receptor (CD20) mediated cellular association of RTX conjugated mixed micelles; competition study was conducted. In this experiment we were looking at the

reduction of the cellular association with our micellar systems in terms of the reduction of the percentage of cells that were positive for both Cy3 and Cy5.5 when pretreated with the free RTX. The results of the competition study where the cells were pretreated with free RTX prior to the treatment with targeted formulation were as following: significant reduction of the cellular association with RTX-MM-$PCL_{15,}$ RTX-MM-PCL_{22} and RTX-MM-$PBCL_{22}$ on the KG-15 compared to the association of those micellar formulations without the pretreatment with free RTX (unpaired student t test, $P<0.05$). In contrast, pretreating the SUP-M2 cells with free RTX didn't significantly change the association of the targeted mixed micelles to the SUP-M2 compared to its association without the pretreatment with free RTX.

Furthermore, when conducting the competition study for the plain mixed micelles (tagged only with Cy3) on both cell lines (KG-15 and SUP-M2) we were looking for the reduction of the percentage of cells that were positive for Cy3, The results showed no significant difference in the association of the plain MM-$PCL_{15,}$ MM-PCL_{22} and MM-$PBCL_{22}$ when pretreated with free mAb compared to the association of those micellar systems without pretreatment with the free RTX on both cell lines (unpaired student t test $P<0.05$).

Moreover, when monitoring the percentage of cells that were only positive for Cy5.5 after conducting the competition study, we found that for KG-15 cells the association of the targeted micelles significantly dropped compared to the association of those micellar formulation without the pretreatment free RTX(unpaired student t test $P<0.05$). On the other hand, there were no significant differences in the percentage of Cy5.5 positive with or without the pretreatment with free RTX on the SUP-M2 cells (unpaired student t test $P<0.05$).

Those results pointed to the important role of the rituximab and CD20 interaction in enhancing the association of the micellar system to the CD20 positive cells.

MM-PCL$_{15}$

A-

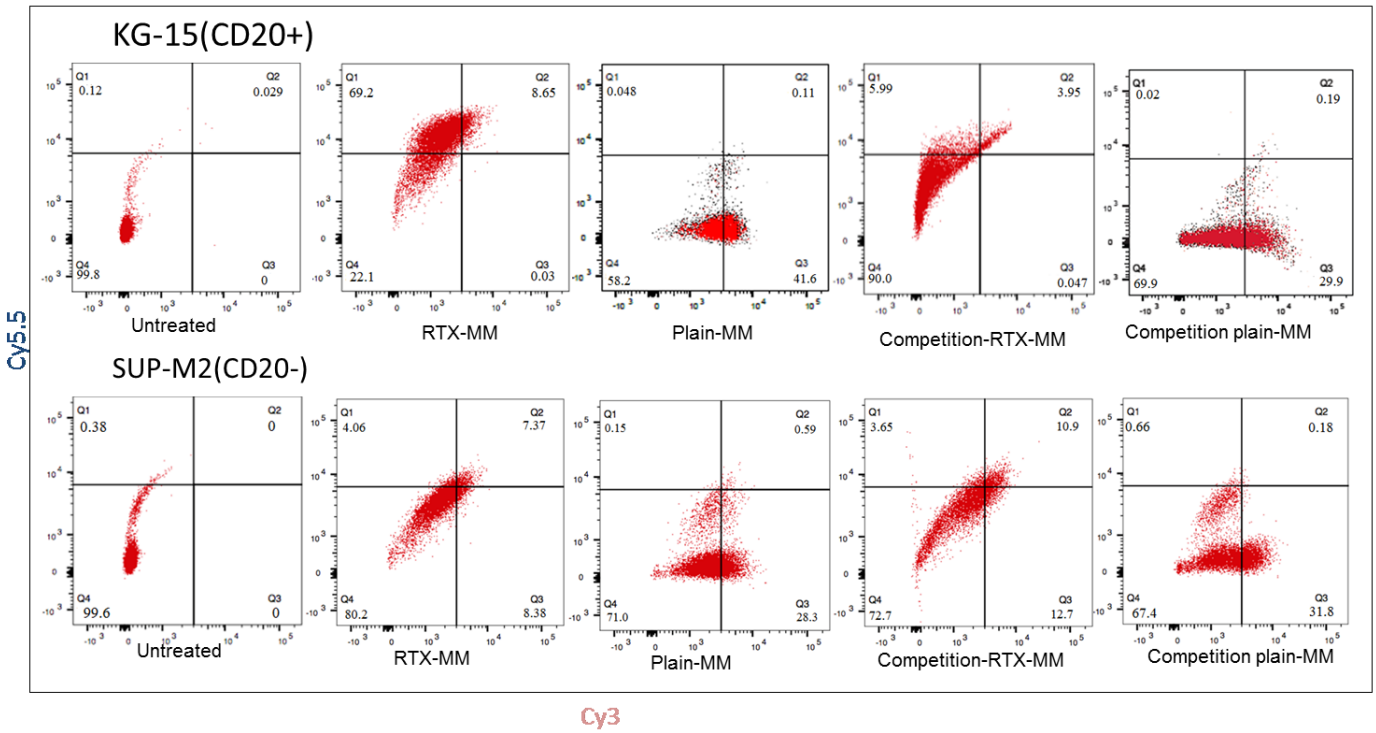

B-

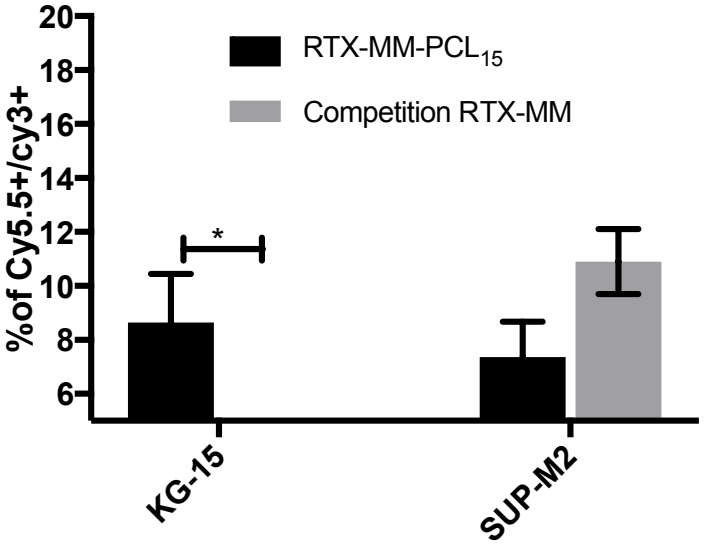

MM-PCL$_{22}$

A-

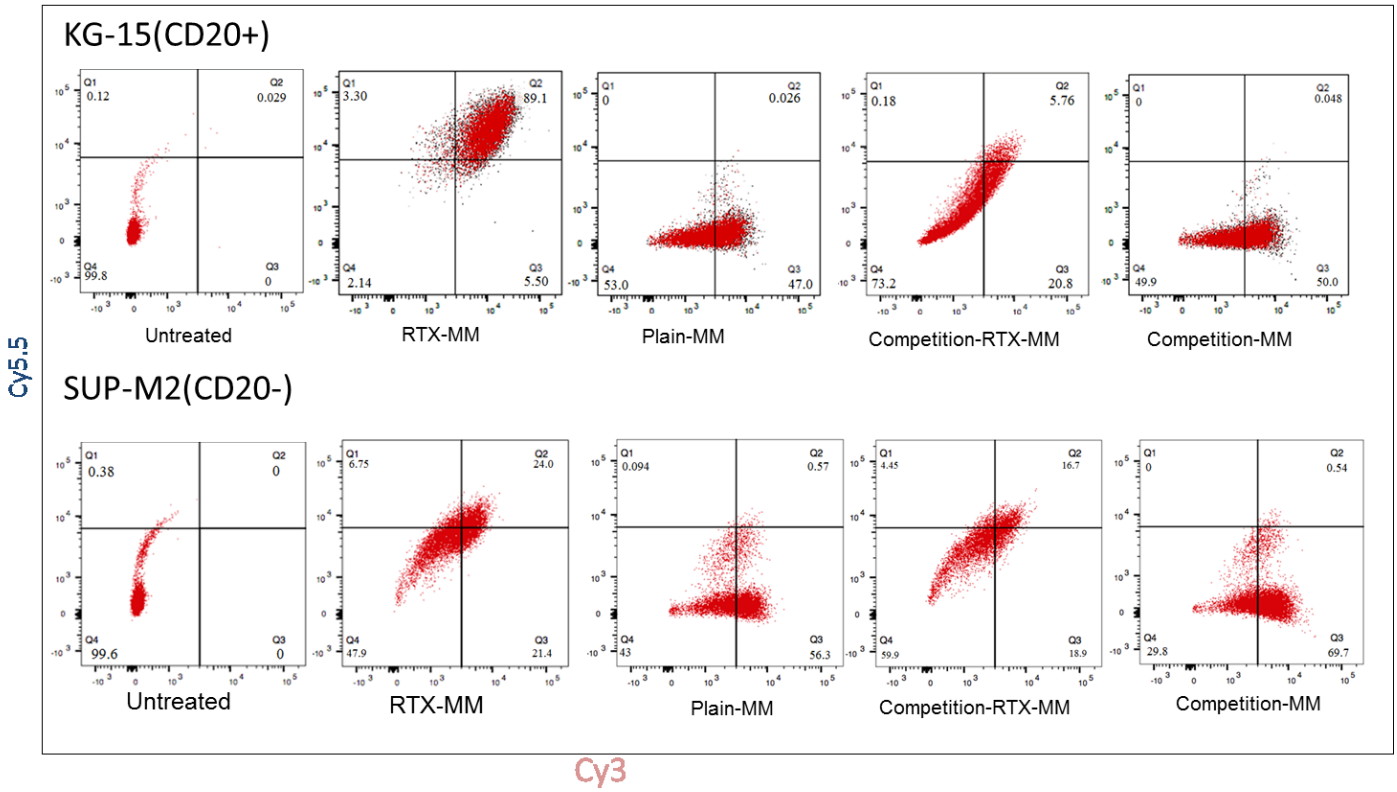
KG-15(CD20+)
Untreated
RTX-MM
Plain-MM
Competition-RTX-MM
Competition-MM
SUP-M2(CD20-)
Untreated
RTX-MM
Plain-MM
Competition-RTX-MM
Competition-MM
Cy5.5
Cy3

B-

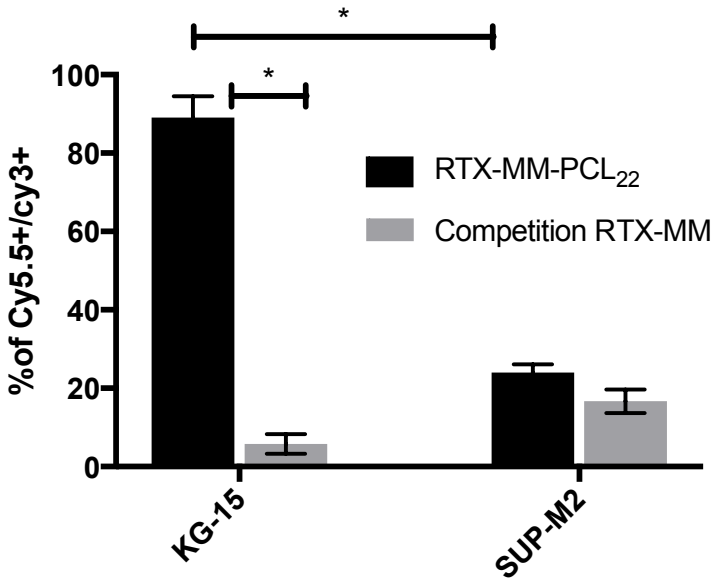
%of Cy5.5+/cy3+
100
80
60
40
20
0
*
*
RTX-MM-PCL22
Competition RTX-MM
KG-15
SUP-M2

MM-PBCL$_{22}$

A-

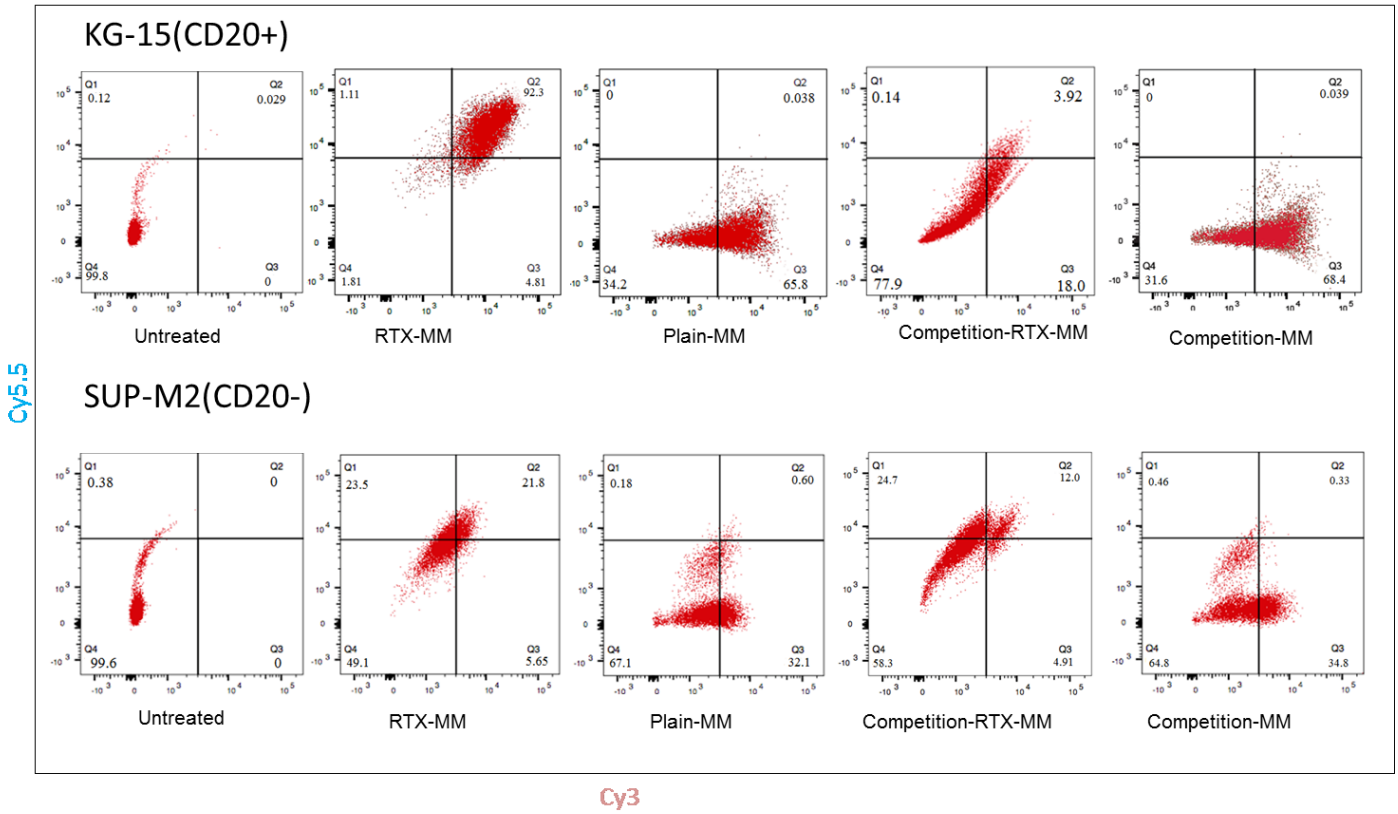
KG-15(CD20+)
Q1 0.12
Q2 0.029
Q4 99.8
Q3 0
Untreated
Q1 1.11
Q2 92.3
Q4 1.81
Q3 4.81
RTX-MM
Q1 0
Q2 0.038
Q4 34.2
Q3 65.8
Plain-MM
Q1 0.14
Q2 3.92
Q4 77.9
Q3 18.0
Competition-RTX-MM
Q1 0
Q2 0.039
Q4 31.6
Q3 68.4
Competition-MM
SUP-M2(CD20-)
Q1 0.38
Q2 0
Q4 99.6
Q3 0
Untreated
Q1 23.5
Q2 21.8
Q4 49.1
Q3 5.65
RTX-MM
Q1 0.18
Q2 0.60
Q4 67.1
Q3 32.1
Plain-MM
Q1 24.7
Q2 12.0
Q4 58.3
Q3 4.91
Competition-RTX-MM
Q1 0.46
Q2 0.33
Q4 64.8
Q3 34.8
Competition-MM
Cy5.5
Cy3

B-

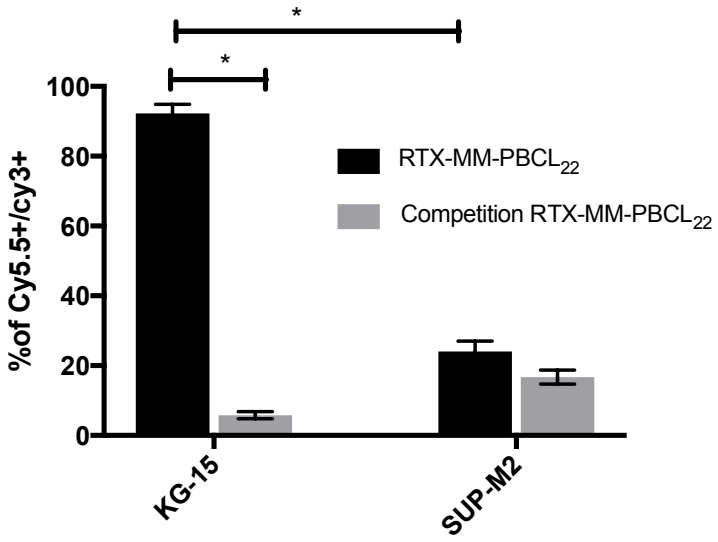
*
*
100
80
60
40
20
0
%of Cy5.5+/cy3+
RTX-MM-PBCL22
Competition RTX-MM-PBCL22
KG-15
SUP-M2

Figure 3-5 A- Flow cytometry dotplot of the association of plain micelle, RTX modified micelles as well as the competition study with free RTX by both KG-15 (CD20+) and SUP-M2 (CD20-) cells. Micelles were labeled with either Cy3 at the end of PCL and PBCL block, and/or Cy5.5 on the conjugated RTX. In each graph, the bottom left section shows the population of cells negative for both Cy5.5 and Cy3; the top left section shows the population of cells positive for Cy5.5 only; the bottom right section shows the population of cells positive for Cy3 only; and the top right section shows the population of cells positive for both Cy5.5 and Cy3.3 (The latter section indicates the population of cells positive for mixed micelles).B. Bar graph showing the percentage of cellular association to Cy3/Cy5.5 positive micelles after 4 h of incubation with or without pretreatment with free RTX on KG-15 and SUP-M2 cells. Each bar represents average association (%) ± SD (n=3). * denotes statistically significant (P < 0.05).

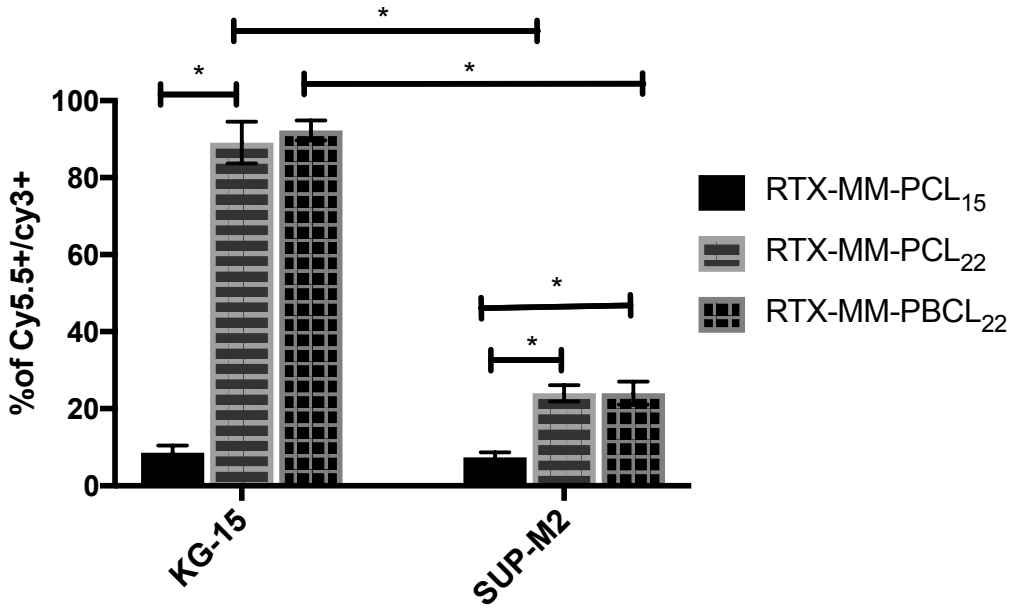

Figure 3-6 The percentage of cellular association to Cy3/Cy5.5 positive micelles after 4 h of incubation with RTX conjugated MM-PCL_{15}, MM-PCL_{22} and MM-$PBCL_{22}$ on KG-15 and SUP-M2 cells. Each bar represents average association (%) ± SD (n=3). * denotes statistically significant (P>0.05).

3.6 Characterzation of PTX loaded polymeric micelles

Solublization of PTX in MM-PCL_{15}, MM-PCL_{22}, MM-$PBCL_{22}$ and its counterpart micelles from single block copolymers was examined [113] Under identical loading conditions, no significant difference in the encapsulation efficacy between PCL_{15} versus MM-$PCL_{15,}$ PCL_{22} micelles versus MM-PCL_{22}; and $PBCL_{22}$ micelles versus MM-$PBCL_{22}$ was observed (unpaired Student's t test, $P>0.05$). Overall, MM-PCL_{22} and MM-$PBCL_{22}$ were shown to have significantly higher encapsulation efficacy than MM-PCL_{15} (One way ANOVA, $P<0.05$). (Table 3-3)

3.7 PTX release from polymeric micelles

The *in-vitro* release profile of PTX from Taxol® and polymeric micelles under study is illustrated in Figure 3-6. Comparison of the release profile between MM-PCL_{15}, MM-PCL_{22} MM-$PBCL_{22}$ with their counterpart micelles prepared from single block copolymers was conducted by f_2 similarity factor ($f_2<50$ is considered significant). In addition to the f_2 factor the unpaired student t-test was also conducted for the purpose of point to point analysis. Our results showed the MM-PCL_{22} significantly slowed down the release of PTX compared to PCL_{22} micelles at 48 h time point (40.7% of PTX release from MM-PCL_{22} compared to 53.1% release from PCL_{22}, unpaired Student's t test, $P<0.05$). However, when measuring the f_2 factor no significant difference between release profile of MM-PCL_{22} and PCL_{22} micelles was observed (f_2=52.3). In contrast, the release of PTX from MM-PCL_{15} after 48h was significantly accelerated compered to its release from PCL_{15} (75.05 versus 46.86% release for MM-PCL_{15} and PCL_{15}, respectively) (unpaired Student's t test, $P<0.05$). When conducting the factor analysis, a significant difference between the release profile of PTX from PCL_{15} and MM-PCL_{15} was also noted (f_2 =10.9). In case of MM-$PBCL_{22}$ there was no significant

difference between release profile of PTX from and $PBCL_{22}$ (58.1 %) and MM-$PBCL_{22}$ (60.75%) at 48 h (unpaired Student's t test, P>0.05). However, when conducting the f_2 similarity factor analysis significant difference in the release profile between $PBCL_{22}$ and MM-$PBCL_{22}$ was shown ($f_2 = 38.4$). Overall, by comparing the release profile of all the prepared mixed micelles, MM-PCL_{22} appeared to have significantly slower release profile, since only 14.7% and 40.7% of PTX was released after 6 and 48h, respectively from this formulation while 55.78% and 75.1% was released from MM-PCL_{15} after 6 and 48h respectively. For the MM-$PBCL_{22}$ 26.6 and 60.8% of PTX was released after 6 and 48h respectively.

Table 3-3 Characteristics of the PTX loaded polymeric micelles under study.

Micelle Name	Average micellar size± SD (dnm)	PDI	PTX Loading content ± SD (Wt%)	Encapsulation efficiency ± SD (%)	PTX release after 48 h (%)
PCL_{15}	-	-	0.55±0.01	14.8±1.50	47.0±5.3
PCl_{22}	-	-	0.79±0.08$^{\$}$	24.7±2.50$^{\$}$	53.0±4.6
$PBCL_{22}$	-	-	0.60±0.04	23.6±2.10$^{\$}$	58.1±8.2
MM-PCL_{15}	80±1.5	0.376±0.01	0.37±0.01$^{\wedge}$	15.0±1.2	75.5±5.1$^{\wedge}$
MM-PCL_{22}	83±0.7	0.217±0.003	0.45±0.03$^{\wedge\Psi}$	23.6±0.5$^{\Psi}$	40.7±4.5$^{\wedge\Psi}$
MM-$PBCL_{22}$	78±0.1	0.148±0.01	0.39±0.03$^{\wedge}$	20.7±0.8$^{\Psi}$	60.75±3.7$^{\Psi}$

$^{\$}$ Significantly different from PCL_{15} micelles

$^{\Psi}$ significantly different from MM-PCL_{15}.

$^{\wedge}$ Significantly different from its counterpart single micelles.

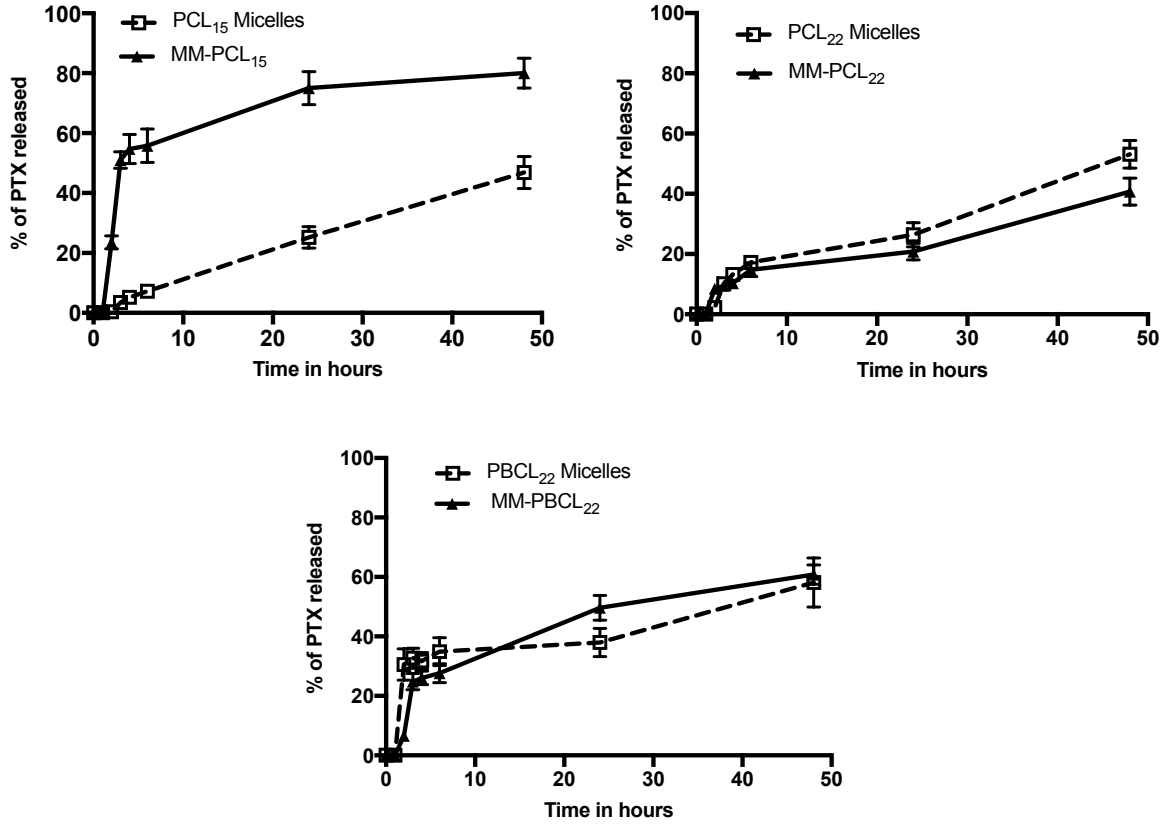

Figure 3-7 *In-vitro* release profile of physically loaded PTX from different micellar formulations at 10% FBS media. Data represent average ± SD (n=3)

3.8 *In-vitro* cytotoxicity

The results of *in-vitro* cytotoxicity of PTX loaded in RTX-MMs versus plain MMs and free PTX against both KG-15 and SUP-M2 cells following 24 and 72 h incubation is illustrated in Figures 3-7 and 3-8, respectively. This study was conducted at a concentration equivalent to 400 ng/mL of PTX. Overall, at 24 hours incubation time irrespective of the cell line used and the core forming block in the mixed micellar formulations of PTX, no significant difference between the cytotoxicity of RTX modified and plain micelles was observed. (Unpaired student's t test, $P>0.05$). However, the free PTX was significantly more cytotoxic than the micellar formulations in both cell lines (Unpaired student's t test, $P<0.05$).

The *in-vitro* cytotoxicity was also studied at 72 hours, For the SUP-M2 cells (CD20-) there was no significant difference between the RTX conjugated mixed micelles loaded with PTX and the PTX plain mixed micelles regardless of the core forming structure (Unpaired student t test $P>0.05$). Additionally, there was no significant difference between the free PTX and the plain mixed micelles loaded with PTX (Unpaired student t test $P>0.05$). For the KG-15(CD20+) cells there were no significant difference in the cytotoxicity between RTX conjugated mixed micelles loaded with PTX and the plain mixed micelles loaded with PTX regardless of the core structure(Unpaired student t test $P>0.05$). Moreover, there was no significant difference between the cytotoxic effect of the free PTX and plain mixed micelles loaded with PTX (Unpaired student t test $P>0.05$).

Furthermore, according to the release profile data of the different micellar formulation prepared (MM-PCL_{15}-PTX, MM-PCL_{22}-PTX and MM-$PBCL_{22}$-PTX), micelles prepared from MM-PCL_{15} had a fast release profile as 75% of PTX was released after 24h while for MM-PCL_{22} only 20% of PTX was released and for MM-$PBCL_{22}$ 50% of PTX was released after 24h. These results hinted that micellar formulation prepared from MM-PCL_{15} might be more cytotoxic to the cells in comparison to the others because of the higher concentration of the free PTX released into the media. However, interestingly that was not the case here as all the formulation had a similar cytotoxicity profile on the cells, indicating that micellar formulation prepared from MM-PCL_{15} might have released some of the loaded PTX during the process of sample preparation and before subjecting this formulation to the cells.

SUP-M2 (CD20-)

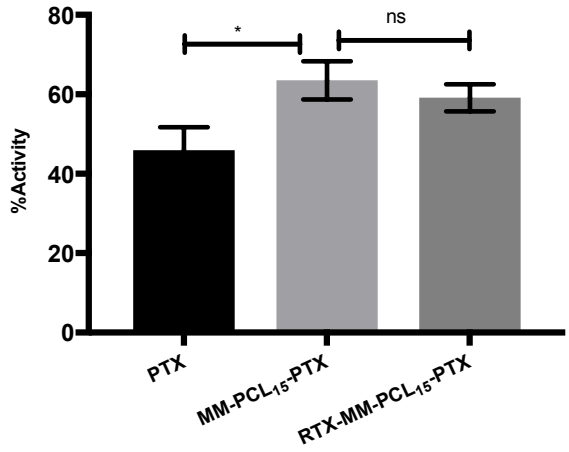
%Activity
80
60
40
20
0
*
ns
PTX
MM-PCL15-PTX
RTX-MM-PCL15-PTX

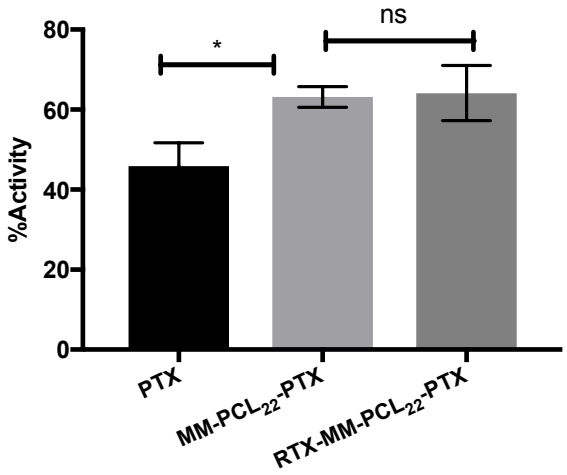
%Activity
80
60
40
20
0
*
ns
PTX
MM-PCL22-PTX
RTX-MM-PCL22-PTX

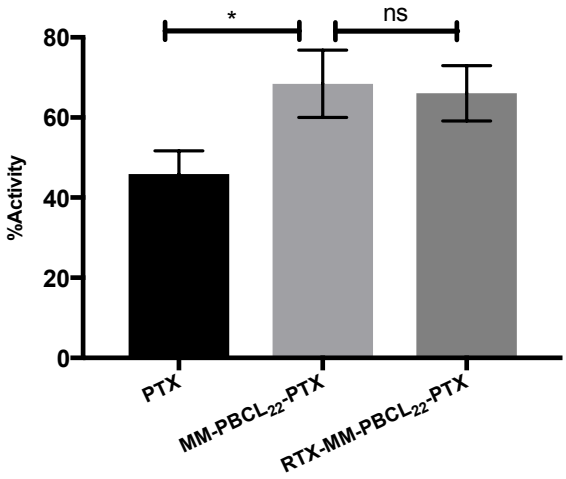
%Activity
80
60
40
20
0
*
ns
PTX
MM-PBCL22-PTX
RTX-MM-PBCL22-PTX

KG-15 (CD20+)

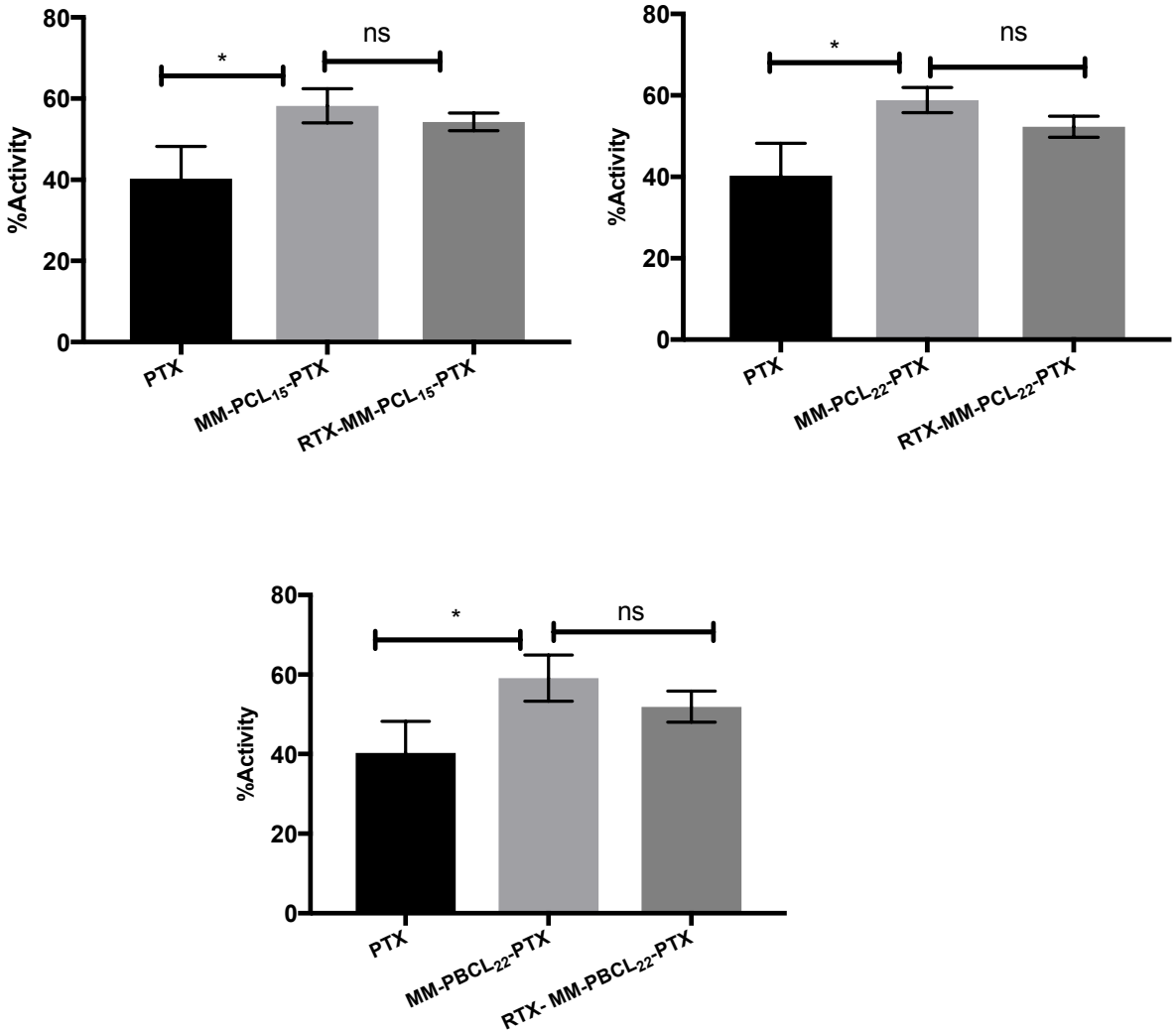

Figure 3-8 *In-vitro* cytotoxicity of PTX encapsulated in RTX conjugated MM-PCL_{15}, RTX conjugated MM-PCL_{22} and RTX conjugated MM-$PBCL_{22}$, in comparison to PTX encapsulated in plain mixed micelles and free PTX against SUP-M2 and KG-15 cells after 24hrs incubation. Data represent average ± SD (n=3) * donates statistically significant difference (Unpaired student's test, P<0.05), while ns donates statistically non-significant (Unpaired student's t test, P>0.05).

SUP-M2 (CD20-)

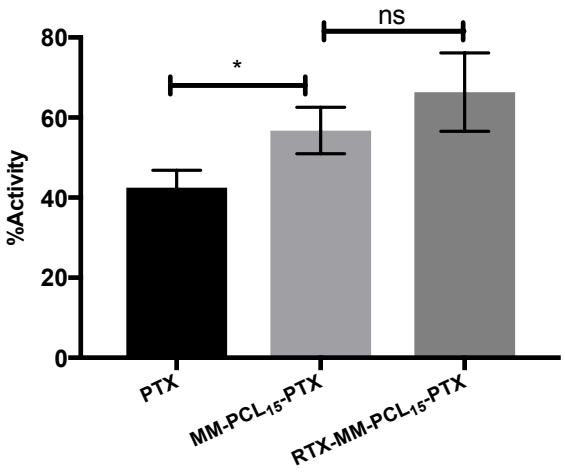
ns
*
80
60
40
20
0
%Activity
PTX
MM-PCL15-PTX
RTX-MM-PCL15-PTX

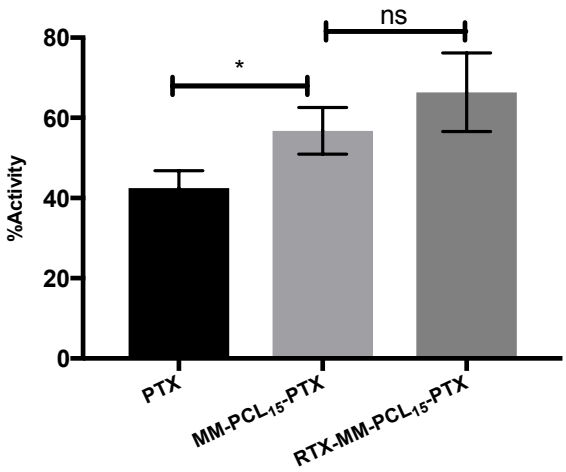
ns
*
80
60
40
20
0
%Activity
PTX
MM-PCL15-PTX
RTX-MM-PCL15-PTX

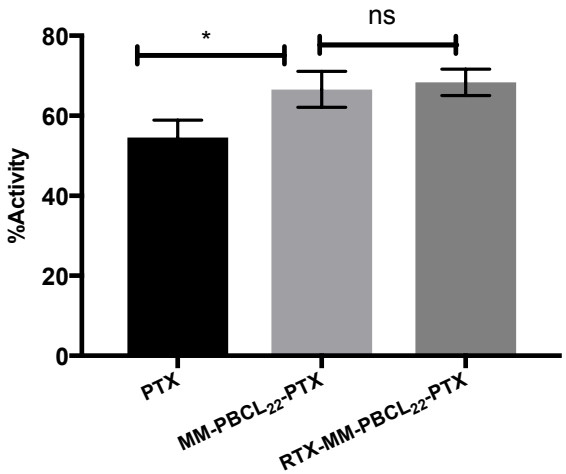
ns
*
80
60
40
20
0
%Activity
PTX
MM-PBCL22-PTX
RTX-MM-PBCL22-PTX

KG-15 (CD20+)

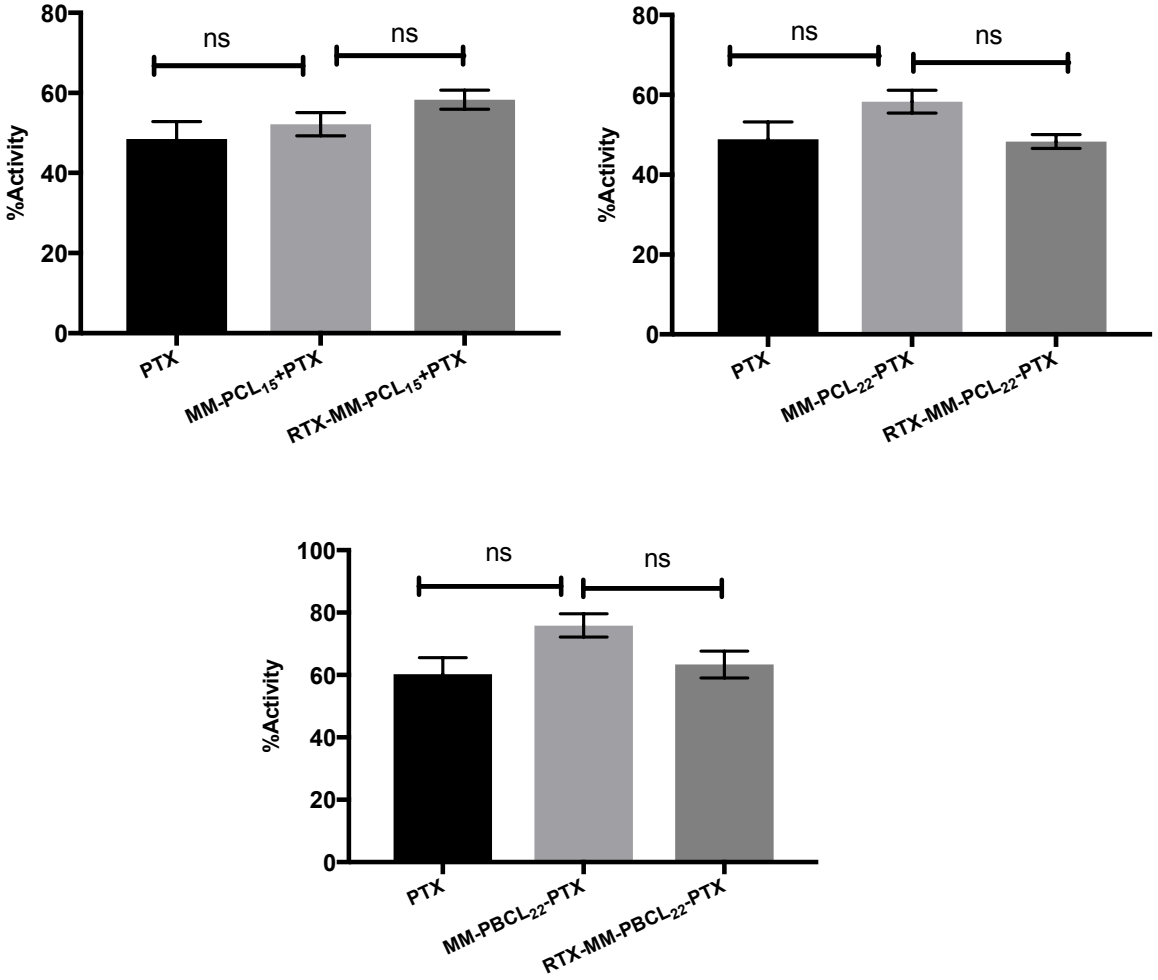

Figure 3-9 *In-vitro* cytotoxicity of PTX encapsulated in RTX conjugated MM-PCL_{15}, RTX conjugated MM-PCL_{22} and RTX conjugated MM-$PBCL_{22}$, in comparison to PTX encapsulated in plain mixed micelles and free PTX against SUP-M2 AND KG-15 cells after 72hrs. Data represent average ± SD (n=3) *donates statistically significant difference (one-way ANOVA P<0.5), while ns donates statistically non-significant (Unpaired student's t test P>0.5).

Chapter Four

Discussion, Conclusion & Future direction

4 Discussion

The main objective of this research is to produce actively targeted immune-micelles prepared by conjugation of mAbs to the micellar surface that can be traced in live animals at the same time. The fate of traceable nanocarriers can be easily followed in biological system, providing opportunities for a better understanding of the relationship between the structures of mAb modified nanocarrier and their cellular uptake and trafficking and/or *in vivo* distribution. For successful development of traceable mAb modified nano-carriers, however, one must insure that the fluorescent tag remains associated with the mAb itself and/or the nanocarrier upon introduction to cells or diluting conditions following intravenous administration to blood. This is more likely by chemical conjugation of the NIR probe to the mAb and/or the nanocarrier itself, rather than physical encapsulation of the dye inside the nanocarrier.

Conjugation of mAbs to the surface of NHS functionalized PEG-phospholipid micelles have been reported before.[113, 114] PEG-phospholipid micelles, however, are found to be mostly not very stable under diluting conditions of the blood and fall apart prematurely before reaching their cellular targets. In this case, the mAb-modified micelle is unlikely to be able to act as a successful actively targeted delivery system due to micellar dissociation in blood leading to early release of incorporated cargo. In this regard, the reported CMC for the inactivated PEG-phospholipid micelles was found to be around 10 μM.[115] The CMC for the functionalized NHS-PEG-DSPE is even higher around 60 μM, reflective if lower thermodynamic stability of these micelles compared to PEG-DSPE micelles.[116] This is in contrast to PEO-PCL and PEO-PBCL polymeric micelles which show lower CMCs at a range of 1 and and 0.25 μM respectively (10 to 100 times less than for the CMC of PEG-DSPE micelles).[117]

Development of traceable antibody modified PEG phospholipid micelles have been mainly achieved through attaching a traceable probe to the mAb or physical encapsulation of the probe inside the core of micelles. For instance, a traceable 2C5 PEG-PE immunomicelles has been reported in the literature that has been developed through conjugating carboxyfluorescein to the 2C5 mAb.[61] Alternatively, loading of DOX (a fluorescent drug) into the PEG-DSPE micelles has also been used to track or image the micelles.[118]

In this research, we examined whether mixing of mAb conjugated PEG-phospholipid micelles with PEO-PCL based block copolymer can lead to the development of stable mAb modified polymeric micelles capable of active drug targeting to their cellular targets. This was achieved through mixing of Cy5 tagged rituximab modified PEG-DSPE with Cy3 tagged PEO-PCL or PEO-PBCL block copolymers of different core length and following the specific association of Cy3/Cy5.5 tagged mixed micelles versus individual Cy3 tagged PEO-PCL or Cy5.5 tagged RTX-PEG-DSPE micelles by CD20 positive or negative cells. Since the Cy3 azide was chemically conjugated into the core of the micelles and the Cy5.5 NHS ester dye was conjugated to the RTX on the distal of the shell of the micellar system, no interference between the two dyes were expected. Stable RTX-conjugated mixed micellar formulations were expected to show high proportion of both Cy5.5 and Cy3+ cells for cell lines overexpressing CD20 thereby have high uptake of the encapsulated chemotherapeutic agent by these cells compared to cells not expressing CD20. Besides, existence of conjugated dyes having different emission wavelengths with minimal interference will provide an opportunity for following the fate of each component in the micellar structure, thus enabling the assessment of the stability of micellar structure *in vivo*.

Rituximab was covalently attached to the distal end of the polymeric micelles through the reaction of reactive NHS ester end of our NHS-PEG-DSPE micelles with the aliphatic free amine from the lysine of RTX to form a stable amide bond. This reaction was found to be appropriate for our purpose for several reasons. Initially, the reaction is simple and can be carried out in aqueous media. In addition to that the reaction does not require extreme environment to proceed, since the amino group from the mAb is a good nucleophile at pH=8. The nucleophile amine will then attack the carboxyl group of the NHS ester from the micelle to form a stable amide bond. More importantly the complementary determining region (CDR) of RTX will not be inactivated by this reaction, since; the CDR doesn't include any lysine.[119-121] Furthermore, conjugating the RTX on the surface of the micelles is not expected to increase the size of micelles significantly. In this work we successfully attached RTX on the surface of the micelles without significant change in the size of the micelles (23 ± 2.1 nm for plain PEG-DSPE micelles vs 30 ± 5.7 nm for the RTX-PEG-DSPE micelles).

For the development of Cy3 tagged PEO-PCL based micelles, we prepared PEO-PCL-PPCL and PEO-PBCL-PPCL block copolymers, first. Cy3 was then conjugated to the PPCL end of the block polymers as described in a previous work by our group (Garg *et al*. Biomaterials, In press). We then prepared micelles from these block copolymers and co-incubated the Cy3 tagged PEO-PCL based micelles with RTX conjugated NHS-PEG-DSPE micelles. This method of preparation for mAb modified micelles is similar to the post insertion method that is widely adopted in the literature for coupling antibodies on the surface of liposomes. This technique basically starts with reacting the mAb ligand with a reactive end of PEG-phospholipid micelles following by co-incubating these micelles with a more thermodynamically and kinetically stable micelle structure that can also be preloaded with a drug. It is assumed that the ligands modified PEG-phospholipids can spontaneously insert into the structure of the more stable micelles to form a stable mixed immunomicelles.[61, 122,

[123] the validity of this assumption for a mixture of RTX modified PEG-phospholipids and PEO-PBCL or PEO-PCLs of different PCL length was studied here. The effect of poly(ester) structure (PCL versus PBCL) on the micellar stability, targeted cellular association and PTX delivery was investigated, as well.

Formation of mixed micelles following co-incubation was investigated following changes in the average dimeter of the two micellar population as a function of time (Figure 3-3). We observed co-existence of two populations particles at time zero for all mixed micelles, which gradually converted to one population over time following 24h incubation, implying insertion of PEG-phospholipid micelles in to the PEO-poly(ester) micelles upon incubation in this study.

We then studied the thermodynamic and kinetic stability of mixed micelles prepared above. For micelles prepared from a single block copolymer, previous studies have shown the direct correlation between the length of the hydrophobic chain and the thermodynamic stability of polymeric micelles as reflected by a decrease in the CMC of block copolymers.[72, 124] Increasing the hydrophobicity of the polymer has been shown to lead to improvements in the kinetic stability of micelles, as well.[125] Furthermore, our group tested the effect of the pendent group on the PCL segment of the PEO-PCL on the stability of the polymeric micellar system and found the presence of benzyl carboxylate pendent group to improve both thermodynamic and the kinetic stability of PEO-PBCL compared to PEO-PCL micelles.[126]

In our studies here, mixing of the NHS-PEG-DSPE micelles with PEO-PCL-PPCL with different hydrophobic domain lengths or with PEO-PBCL-PPCL appeared to lead to a significant change in the micellar size, thermodynamic and kinetic stability. The average diameter of the mixed micelles from MM-PCL_{15} (78 nm), MM-PCL_{22} (84 nm) and MM-

$PBCL_{22}$ (93 nm) was significantly increased compared to micelles forming by single block copolymers: (PCL_{15},57 nm), $PCL_{22,}$ 50 nm; and $PBCL_{22,}$ 71 nm) (Table 3-1). Also the size of mixed micelles showed an increasing trend moving from MM-PCL_{15} to MM-PCL_{22} to MM-PBCL-$_{22}$. This trend was not seen for micelles from single block copolymers.

In terms of thermodynamic stability, mixing of PEG-PSPE appeared to lower the thermodynamic stability (increase the CMC) of PEO-poly(esters) under current study. This effect was more significant for PEO-PCL_{15} than PEO-PCL_{22} and PEO-$PBCL_{22}$, however. when comparing mixed micelles versus micelles from single block copolymers, Mixed micelles prepared from PCL_{15} based block copolymer or MM-PCL_{15} (which has the shorter hydrophobic segment) have shown significantly lower thermodynamic stability compared to MM-PCL_{22} (longer hydrophobic segment) and MM-$PBCL_{22}$ (benzoyl carboxylate pending group). Additionally, the MM-$PBCL_{22}$ was the most thermodynamically stable system among the three mixed micelles (Table 3-1).

In terms of kinetic stability, mixed micelles in general showed higher stability compared to PEG-DSPE ones. Among the three mixed micellar structures, MM-$PBCL_{22}$ was found to be the most kinetically structure, followed by MM-PCL_{22} and then MM-PCL_{15} (Figure 3-4).

We then investigated the formation of mixed micelles and their stability in cell media, by comparing the association of Cy5.5/Cy3 dye with CD20 positive versus CD20 negative cells for MM-PCL15, MM-PCL22 and MM-PBCL22. Several researches have proven that the conjugation of monoclonal antibodies on the surface of the PEO-PCL and PEG-PE micelles can improve their uptake by target cells up to 2 times. [87, 89] In our work, we reacted the RTX with NHS-PEG-DSPE in very low ratio 1:100 Molar ratio for the purpose of having low

density of mAb on the surface so it doesn't compromise the stealth properties provided by the PEG.[122] Despite the low RTX density, the RTX- conjugated MM-PCL_{22} and MM-$PBCL_2$) show significantly increased association toward the CD20+ cells. This was evidenced by up to significant increase in the Cy5.5/Cy3+ population of cells for KG15 cells treated with RTX modified MMs in comparison to the same cells treated with plain MMs. A 3.7(RTX- MM-PCL_{22}) and 4.2-folds (RTX- MM-$PBCL_{22}$) increase in the Cy5.5/Cy3+ population of KG-15 over SUP-M2 cells was also noted for RTX-MM treatment). This can be attributed mainly to the high affinity and selectivity of RTX toward its target and also to the nature of the CD20 antigen itself as it expressed abundantly on the surface of the B-cells and it is will exposed.[9, 27, 122] For RTX- MM-PCL_{15} micelles, the dotplot graph (Figure 3-5) showed the lowest population of Cy5.5/Cy3+ cells, instead a high population of Cy5 positive cells was observed. This observation point to instability of MM-PCL15 and its rapid dissociation to two separate micellar population consisting of Cy5.5 labeled RTX-PEG-PSPE and Cy3 labeled PEO-PCL15 micelles. This is in line with our earlier observation on the kinetically instability of these micelles.

We have chosen to encapsulate PTX in the MM formulations of this study. This selection was based on a previous study where PEO_{45}-PCL_{17} micelles have shown high encapsulation efficiency (EE) of 99.2% and drug loading (DL) of 14.89% for PTX. The release profile of PTX from these formulation was also shown to be relatively slow as only 35% of PTX was released from these micelles after 48h (versus 90 % release for free drug).[127] Slow drug release from the carrier is a prerequisite for its targeted delivery by the carrier implying similar *in vivo* fate for the carrier and the drug following systemic administration. In the current study the encapsulation and the release profile of PTX from MM-PCL_{15}, MM-PCL_{22} and MM-$PBCL_{22}$ in comparison with its counterpart micelles from single block copolymers

was studied. Our results pointed to similar size between drug loaded and empty mixed micelles. In comparison to the formulation noted above, our micellar formulations had an encapsulation efficacy of 15, 23.6 and 20.7% and drug loading of 0.37, 0451 and 0.39% for MM-PCL_{15}, MM-PCL_{22} and MM-$PBCL_{22}$ respectively. Additionally the release of PTX from MM-PCL_{15}, MM-PCL_{22} and MM-$PBCL_{22}$ formulation after 48h was 75, 40.7 and 60.75% respectively. Overall among different mixed micellar formulation, MM-PCL_{22} showed to have the best EE and release profile (Table 3-3 and Figure 3-6). These results were also in line with our previous lab findings that shows micelles from PEO-PCL (with long hydrophobic chain) are better vehicle for PTX than PEO-PCL (short hydrophobic segment and PEO-PBCL.[128]

Our results showed no significant difference between the cytotoxicity of RTX conjugated mixed micelles loaded with PTX and the plain mixed micelles loaded with PTX irrespective of the CD 200 positivity in the cells used for this study (Figure 3-7 and 3-8). RTX is a non-internalizing mAb which means that the nanocarrier with the drug will not be expected to enter the targeted cells and release the drug intracellularly, but may rather release the drug in the vicinity of cancer cells and to the extracellular space.[14, 122] With the later scenario happening one cannot expect to see any difference in the cytotoxicity *in-vitro* since the drug will be released eventually in the media within the 24 and 48h incubation time used in this study.

5 Conclusions

In this study, we were able to successfully develop RTX modified mixed polymeric micelles without jeopardizing the functionality of the mAb and the stability of the nanocarrier. This system was also successfully designed to be traceable using two different emission wavelengths, each representing one component within the mixed micellar population. We also reported on the positive impact of a core with higher hydrophobicity on the stability of the RTX modified mixed micelles and their specific targeting of CD20 positive cells. We also showed that pending benzoyl carboxylate group on the caprolactone (MM-PBCL$_{22}$) to significantly improve the thermodynamic and kinetic stability of mixed micelles leading to better RTX micellar specificity for the CD20 positive cells.

In general, we found a positive correlation between the kinetic stability of mixed micelles and their targeting properties for CD20 positive cells. In other words, micelles, which were kinetically stable when incubated with SDS (MM-PCL$_{22}$ and MM-PBCL$_{22}$), managed to associate with their target cell and remain intact more effectively. In contrast MM-PCL$_{15}$, which was not stable in the presence of SDS, also broke down in the media Finally the association of RTX conjugated mixed micelles prepared from PCL 22 or PBCL 22 based block copolymers to its targeted cells (KG-15) was significantly higher than the plain micelles and also 3.7 and 4.2 fold respectively higher than its association with CD20- cells (SUP-M2), pointing to the suitability of these two structures for active targeting of CD20 positive NHL cells.

In PTX delivery and encapsulation, we concluded the MM-PCL$_{22}$ to have the best EE among the mixed micellar formulation prepared under the same conditions. Additionally, MM-PCL$_{22}$ had the slowest release profile compared to the other mixed micelles formulation. However, our *in-*

vitro cytotoxicity study did not show a significant difference in the cytotoxic effect of encapsulated PTX in RTX modified mixed micelles compared to their plain counterparts in in KG-15 cells (CD20+) and SUP-M2 cells (CD20-) at both 24 and 72 hours. This was attributed to the non-internalizing properties of RTX in addition to the release of cytotoxic drug concentrations form MM formulations at these incubation periods.

6 Future direction

1-In this study we are able to design a stable mixed immunomicelles system and study its *in-vitro* association with its target cells and also its *in-vitro* cytotoxicity. Conducting an *in-vivo* tissue distribution study of our NIR labeled RTX conjugated mixed micelles on a lymphoma bearing mice model and studying the specificity of this system to accumulate with its target compared to the plain mixed micelles and the free drug is warranted. Additionally, the bio distribution of drug loaded RTX MMs can be compared to that of plain ones in tumor bearing animal models. Moreover, the cytotoxic effect of drug loaded in RTX conjugated micelles can be compared to that of the free drug and the plain mixed micelles *in vivo*.

2-Conjugating different densities of RTX on the surface of the micelles and therefore, optimizing the ideal density of the mAb on the surface that can cause maximum association with its target without jeopardizing the stealth properties of the micellar system can be carried out.

3- The developed micellar system can be used to incorporate drugs that are clinically more relevant to the treatment of NHL, like doxorubicin, or they can be used for the delivery of drug combination to tumors.

4- In this study we are able to design traceable immunomicelles. These micelles can be traced in vivo to define the time of maximum nanocarrier accumulation in tumor. One can than give a dose of radiation accurately to only the tumor cite. The combination of radiation and chemotherapy will then maximize the therapeutic outcome.

7 Limitation

1-In this study we were not able to measure\calculate how much mAb were conjugated on the surface of each micelle, since it was difficult to estimate the molecular weight of the micelles. Instead we have reported on the conjugation efficiency and w/w ratio of conjugated mAb for PEG-DSPE block copolymer.

2- Paclitaxel is not the first choice for lymphoma tumor. Other drugs such as doxorubicin could have been used which are clinically more relevant.

3-The kinetic and thermodynamic stability the RTX conjugated mixed micellar system was not studied. Instead, these parameters were measured for MMs without RTX modification. If we would have conjugated the RTX to the micellar system we will need to purify it to remove the free antibody, this process will leave the concentration of the micelles unknown. And in order to

measure the kinetic and thermodynamic stability of the micelles we need to know the exact concentration of the micelles.

References

References

1. Sabattini, E., et al., *WHO classification of tumours of haematopoietic and lymphoid tissues in 2008: an overview.* Pathologica, 2010. **102**(3): p. 83-7.
2. Rajyaguru, D.J., et al., *Intravascular large B-cell lymphoma in the United States (US): a population-based study using Surveillance, Epidemiology, and End Results program and National Cancer Database.* Leuk Lymphoma, 2017: p. 1-9.
3. Committee, C.C.S.s.A. *Cancer Statistics.* 2017; Available from: http://www.cancer.ca/~/media/cancer.ca/CW/cancer information/cancer 101/Canadian cancer statistics/Canadian-Cancer-Statistics-2017-EN.pdf?la=en.
4. Dotan, E., C. Aggarwal, and M.R. Smith, *Impact of Rituximab (Rituxan) on the Treatment of B-Cell Non-Hodgkin's Lymphoma.* P t, 2010. **35**(3): p. 148-57.
5. Ku, M., G. Chong, and E.A. Hawkes, *Tumour cell surface antigen targeted therapies in B-cell lymphomas: Beyond rituximab.* Blood Rev, 2017. **31**(1): p. 23-35.
6. Tedder, T.F. and P. Engel, *CD20: a regulator of cell-cycle progression of B lymphocytes.* Immunol Today, 1994. **15**(9): p. 450-4.
7. Stashenko, P., et al., *Characterization of a human B lymphocyte-specific antigen.* J Immunol, 1980. **125**(4): p. 1678-85.
8. Cragg, M.S. and M.J. Glennie, *Antibody specificity controls in vivo effector mechanisms of anti-CD20 reagents.* Blood, 2004. **103**(7): p. 2738-43.

9. Golay, J., et al., *Biologic response of B lymphoma cells to anti-CD20 monoclonal antibody rituximab in vitro: CD55 and CD59 regulate complement-mediated cell lysis.* Blood, 2000. **95**(12): p. 3900-8.

10. Pescovitz, M.D., *Rituximab, an anti-cd20 monoclonal antibody: history and mechanism of action.* Am J Transplant, 2006. **6**(5 Pt 1): p. 859-66.

11. Solimando, A.G., et al., *Targeting B-cell non Hodgkin lymphoma: New and old tricks.* Leuk Res, 2016. **42**: p. 93-104.

12. Okroj, M., A. Osterborg, and A.M. Blom, *Effector mechanisms of anti-CD20 monoclonal antibodies in B cell malignancies.* Cancer Treat Rev, 2013. **39**(6): p. 632-9.

13. Gelderman, K.A., S. Lam, and A. Gorter, *Inhibiting complement regulators in cancer immunotherapy with bispecific mAbs.* Expert Opin Biol Ther, 2005. **5**(12): p. 1593-601.

14. Glennie, M.J., et al., *Mechanisms of killing by anti-CD20 monoclonal antibodies.* Mol Immunol, 2007. **44**(16): p. 3823-37.

15. Klein, C., et al., *Epitope interactions of monoclonal antibodies targeting CD20 and their relationship to functional properties.* MAbs, 2013. **5**(1): p. 22-33.

16. Ivanov, A., et al., *Monoclonal antibodies directed to CD20 and HLA-DR can elicit homotypic adhesion followed by lysosome-mediated cell death in human lymphoma and leukemia cells.* J Clin Invest, 2009. **119**(8): p. 2143-59.

17. Honeychurch, J., et al., *Antibody-induced nonapoptotic cell death in human lymphoma and leukemia cells is mediated through a novel reactive oxygen species-dependent pathway.* Blood, 2012. **119**(15): p. 3523-33.

18. Shan, D., J.A. Ledbetter, and O.W. Press, *Apoptosis of malignant human B cells by ligation of CD20 with monoclonal antibodies.* Blood, 1998. **91**(5): p. 1644-52.

19. Pedersen, I.M., et al., *The chimeric anti-CD20 antibody rituximab induces apoptosis in B-cell chronic lymphocytic leukemia cells through a p38 mitogen activated protein-kinase-dependent mechanism.* Blood, 2002. **99**(4): p. 1314-9.

20. Teeling, J.L., et al., *Characterization of new human CD20 monoclonal antibodies with potent cytolytic activity against non-Hodgkin lymphomas.* Blood, 2004. **104**(6): p. 1793-800.

21. Kohler, G. and C. Milstein, *Continuous cultures of fused cells secreting antibody of predefined specificity.* Nature, 1975. **256**(5517): p. 495-7.

22. Smolewski, P. and T. Robak, *The preclinical discovery of rituximab for the treatment of non-Hodgkin's lymphoma.* Expert Opin Drug Discov, 2015. **10**(7): p. 791-808.

23. Zhang, C., *Hybridoma technology for the generation of monoclonal antibodies.* Methods Mol Biol, 2012. **901**: p. 117-35.

24. Little, M., et al., *Of mice and men: hybridoma and recombinant antibodies.* Immunol Today, 2000. **21**(8): p. 364-70.

25. Press, O.W., et al., *Monoclonal antibody 1F5 (anti-CD20) serotherapy of human B cell lymphomas.* Blood, 1987. **69**(2): p. 584-91.

26. Liu, A.Y., et al., *Production of a mouse-human chimeric monoclonal antibody to CD20 with potent Fc-dependent biologic activity.* J Immunol, 1987. **139**(10): p. 3521-6.

27. Reff, M.E., et al., *Depletion of B cells in vivo by a chimeric mouse human monoclonal antibody to CD20.* Blood, 1994. **83**(2): p. 435-45.

28. Maloney, D.G., et al., *Phase I clinical trial using escalating single-dose infusion of chimeric anti-CD20 monoclonal antibody (IDEC-C2B8) in patients with recurrent B-cell lymphoma.* Blood, 1994. **84**(8): p. 2457-66.

29. Maloney, D.G., et al., *IDEC-C2B8 (Rituximab) anti-CD20 monoclonal antibody therapy in patients with relapsed low-grade non-Hodgkin's lymphoma.* Blood, 1997. **90**(6): p. 2188-95.

30. Berinstein, N.L., et al., *Association of serum Rituximab (IDEC-C2B8) concentration and anti-tumor response in the treatment of recurrent low-grade or follicular non-Hodgkin's lymphoma.* Ann Oncol, 1998. **9**(9): p. 995-1001.

31. *<RituxanIV_PM_E-2.pdf>*.

32. Smith, M.R., *Rituximab (monoclonal anti-CD20 antibody): mechanisms of action and resistance.* Oncogene, 2003. **22**(47): p. 7359-68.

33. Reagan, P.M. and J.W. Friedberg, *Reassessment of Anti-CD20 Therapy in Lymphoid Malignancies: Impact, Limitations, and New Directions.* Oncology (Williston Park), 2017. **31**(5): p. 402-11.

34. Rose, A.L., B.E. Smith, and D.G. Maloney, *Glucocorticoids and rituximab in vitro: synergistic direct antiproliferative and apoptotic effects.* Blood, 2002. **100**(5): p. 1765-73.

35. Helmberg, A., et al., *Glucocorticoid-induced apoptosis of human leukemic cells is caused by the repressive function of the glucocorticoid receptor.* Embo j, 1995. **14**(3): p. 452-60.

36. Chow, K.U., et al., *Anti-CD20 antibody (IDEC-C2B8, rituximab) enhances efficacy of cytotoxic drugs on neoplastic lymphocytes in vitro: role of cytokines, complement, and caspases.* Haematologica, 2002. **87**(1): p. 33-43.

37. Wu, L., et al., *lenalidomide enhances natural killer cell and monocyte-mediated antibody-dependent cellular cytotoxicity of rituximab-treated CD20+ tumor cells.* Clin Cancer Res, 2008. **14**(14): p. 4650-7.

38. Smolewski, P., et al., *Proapoptotic activity of alemtuzumab alone and in combination with rituximab or purine nucleoside analogues in chronic lymphocytic leukemia cells.* Leuk Lymphoma, 2005. **46**(1): p. 87-100.

39. Coiffier, B., et al., *CHOP chemotherapy plus rituximab compared with CHOP alone in elderly patients with diffuse large-B-cell lymphoma.* N Engl J Med, 2002. **346**(4): p. 235-42.

40. Feugier, P., et al., *Long-term results of the R-CHOP study in the treatment of elderly patients with diffuse large B-cell lymphoma: a study by the Groupe d'Etude des Lymphomes de l'Adulte.* J Clin Oncol, 2005. **23**(18): p. 4117-26.

41. Scott, A.M., J.D. Wolchok, and L.J. Old, *Antibody therapy of cancer.* Nat Rev Cancer, 2012. **12**(4): p. 278-87.

42. Wu, A.M. and P.D. Senter, *Arming antibodies: prospects and challenges for immunoconjugates.* Nat Biotechnol, 2005. **23**(9): p. 1137-46.

43. Witzig, T.E., *Yttrium-90-ibritumomab tiuxetan radioimmunotherapy: a new treatment approach for B-cell non-Hodgkin's lymphoma.* Drugs Today (Barc), 2004. **40**(2): p. 111-9.

44. Parslow, A.C., et al., *Antibody-Drug Conjugates for Cancer Therapy.* Biomedicines, 2016. **4**(3).

45. Jiang, L., et al., *A novel antibody-drug conjugate anti-CD19(Fab)-LDM in the treatment of B-cell non-Hodgkin lymphoma xenografts with enhanced anticancer activity.* J Drug Target, 2016. **24**(1): p. 47-57.

46. Mehta, A. and A. Forero-Torres, *Development and Integration of Antibody-Drug Conjugate in Non-Hodgkin Lymphoma.* Curr Oncol Rep, 2015. **17**(9): p. 41.

47. Peer, D., et al., *Nanocarriers as an emerging platform for cancer therapy.* Nat Nano, 2007. **2**(12): p. 751-760.

48. Lopes de Menezes, D.E., L.M. Pilarski, and T.M. Allen, *In vitro and in vivo targeting of immunoliposomal doxorubicin to human B-cell lymphoma.* Cancer Res, 1998. **58**(15): p. 3320-30.

49. Wu, C., et al., *Potentiating antilymphoma efficacy of chemotherapy using a liposome for integration of CD20 targeting, ultra-violet irradiation polymerizing, and controlled drug delivery.* Nanoscale Res Lett, 2014. **9**(1): p. 447.

50. Zhou, S., et al., *Intracellular pH-responsive and rituximab-conjugated mesoporous silica nanoparticles for targeted drug delivery to lymphoma B cells.* J Exp Clin Cancer Res, 2017. **36**(1): p. 24.

51. Chiu, G.N., et al., *CD20 cross-linking achieved following treatment with liposomal rituximab results in significant cytotoxic activity in B-cell lymphomas including mantle cell lymphoma cell lines.* Cancer Research, 2014. **65**(9 Supplement): p. 327.

52. Meissner, J.M., et al., *Novel antisense therapeutics delivery systems: In vitro and in vivo studies of liposomes targeted with anti-CD20 antibody.* J Control Release, 2015. **220**(Pt A): p. 515-28.

53. Voltan, R., et al., *Nanoparticles engineered with rituximab and loaded with Nutlin-3 show promising therapeutic activity in B-leukemic xenografts.* Clin Cancer Res, 2013. **19**(14): p. 3871-80.

54. Popov, J., et al., *Multivalent rituximab lipid nanoparticles as improved lymphoma therapies: indirect mechanisms of action and in vivo activity.* Nanomedicine (Lond), 2011. **6**(9): p. 1575-91.

55. Azadbakht, B., et al., *Preparation and evaluation of APTES-PEG coated iron oxide nanoparticles conjugated to rhenium-188 labeled rituximab.* Nuclear Medicine and Biology. **48**: p. 26-30.

56. Prabhu, R.H., V.B. Patravale, and M.D. Joshi, *Polymeric nanoparticles for targeted treatment in oncology: current insights.* Int J Nanomedicine, 2015. **10**: p. 1001-18.

57. Moretton, M.A., et al., *A glucose-targeted mixed micellar formulation outperforms Genexol in breast cancer cells.* Eur J Pharm Biopharm, 2017. **114**: p. 305-316.

58. Kapishon, V., et al., *Oseltamivir-conjugated polymeric micelles prepared by RAFT living radical polymerization as a new active tumor targeting drug delivery platform.* Biomaterials Science, 2016. **4**(3): p. 511-521.

59. Meng, Y., et al., *TKD peptide as a ligand targeting drug delivery systems to memHsp70-positive breast cancer.* Int J Pharm, 2016. **498**(1-2): p. 40-8.

60. Palanca-Wessels, M.C., et al., *Anti-CD22 antibody targeting of pH-responsive micelles enhances small interfering RNA delivery and gene silencing in lymphoma cells.* Mol Ther, 2011. **19**(8): p. 1529-37.

61. Torchilin, V.P., et al., *Immunomicelles: targeted pharmaceutical carriers for poorly soluble drugs.* Proc Natl Acad Sci U S A, 2003. **100**(10): p. 6039-44.

62. Ahn, J., et al., *Antibody fragment-conjugated polymeric micelles incorporating platinum drugs for targeted therapy of pancreatic cancer.* Biomaterials, 2015. **39**: p. 23-30.

63. Noh, T., et al., *Block copolymer micelles conjugated with anti-EGFR antibody for targeted delivery of anticancer drug.* Journal of Polymer Science Part A: Polymer Chemistry, 2008. **46**(22): p. 7321-7331.

64. Mathews, A.S., et al., *Peptide Modified Polymeric Micelles Specific for Breast Cancer Cells.* Bioconjugate Chemistry, 2013. **24**(4): p. 560-570.

65. Xiong, X.B., et al., *Multifunctional polymeric micelles for enhanced intracellular delivery of doxorubicin to metastatic cancer cells.* Pharm Res, 2008. **25**(11): p. 2555-66.

66. Hoang, B., et al., *Active targeting of block copolymer micelles with trastuzumab Fab fragments and nuclear localization signal leads to increased tumor uptake and nuclear localization in HER2-overexpressing xenografts.* Mol Pharm, 2013. **10**(11): p. 4229-41.

67. Biswas, S., et al., *Recent advances in polymeric micelles for anti-cancer drug delivery.* Eur J Pharm Sci, 2016. **83**: p. 184-202.

68. Kwon, G.S. and K. Kataoka, *Block copolymer micelles as long-circulating drug vehicles.* Advanced Drug Delivery Reviews, 1995. **16**(2): p. 295-309.

69. Nishiyama, N. and K. Kataoka, *Current state, achievements, and future prospects of polymeric micelles as nanocarriers for drug and gene delivery.* Pharmacol Ther, 2006. **112**(3): p. 630-48.

70. Adams, M.L., A. Lavasanifar, and G.S. Kwon, *Amphiphilic block copolymers for drug delivery.* J Pharm Sci, 2003. **92**(7): p. 1343-55.

71. *Martin's physical pharmacy and pharmaceutical sciences : physical chemical and biopharmaceutical principles in the pharmaceutical sciences*, P.J. Sinko, Editor.

72. Owen, S.C., D.P.Y. Chan, and M.S. Shoichet, *Polymeric micelle stability.* Nano Today, 2012. **7**(1): p. 53-65.

73. Dvorak, H.F., et al., *Vascular permeability factor/vascular endothelial growth factor, microvascular hyperpermeability, and angiogenesis.* Am J Pathol, 1995. **146**(5): p. 1029-39.

74. Seymour, L.W., et al., *Effect of molecular weight (Mw) of N-(2-hydroxypropyl)methacrylamide copolymers on body distribution and rate of excretion after subcutaneous, intraperitoneal, and intravenous administration to rats.* J Biomed Mater Res, 1987. **21**(11): p. 1341-58.

75. Kwon, G., et al., *Enhanced tumor accumulation and prolonged circulation times of micelle-forming poly (ethylene oxide-aspartate) block copolymer-adriamycin conjugates.* Journal of Controlled Release, 1994. **29**(1): p. 17-23.

76. Lavasanifar, A., J. Samuel, and G.S. Kwon, *Poly(ethylene oxide)-block-poly(L-amino acid) micelles for drug delivery.* Adv Drug Deliv Rev, 2002. **54**(2): p. 169-90.

77. Kataoka, K., A. Harada, and Y. Nagasaki, *Block copolymer micelles for drug delivery: design, characterization and biological significance.* Advanced Drug Delivery Reviews, 2001. **47**(1): p. 113-131.

78. Hu, D.S.-G. and H.-J. Liu, *Structural analysis and degradation behavior in polyethylene glycol/poly(L-lactide) copolymers.* Journal of Applied Polymer Science, 1994. **51**(3): p. 473-482.

79. Fan, Z., et al., *Adding Vitamin E-TPGS to the Formulation of Genexol-PM: Specially Mixed Micelles Improve Drug-Loading Ability and Cytotoxicity against Multidrug-Resistant Tumors Significantly.* PLOS ONE, 2015. **10**(4): p. e0120129.

80. Zhang, B., et al., *Targeting fibronectins of glioma extracellular matrix by CLT1 peptide-conjugated nanoparticles.* Biomaterials, 2014. **35**(13): p. 4088-98.

81. Li, X., et al., *A folate modified pH sensitive targeted polymeric micelle alleviated systemic toxicity of doxorubicin (DOX) in multi-drug resistant tumor bearing mice.* Eur J Pharm Sci, 2015. **76**: p. 95-101.

82. Wang, Y., et al., *Specific cell targeting with APRPG conjugated PEG–PLGA nanoparticles for treating ovarian cancer.* Biomaterials, 2014. **35**(3): p. 983-992.

83. Ge, H., et al., *Preparation, characterization, and drug release behaviors of drug nimodipine-loaded poly(epsilon-caprolactone)-poly(ethylene oxide)-poly(epsilon-caprolactone) amphiphilic triblock copolymer micelles.* J Pharm Sci, 2002. **91**(6): p. 1463-73.

84. Peng, C.L., et al., *Self-assembled star-shaped chlorin-core poly(epsilon-caprolactone)-poly(ethylene glycol) diblock copolymer micelles for dual chemo-photodynamic therapies.* Biomaterials, 2008. **29**(26): p. 3599-608.

85. Cuong, N.-V., Y.-L. Li, and M.-F. Hsieh, *Targeted delivery of doxorubicin to human breast cancers by folate-decorated star-shaped PEG-PCL micelle.* Journal of Materials Chemistry, 2012. **22**(3): p. 1006-1020.

86. Xu, P., et al., *Highly stable core-surface-crosslinked nanoparticles as cisplatin carriers for cancer chemotherapy.* Colloids Surf B Biointerfaces, 2006. **48**(1): p. 50-7.

87. Liao, C., et al., *Targeting EGFR-overexpressing tumor cells using Cetuximab-immunomicelles loaded with doxorubicin and superparamagnetic iron oxide.* European Journal of Radiology, 2011. **80**(3): p. 699-705.

88. Benahmed, A., M. Ranger, and J.-C. Leroux, *Novel Polymeric Micelles Based on the Amphiphilic Diblock Copolymer Poly(N-vinyl-2-pyrrolidone)-block-poly(D,L-lactide).* Pharmaceutical Research, 2001. **18**(3): p. 323-328.

89. Perche, F., N.R. Patel, and V.P. Torchilin, *Accumulation and toxicity of antibody-targeted doxorubicin-loaded PEG-PE micelles in ovarian cancer cell spheroid model.* J Control Release, 2012. **164**(1): p. 95-102.

90. Zhao, B.J., et al., *The antiangiogenic efficacy of NGR-modified PEG-DSPE micelles containing paclitaxel (NGR-M-PTX) for the treatment of glioma in rats.* J Drug Target, 2011. **19**(5): p. 382-90.

91. Bae, Y. and K. Kataoka, *Intelligent polymeric micelles from functional poly(ethylene glycol)-poly(amino acid) block copolymers.* Adv Drug Deliv Rev, 2009. **61**(10): p. 768-84.

92. Vega, J., et al., *Targeting doxorubicin to epidermal growth factor receptors by site-specific conjugation of C225 to poly(L-glutamic acid) through a polyethylene glycol spacer.* Pharm Res, 2003. **20**(5): p. 826-32.

93. Song, W., et al., *Anti-tumor efficacy of c(RGDfK)-decorated polypeptide-based micelles co-loaded with docetaxel and cisplatin.* Biomaterials, 2014. **35**(9): p. 3005-14.

94. Stage, T.B., T.K. Bergmann, and D.L. Kroetz, *Clinical Pharmacokinetics of Paclitaxel Monotherapy: An Updated Literature Review.* Clin Pharmacokinet, 2017.

95. Miller, T.P., et al., *A phase I/II trial of paclitaxel for non-Hodgkin's lymphoma followed by paclitaxel plus quinine in drug-resistant disease.* Anticancer Drugs, 1998. **9**(2): p. 135-40.

96. Mathew, A.E., et al., *Synthesis and evaluation of some water-soluble prodrugs and derivatives of taxol with antitumor activity.* Journal of Medicinal Chemistry, 1992. **35**(1): p. 145-151.

97. Singla, A.K., A. Garg, and D. Aggarwal, *Paclitaxel and its formulations.* International Journal of Pharmaceutics, 2002. **235**(1): p. 179-192.

98. Lee, K.S., et al., *Multicenter phase II trial of Genexol-PM, a Cremophor-free, polymeric micelle formulation of paclitaxel, in patients with metastatic breast cancer.* Breast Cancer Res Treat, 2008. **108**(2): p. 241-50.

99. Cabral, H. and K. Kataoka, *Progress of drug-loaded polymeric micelles into clinical studies.* J Control Release, 2014. **190**: p. 465-76.

100. Hamaguchi, T., et al., *NK105, a paclitaxel-incorporating micellar nanoparticle formulation, can extend in vivo antitumour activity and reduce the neurotoxicity of paclitaxel.* Br J Cancer, 2005. **92**(7): p. 1240-6.

101. Kato, K., et al., *Phase II study of NK105, a paclitaxel-incorporating micellar nanoparticle, for previously treated advanced or recurrent gastric cancer.* Invest New Drugs, 2012. **30**(4): p. 1621-7.

102. Green, M.R., et al., *Abraxane, a novel Cremophor-free, albumin-bound particle form of paclitaxel for the treatment of advanced non-small-cell lung cancer.* Ann Oncol, 2006. **17**(8): p. 1263-8.

103. Vakil, R. and G.S. Kwon, *Poly(ethylene glycol)-b-poly(epsilon-caprolactone) and PEG-phospholipid form stable mixed micelles in aqueous media.* Langmuir, 2006. **22**(23): p. 9723-9.

104. Mahmud, A., X.-B. Xiong, and A. Lavasanifar, *Novel Self-Associating Poly(ethylene oxide)-block-poly(ε-caprolactone) Block Copolymers with Functional Side Groups on the Polyester Block for Drug Delivery.* Macromolecules, 2006. **39**(26): p. 9419-9428.

105. Xiong, X.B., et al., *Amphiphilic block co-polymers: preparation and application in nanodrug and gene delivery.* Acta Biomater, 2012. **8**(6): p. 2017-33.

106. Garg, S.M., et al., *Application of Click Chemistry in the Preparation of Poly(ethylene oxide)-block-poly(ε-caprolactone) with Hydrolyzable Cross-Links in the Micellar Core.* Macromolecules, 2011. **44**(7): p. 2058-2066.

107. Lecomte, P., R. Riva, and C. Jerome, *Synthesis of Functionalized Aliphatic Polyesters by the "Click" Copper-Catalyzed Alkyne—Azide Cycloaddition*, in *New Smart Materials via Metal Mediated Macromolecular Engineering*, E. Khosravi, Y. Yagci, and Y. Savelyev, Editors. 2009, Springer Netherlands: Dordrecht. p. 77-91.

108. *<nhs-ester-labeling.pdf>*.

109. Topel, Ö., et al., *Determination of critical micelle concentration of polybutadiene-block-poly(ethyleneoxide) diblock copolymer by fluorescence spectroscopy and dynamic light scattering.* Journal of Molecular Liquids, 2013. **177**: p. 40-43.

110. Soleymani Abyaneh, H., et al., *Rational design of block copolymer micelles to control burst drug release at a nanoscale dimension.* Acta Biomaterialia, 2015. **24**: p. 127-139.

111. Shahin, M., et al., *Decoration of polymeric micelles with cancer-specific peptide ligands for active targeting of paclitaxel.* Biomaterials, 2011. **32**(22): p. 5123-33.

112. Zhao, X., et al., *Enhanced Stability of Polymeric Micelles Based on Postfunctionalized Poly(ethylene glycol)-b-poly(γ-propargyl l-glutamate): The Substituent Effect.* Biomacromolecules, 2012. **13**(5): p. 1315-1322.

113. Wang, R., et al., *Application of poly(ethylene glycol)-distearoylphosphatidylethanolamine (PEG-DSPE) block copolymers and their derivatives as nanomaterials in drug delivery.* Int J Nanomedicine, 2012. **7**: p. 4185-98.

114. Wu, H., L. Zhu, and V.P. Torchilin, *pH-sensitive poly(histidine)-PEG/DSPE-PEG co-polymer micelles for cytosolic drug delivery.* Biomaterials, 2013. **34**(4): p. 1213-22.

115. Lukyanov, A.N., et al., *Polyethylene glycol-diacyllipid micelles demonstrate increased acculumation in subcutaneous tumors in mice.* Pharm Res, 2002. **19**(10): p. 1424-9.

116. Salmaso, S., et al., *pH-sensitive PEG-based micelles for tumor targeting.* J Drug Target, 2011. **19**(4): p. 303-13.

117. !!! INVALID CITATION !!! [117].

118. Dong, Q., et al., *Isomeric folate-conjugated polymeric micelles bind to folate receptors and display anticancer effects.* Asian Pac J Cancer Prev, 2014. **15**(17): p. 7363-9.

119. Brinkley, M., *A brief survey of methods for preparing protein conjugates with dyes, haptens and crosslinking reagents.* Bioconjugate Chemistry, 1992. **3**(1): p. 2-13.

120. Du, J., et al., *Structural basis for recognition of CD20 by therapeutic antibody Rituximab.* J Biol Chem, 2007. **282**(20): p. 15073-80.

121. Du, J., et al., *Crystal structure of chimeric antibody C2H7 Fab in complex with a CD20 peptide.* Mol Immunol, 2008. **45**(10): p. 2861-8.

122. Torchilin, V.P., *Passive and active drug targeting: drug delivery to tumors as an example.* Handb Exp Pharmacol, 2010(197): p. 3-53.

123. Ishida, T., D.L. Iden, and T.M. Allen, *A combinatorial approach to producing sterically stabilized (Stealth) immunoliposomal drugs.* FEBS Lett, 1999. **460**(1): p. 129-33.

124. Gaucher, G., et al., *Block copolymer micelles: preparation, characterization and application in drug delivery.* Journal of Controlled Release, 2005. **109**(1–3): p. 169-188.

125. Van Domeselaar, G.H., et al., *Application of solid phase peptide synthesis to engineering PEO–peptide block copolymers for drug delivery.* Colloids and Surfaces B: Biointerfaces, 2003. **30**(4): p. 323-334.

126. Garg, S.M., M.R. Vakili, and A. Lavasanifar, *Polymeric micelles based on poly(ethylene oxide) and alpha-carbon substituted poly(varepsilon-caprolactone): An in vitro study on the effect of core forming block on polymeric micellar stability, biocompatibility, and immunogenicity.* Colloids Surf B Biointerfaces, 2015. **132**: p. 161-70.

127. Gong, C., et al., *Improving anti-tumor activity with polymeric micelles entrapping paclitaxel in pulmonary carcinoma.* Nanoscale, 2012. **4**(19): p. 6004-17.

128. Shahin, M. and A. Lavasanifar, *Novel self-associating poly(ethylene oxide)-b-poly(epsilon-caprolactone) based drug conjugates and nano-containers for paclitaxel delivery.* Int J Pharm, 2010. **389**(1-2): p. 213-22.

Appendix

Appendix

Assessing the effect of polymer stereochemistry in selective solublization of one enantiomer from a racemic mixture of a compound with chiral carbon

Abstract

Purpose: The stereochemistry of the polymer has shown to have a significant impact on its intrinsic properties. The aim of this study was to assess the effect of polymer stereochemistry of the core forming self-associating block copolymers on the solublization of optically active and hydrophobic molecules. Polymeric micelles composed of stereo-active polylactide segments as the hydrophobic part (core-forming block) were selected for this purpose.

Method: Methoxy poly(ethylene glycol)-b-poly(lactides) (PEO-b-PLA) of different stereo-chemistries, i.e., MPEG-PDLA, MPEG-PLLA and MPEG-PDLLA, were synthesized by ring opening polymerization of D-Lactide, L-Lactide or D,L-Lactide, respectively using methoxy PEG as initiator and stannous octoate as catalyst. H^1NMR (600 MHz) was used to characterize the synthesized polymers and calculate their molecular weight. The α-benzyl carboxylate ε-caprolactone (BCL) was encapsulated into the di-block polymers by solvent evaporation method. UV-VIS Spectrophotometer was used to determine the loading capacity. After separating the loaded polymer from the free monomer by ultrafiltration, the optical activity of the loaded micelles, and the filtrate was measured using polarimeter.

Results: H^1NMR confirmed the successful synthesis of block copolymers at expected molecular weights. Polymeric micelles with stereo regular cores appeared to provide significantly better loading efficiency for BCL than those with non-stereo regular cores. Block copolymer micelles with PDLA appeared to have a significantly better loading capacity for BCL than those with the

PLLA core. Optical rotation results showed that polymeric micelles with different stereo configuration under study have no preference for selective solubilization of one enantiomer of BCL from its racemic mixture.

Conclusion: The stereochemistry of the core appeared to have no effect on selective solublization of the optically active model material under study. However, micelles with stereo regular core appeared to have better loading capacity for racemic BCL compared to micelles with optically inactive cores.

1-Introduction

Polymeric micelles are self-assembled block copolymers, consisting of a hydrophilic shell, and a hydrophobic core in an aqueous media [1]. Polymeric micelles are widely used as drugs delivery system to solubilize poorly water-soluble drugs or to obtain targeted drug delivery [2].

The stereochemistry of a polymer has shown to have a significant impact on its intrinsic properties. For instance previous studies showed that block copolymer micelles with stereo-regular structures can form semi crystalline cores and show better kinetic stability than those without stereo-regular blocks that form amorphous cores. Furthermore, other studies illustrated that block copolymers with semi crystalline cores may show faster release rate compared to the micelles with amorphous cores [3],[4],[5]. The effect of stereo regularity of the core on the solubilization of particular compounds especially those with chiral carbon centers have not been given too much attention, however.

The aim of this study was to assess the effect of polymer stereochemistry in core forming block of self-associating block copolymers on the solublization of optically active and hydrophobic molecules. Polymeric micelles composed of stereo-active polylactide segments as the hydrophobic part (core-forming block) were selected for this purpose.

Lactide has two chiral carbons and three different enantiomers (D-Lactide, L-Lactide and the Meso- Lactide) [6]. In this study, upon polymerization of each of D- or L-lactide pure monomers with methoxy poly(ethylene glycol) (PEG), block copolymers of PEG-b-poly(D-lactide) (PEG-PDLA) and PEG-b-poly (L-lactide) (PEG-PLLA) were prepared, respectively. We also used a racemic 50:50 mixture of D- and L- lactide in a separate polymerization reaction to produce MPEG-PDLLA block copolymers. MPEG-PLA block copolymers with different stereochemistry in the PLA block were then used for the solubilization of a racemic mixture of a chiral low

molecular weight compounds, i.e., benzyl carboxylate-ε-caprolactone. The effect of PLA stereochemistry on the total solubilization of the racemic mixture of BCL as well as selective solubilization of a single enantiomer from this racemic mixture was then assessed.

2. Materials and Methods

2.1. Materials:

Methoxy poly(ethylene glycol) (average molecular weight 5000 $gmol^{-1}$) and stannous Octoate were purchased from sigma, St Louis, MO, USA. D-Lactide was a generous gift from Purac, Schiedam, Netherlands. L-Lactide was obtained from Alfa-Aesar, Lancashire, UK. **α**-benzyl carboxylate ε-caprolactone is purchased from Alberta Research Chemical INC (ARCI). Ultra-filtration tubes (Ultracel 3000NMWL) were purchased from Merk Millipore LTD, Cork, Ireland. All the chemicals and reagents used were of analytical grade.

2.2. Methods:

2.2.1. Synthesis of MPEG-PDLA, MPEG-PLLA and MPEG PDLLA 50:50 di-block copolymers

MPEG-PDLA and MPEG-PLLA di-block copolymers were synthesized by ring opening polymerization of D-Lactide or L-Lactide, respectively using methoxy poly (ethylene glycol) as an initiator and stannous octoate as a catalyst. For the preparation of MPEG-PDLLA 50:50 a racemic mixture of D- and L lactide at equal molar ratio was used, the MPEG-PDLLA block copolymer was synthesized previously in our lab by the same method.[5]. The methoxy poly (ethylene glycol) 5000$gmol^{-1}$ (0.5mg), D-Lactide (0.5g) and L-Lactide (0.5g) were left in the oven at 65^{o}C under vacuum overnight. Stannous Octoate (6 drops) was added to each of the

vials. Vials were sealed under vacuum. The reaction was preceded by placing the vials in the oven at 160c^{o} for 7 hours and vortexing them every 30 minutes hours. Cooling the vials at room temperature overnight terminated the reaction. The synthesized polymers were purified by adding dichloromethane (18 mL) to each vial and centrifuging it for 7 minute. The supernatant was slowly decanted into n-hexane (150mL) and stirred for 10 minutes, the solution was placed in the fridge for 2 hours and finally the hexane was decanted and the precipitate was collected. The samples were dissolved in chloroform D ($CDCL_3$) and then subjected to ^{1}H NMR spectroscopy 600MHz (Bruker 300 AM; Billerica MA) for characterization.

2.2.2. Self-assembly of MPEG-PDLA, MPEG-PLLA and MPEG-PDLLA di-block copolymers

The MPEG-PDLA, MPEG-PLLA and MPEG-PDLLA micelles were prepared by solvent evaporation method. This was achieved by adding 4 mL THF to 30 mg of the di-block copolymer, followed by drop-wise addition of this solution to 7.5mL doubly distilled water under stirring. The solutions were left overnight to allow evaporation of the THF.

2.2.3. Determination of micellar size and size distribution: The hydrodynamic diameter of micelles (4 mg/mL) was measured using dynamic light scattering (DLS) ZETA-Sizer Nano (Malvern Instruments Ltd., Malvern, UK). The analysis was performed at a scattering angle of 173^{o} at 25 C^{o}.

2.2.4. Encapsulation of α-benzoyl carboxylate ε-caprolactone in to MPEG-PDLA, MPEG-PLLA and MPEG-PDLLA micelles

Loading of the micelles was accomplished by dissolving 30 mg of the polymer and 10 mg of BCL in 4 mL THF. The BCL solution was added slowly to the polymer solution. Under the fume hood the THF solution was added drop wise to 7.5mL double distilled water under magnetic stirring for one day to allow evaporation of THF.

2.2.5. Ultra-Filtration of the prepared polymeric micelles

The polymer plus BCL solutions were poured into the ultra-filtration tubes (Am icon - Utra-4 centrifugal filter with molecular sieve 3000 NMWL) and placed in the centrifuge (MSE Mistral 2000) for 40 minutes at 3600× G. The supernatant and the filtrate were freeze dried for 24 hours in separate vials.

2.2.6. Determination of the encapsulation efficiency

The loading capacity of the micelles for BCL were determined by UV-VIS Spectrophotometer (Beckman Coulter DU. 730) at λ max=256 nm.

The supernatant was diluted with 2 mL water and 2 mL methanol to destroy the micelle and the absorbance was measured. The concentration of the supernatant was calculated from the calibration curve. Furthermore, the encapsulation efficiency was calculated from the following equation

Encapsulation efficiency % = the amount of encapsulated BCL the total feeding amount of BCL×100

Loading Efficiency (W\W %) = the amount of loaded BCL (mg) total amount of copolymer (mg)×100.

2.2.7. Optical activity measurement

The freeze-dried supernatant, filtrate and samples before ultracentrifugation were dissolved in 5mL THF sonicated for 10 minutes and their optical activity was measured immediately using a polarimeter (Perkin Elmer 241, USA). The optical activity was measured at 25^{O} C using the sodium D-line (λ max =589 nm).

The following equation was used to calculate the specific rotation:

$$[\alpha]_l^T = \alpha/lc$$

Where:

$[\alpha]_l^T$ = Specific rotation in degrees. l is the wavelength of light used for the observation . T is the temperature in C^o

α = observed rotation in degrees.

l = cell path length in decimeters. (1decimeter).

c = concentration in g ml^{-1} for a pure liquid compound.

2.2.8. Statistical Analysis

All experiments were conducted in triplicate. Data is reported as average SD. Statistical analysis was done by using one way ANOVA with Tukey post-test analysis. For non-linear regression analysis the significance level [α] was set at 0.05. Graph pad prism was used (version 6.0. Graph pad software, INC., La Jolla,CA, USA).

3. Results

3.1. Synthesis and characterization of MPEG-PDLA, MPEG-PLLA and MPEG-PDLLA

The MPEG-PLA block copolymer with different stereo configuration was synthesized by ring opening polymerization of the lactide by the hydroxyl group of the MPEG (macro-initiator) using stannous Octoate as a catalyst [7], [8]. H^1NMR was used to characterize the synthesized block copolymer and to confirm its purity. The correspondence proton peaks at δ =1.5 ppm (3H) and 5.09 ppm (1H) represents the methine and the methyl proton signals, respectively of the lactide moiety. While the proton peaks at δ= 3.312ppm (3H) corresponds to the proton signal of the methoxy segment and 3.577ppm (4H) relates to the proton signal ethylene moiety of the MPEG. Moreover, the degree of polymerization was calculated from the H^1NMR based on the peak intensity ratio of the protons from the ethylene moiety of the MPEG (3.577ppm); where the intensity was 8.39 for the MPEG-PDLA and 7.70 for the MPEG-PLLA; to peak intensity of the proton from the chiral carbon of the lactide (5.09ppm) where the intensity was 1.figure (1.1),(1.2). In addition to that the yield of polymerization was calculated from the following equation. Details are summarized in table (1.1)

$$\text{Yield (W\W \%)} = (\text{Actual weight})/ (\text{Theoretical weight}) \times 100$$

Table (1.1): Molecular weight and the yield of the block copolymer

Sample ID	Degree of Polymerization	$M_{n\,(}$ gmol$^{-1)}$	Yield %	PLA (W %)
MPEG-PDLA	54	8888	78.3%	43.74%
MPEG-PLLA	59	9248	78%	45.93%
MPEG-PDLLA	40	7868	70%	36.45%

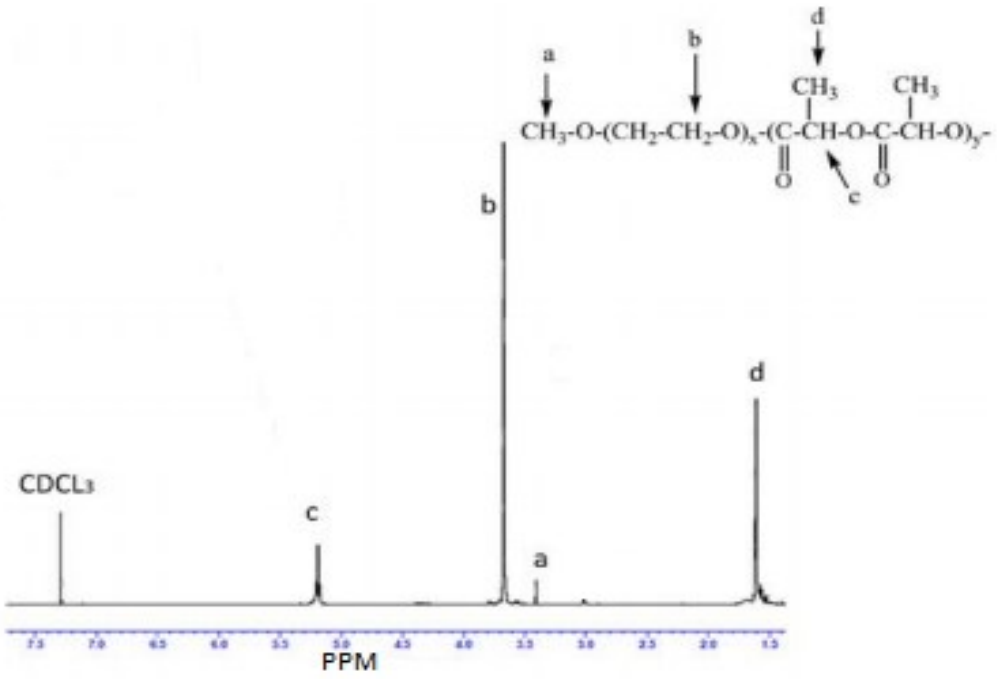

Figure (1.2): H1NMR Spectrum of MPEG-PLA

3.2. Determination of the micellar size and size distribution.

The characteristics of the prepared polymeric micelles were summarized in table (1.2). The Z-average diameters of the prepared micelles were all below 60nm with relatively low polydispersity index.

3.3. Determination of the encapsulation efficiency

Using different weights of BCL and dissolving it in a solvent system consisting of 2mL water and 2mL methanol the UV absorbance were measured and a calibration curve was conducted by plotting the absorbance in nm against the concentration in mg\mL.

The absorbance of the unknowns (MPEG-PDL+BCL, MPEG-PLLA+BCL and MPEG-PDLLA+BCL) was measured and the concentration of the unknowns was determined from the

calibration curve. The amount of BCL loaded was then calculated by multiplying the BCL concentration by the sample volume.

Furthermore, the encapsulation efficiency (EE) and the loading capacity were calculated and the results are summarized in the following table (1.4)

Polymeric micelles with stereo regular core appeared to have significantly better loading capacity than those with non-stereo regular core. In the other hand the block copolymer with D- lactide segment appeared to have a significant better loading capacity than the one with the L-lactide segment.

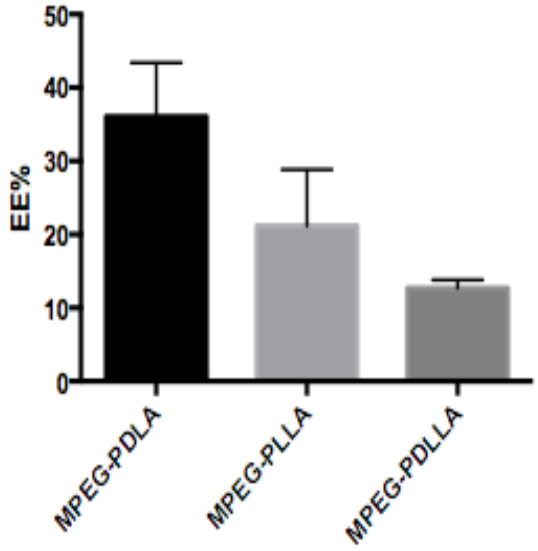

Figure (1.3): The effect of the polymer stereochemistry on the solublization of BCL. The data was obtained by measuring the loaded BCL by UV-VIS Spectrophotometer.

Table (1.4): Loading and encapsulation efficiency of BCL into the block co-polymer

Name	Diameter ±SD (dnm)	PDI ±SD	EE (%) ±SD	Monomer Loading(%)±SD
MPEG-PDLA	40±0.35	0.37 ± 0.001	36.05±7.37	12.016±2.45
MPEG-PDLA+BCL	49±0.36	0.21 ± 0.003		
MPEG-PLLA	50 ±0.46	0.25 ± 0.006	21.17±7.7	7.049±2.57
MPEG-PLLA+BCL	55±0.20	0.14 ± 0.018		
MPEG-PDLLA	56±0.29	0.162 ± 0.002	12.66±1.13	4.586±0.39
MPEG-PDLLA+BCL	61±0.24	0.121 ± 0.005		

3.4. Measuring the optical activity

Perkin Elmer Polarimeter was used to measure the optical rotation at $25C^{O}$ using the sodium D-line lamp at λmax =589nm. The results for the raw and the specific optical rotation are summarized in the table below (Table 1.3). The results showed that both polymeric micelles with different stereo configuration have no preference to selectively solubilizing one enantiomer from a racemic mixture. In other words all row optical rotation measurement from the unloaded BCL (filtrate) appeared to have no optical activity. Furtermore, the di block copolymer containing the racemic mixture lactide segment showed to have no selectivity toward the racemic mixture of BCL.

Moreover, the specific rotation calculated for each di block copolymer had a positive or negative value that correlates with the % optical rotation. Weight of the poly D-lactide or the poly L-lactide respectively Table (1.1).

Notes:

1- Row optical rotation below -\+ 0.005 is considered zero.

2-The specific rotation of the pure enantiomer either PDLA or PLLA is between 140-150

Table (1.2): Optical activity measurements

Sample		Average optical rotation ±SD	Specific rotation $[\alpha]_l^T$
MPEG-PDLA	Unfiltered	0.1918± 0.001	51.52±2.6
	Supernatant	0.35240 ± 0.001	55.79±4.2
	Filtrate	0.00020± 0.000	0.17±0.001
MPEG-PDLA + BCL	Unfiltered	0.19180± 0.001	51.52±1.5
	Supernatant	0.13560 ± 0.001	51.35±2.4
	Filtrate	0.000 ±0.000	0.00±0.00
MPEG-PLLA	Unfiltered	-0.16400± 0.001	-59.41±5.1
	Supernatant	-0.17280± 0.001	-54.40±3.2
	Filtrate	-0.00060± 0.001	-0.51±0.1
MPEG-PLLA +BCL	Unfiltered	-0.37920± 0.001	-48.73±1.9
	Supernatant	-0.11580± 0.000	-53.01±3.1
	Filtrate	-0.0008± 0.000	-0.83±0.4
MPEG-PDLLA	Unfiltered	0.00 ± 0.00	0.00±0.001
	Supernatant	0.001180± 0.00	0.89±0.2
	Filtrate	0.00±0.00	0.00±0.004
MPEG-PDLLA+BCL	Unfiltered	0.0± 0.00	0.00±0.00
	Supernatant	0.00± 0.00	0.00±0.00
	Filtrate	-0.00040± 0.001	-0.27±0.001

BCL Control	Supernatant	0.00±0.00	0.00±0.00
	Filtrate	0.00120	0.84±0.5

4. Discussion

The use of polymeric micelles as drug delivery systems has many advantages. In addition to its ability of providing targeted and sustained release to the site of action, polymeric micelles has the ability to solubilize and retain hydrophobic drugs in its core i.e. works as a drug reservoir [9]. Polymeric micelles appear to be the most promising drug delivery system in clinical trials, due to its relatively small size and enhanced stability [10]. In addition to that, the core of the micelle can be simply varied to meet specific requirement. For instance by varying the structure of the micelles core we can increase the loading capacity of the system [11], or enhance the kinetic or dynamic stability. In this study we assessed the effect of core stereochemistry on selective solublization of one enantiomer over the other. From the experiments conducted neither did the PDLA micelle nor the PLLA micelles showed to have any selectivity toward any of the BCL enantiomers. In other words the results of the optical activity of the unloaded monomer from all the micelles groups with different stereochemistry (MPEG-PDLA, MPEG-PLLA, and MPEG- PDLLA) were all neutral. This may be due to the fact the stereochemistry of the monomers might be different than that of the synthesized polymer. Monomers stereochemistry can be dextro, levo or meso. However the polymer stereochemistry can be divided to isotactic, syndiotactic or atactic depending on the stereochemistry of the monomer forming it. For instance if the monomer forming the polymer was either D or L then the polymer stereochemistry will be isotactic. Furthermore, if the monomer forming the polymer was either meso or racemic mixture than the stereochemistry of the polymer will be either syndiotactic or atactic [12]. From this explanation we can conclude that polymers formed from

either the D-Lactide or the L-Lactide will form isotactic polymer and have the same properties without any ability to selectively solubilize any enantiomer. However the loading capacity of the MPEG-PDLA showed to be significantly more than that of the MPEG-PDLLA micelle but not significantly different from that of the MPEG-PLLA micelle. The better loading efficacy seems to be related to the formation of more crystalline core when using stereo regular polymer (MPEG-PDLA and MPEG-PLLA) compared to the formation of amorphous core when using non-stereoregular polymer (MPEG-PDLLA). The formation of crystalline core leads to more kinetically stable micelle and therefore might lead to better loading capacity.

5. Conclusion

We can conclude that both polymeric micelles with different stereo configuration have no preference to selectively solubilize one enantiomer from a racemic mixture. Furthermore, In the other hand the block copolymer micelles with D- lactide segment trend to have better loading capacity than the one with the L-lactide segment for BCL.

References

1-Kwon, Glen S, and Kazunori Kataoka. "Block copolymer micelles as long-circulating drug vehicles." *Advanced drug delivery reviews* 16.2 (1995): 295-309.

2- Feng, Kun et al. "Chirality plays critical roles in enhancing the aqueous solubility of nocathiacin I by block copolymer micelles." *Journal of Pharmacy and Pharmacology* 65.1 (2013): 64-71.

3-Kang N, Perron ME, Prud'homme RE, Zhang Y, Gaucher G, Leroux JC. Stereocomplex block copolymer micelles: coreshell nanostructures with enhanced stability. Nano Lett. 2005;5(2):315–9.

4-Agrawal SK, Sanabria-DeLong N, Coburn JM, Tew GN, Bhatia SR. Novel drug release profiles from micellar solutions of PLA-PEO-PLA triblock copolymers. J Controlled Release. 2006;112(1):64–71.

5-Abyaneh, Hoda Soleymani et al. "Rationale design of block copolymer micelles to control burst drug release at a nanoscale dimension." *Acta biomaterialia* (2015).

6-Inkinen S, Hakkarainen M, Albertsson AC, Sodergard A. From lactic acid to poly(lactic acid) (PLA): characterization and analysis of PLA and its precursors. Biomacromolecules. 2011;12(3):523–32.

7- Drumright, Ray E, Patrick R Gruber, and David E Henton. "Polylactic acid technology." *Advanced materials* 12.23 (2000): 1841-1846.

8- Keith A. Porter, Ring Opening Polymerization of Lactide for The synthesis of Poly (Lactic Acid), March 2006.

9-Aw, Moom Sinn, Mima Kurian, and Dusan Losic. "Polymeric micelles for multidrug delivery and combination therapy." *Chemistry–A European Journal* 19.38 (2013): 12586-12601.

10- Jones, Marie-Christine, and Jean-Christophe Leroux. "Polymeric micelles–a new generation of colloidal drug carriers." *European journal of pharmaceutics and biopharmaceutics* 48.2 (1999): 101-111.

11-Garg, Shyam M, Mohammad Reza Vakili, and Afsaneh Lavasanifar. "Polymeric micelles based on poly (ethylene oxide) and α-carbon substituted poly (ε-caprolactone): An in vitro study on the effect of core forming block on polymeric micellar stability, biocompatibility, and immunogenicity." *Colloids and Surfaces B: Biointerfaces* 132 (2015): 161-170.

12- Ovitt, Tina M, and Geoffrey W Coates. "Stereochemistry of lactide polymerization with chiral catalysts: new opportunities for stereocontrol using polymer exchange mechanisms." *Journal of the American Chemical Society* 124.7 (2002): 1316-1326